UNIVERSITY OF OKLAHOMA

GRADUATE COLLEGE

NON-NEWTONIAN POWER-LAW FLUID FLOW IN ECCENTRIC ANNULI: CFD SIMULATION AND EXPERIMENTAL STUDY

A DISSERTATION

SUBMITTED TO THE GRADUATE FACULTY

in partial fulfillment of the requirements for the

Degree of

DOCTOR OF PHILOSOPHY

By

CHINENYE CHIBUIKE EXCEL OGUGBUE
Norman, Oklahoma
2009

NON-NEWTONIAN POWER-LAW FLUID FLOW IN ECCENTRIC ANNULI: CFD SIMULATION AND EXPERIMENTAL STUDY

A DISSERTATION APPROVED FOR THE
MEWBOURNE SCHOOL OF PETROLEUM AND GEOLOGICAL ENGINEERING

BY

_____
Dr. Subhash N. Shah, Chair

_____
Dr. Brian P. Grady

_____
Dr. Samuel Osisanya

_____
Dr. Chandra S. Rai

_____
Dr. J. C. Roegiers

To the memory of my Father

To my Mother

ACKNOWLEGDEMENTS

Works of this nature can't be accomplished by an individual effort; hence this section is devoted to appreciating individuals and groups who have contributed in one way or the other to the success of this project. Firstly, my sincere gratitude goes to the Almighty God, for the strength, zeal, and wisdom that He gave me for the completion of this study.

I would like to express my deepest gratitude to my advisor, Dr. Subhash Shah, for his support, critical evaluation and excellent guidance that ensured the successful completion of this work. Sometimes, he showed more confidence in me than I had in myself, which really helped me through my studies. My special thanks go to all the members of my doctoral committee, Dr. Samuel Osisanya, Dr. Brian Grady, Dr. Jean-Claude Roegiers, and Dr. Chandra Rai. I appreciate you all for your teaching, insightful comments, suggestions, and being always available to help.

I also deeply appreciate the help from the research team at Well Construction Technology Center (WCTC). My sincere thanks go to Joe Flenniken for his help and guidance in the experimental phase of this work. Many thanks go to my fellow graduate students, the professors and staff of the Mewbourne School of Petroleum and Geological Engineering (MPGE) for their assistance, encouragement and support during my graduate study.

I would like to also thank members of the Coiled Tubing Consortium for sharing their time, expertise, and resources during the several stages of this work. Special thanks to Mr. Michael Bailey of Halliburton, Mr. Curtis Blount of ConocoPhillips, Dr.

Steven Hill of Schlumberger, and Mr. Bill Aitkens of BJ Services, and others. I am deeply grateful to Dr Bob Gochnour, Bryan Dotson, Chinedu Agbalaka, and Pat Archey for their invaluable advice towards my petroleum engineering career.

Special thanks go to my colleagues in the Society of Petroleum Engineers international and OU Petrobowl team for their contributions to my welfare and development as a petroleum engineering student. I also appreciate help from several members of the University of Oklahoma community: University Libraries, Graduate College, OU Cousins, and the Office of the International Student Services (ISS) are a few.

I am notably grateful to my host parents, Judith and Barbara, and their families for their unique acceptance, hospitality and benevolence. I also wish to thank in a very special way, Dr Godwin Chukwu and Mummy Felicia for always being there for me. To my family in Nigeria; my precious mother, Mrs. E. N. Ogugbue, siblings: Kelechi, Chiemela, Chinanu, Ugochi, Nomso, Mimi and friends, I say thank you for your prayers, patience, and encouragement.

TABLE OF CONTENTS

LIST OF TABLES

LIST OF FIGURES

ABSTRACT

Numerous publications have addressed the problems inherent to calculating wellbore hydraulics in eccentric annulus. The challenge of theoretical and numerical studies of fluid flow in an eccentric annulus is mainly due to the required coordinate systems. CFD modeling provides an alternative approach of investigating fluid flow in such complex geometries. The CFD technique emerged as a result of the current increase in computer processing speed and available memory. This branch of fluid flow analysis complements experimental and theoretical work, providing economically interesting alternatives through the simulation of real flows and allowing an alternative form for theoretical advances under conditions unavailable experimentally.

In this study, results from a series of numerical simulations for the fully developed laminar flow of non-Newtonian power law fluids in eccentric annular geometries, conducted using the computational fluid dynamics (CFD) code FLUENT, are used to investigate the effect of eccentricity, and diameter ratios (ratio of the outer diameter of the inner tubing to the inner diameter of the outer tubing) on axial velocity profiles, the viscosity profile, as well as the axial friction pressure losses. Unlike the uniform velocity profile applicable for every sector in a concentric annulus, the axial velocity profile for an eccentric annulus is altered, with the peak velocities varying with location. A virtual inspection of the velocity profiles in an eccentric annulus shows that the zone of highest shear exists across the narrowing sector of an eccentric annulus; hence this region is noticeably accompanied by a considerable reduction in viscosity.

The friction pressure gradients predicted by the CFD simulations were verified by comparing with the published studies and flow data from a field scale experimental data of a fully eccentric annulus. At a constant flow rate, it is confirmed that frictional pressure losses are decreased with increasing eccentricity. Also, fluids with the stronger non-Newtonian property show a slower rate of decrease in pressure drop as eccentricity increases. A good agreement is obtained with the Haciislamoglu et al. correlation, and the results of this study, especially at low values of eccentricity. At very high eccentricities, data from the CFD model yields lower friction pressure compared to Haciislamoglu et al. correlation. A Haciislamoglu et al. type expression is obtained, incorporating the improved data of this study.

Next, the results of an experimental study carried out to investigate friction pressure behavior of drag reducing polymer solutions flowing turbulently through an eccentric annulus are presented. The experimental set-up includes 30 ft of 3½-in. x 2 3/8-in., 200 ft of 3½-in. x 1¾-in., 69 ft of 5½-in. x 4-in., and 79 ft of 5-in. x 3½-in. fully eccentric annuli. Data analysis enabled the development of a new correlation using Fanning friction factor, generalized Reynolds number, and diameter ratio, all of which can be easily determined in the field, as independent variables. These new correlations for laminar and turbulent flow of drag reducing polymer solutions present an improvement to existing correlations, and also permit undemanding hydraulic program calculations for varying annular configurations.

CHAPTER 1

INTRODUCTION

Fluid flow in annular spaces has received great attention from the oil industry, as engineers routinely encounter Newtonian and non-Newtonian fluid flow through the annulus in both drilling and workover operations. The problem that has received most attention from researchers has been the calculation of the flow field within the annulus. In coiled tubing operations, this situation is usually idealized as that of steady, isothermal, fully developed laminar flow of a non-Newtonian fluid through an annulus consisting of an outer cylindrical casing and an inner non-rotating tubing, which in most cases, is offset (i.e. eccentric) as illustrated in Fig. 1.1.

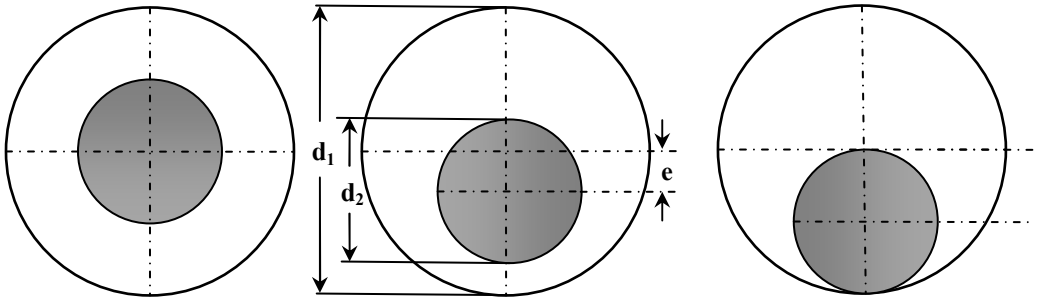

Figure 1.1 Concentric and eccentric annular geometries

In analyzing fluid flow behavior in a wellbore annulus, several investigators traditionally have assumed that the annulus between the drill pipe and the hole or casing is concentric. However, the drill pipe usually is not concentric with the hole, especially during directional drilling when the pipe weight causes a strong tendency for the pipe to

lie against the hole. The main problem, for field calculations, is that eccentricity is not a controllable parameter, except in highly deviated wells where it is reasonable to assume fully eccentric geometry. Also, it is now a well-established fact that frictional pressure losses depend significantly on the exact value of eccentricity for uniformly eccentric annuli. Experimental studies with water (Dodge, 1963), air (Jonsson and Sparrow, 1966), non-Newtonian fluids (Mitsuishi and Aoyagi, 1973) and drilling muds (Zamora et al., 2005) have shown that the pressure drop for flow in an eccentric annulus decreases as the eccentricity increases. Moises and Shah (2000) reported that the annular pressure losses in a fully eccentric annulus could be as low as 40% of the value in concentric annulus. Eccentricity, ξ, is defined by:

$$\xi = \frac{e}{R_o - R_i} \tag{1.1}$$

with "e" the distance between the centre's of the inner and outer pipes and R_i and R_o the inner and outer radii (*see* ***Figure 1.1***). Hence, eccentricity is a dimensionless parameter which is equal to zero for a concentric annulus and is equal to one for a fully eccentric annulus. As discussed by Haciislamoglu (1989), accounting for eccentricity will enhance the accuracy of numerous mathematical models used in drilling hydraulics since many of these models depend heavily upon the velocity profile and the frictional pressure losses in the annulus.

Therefore, the research area of Non-Newtonian flow through eccentric annuli has been concentrated in developing several analytical models to illustrate the effects of eccentricity on velocity and viscosity profiles, and frictional pressure loss gradient. Since there is no simple analytical solution to such a problem, researchers often

incorporate simplifying assumptions to avoid the development of complicated mathematical models (Heyda, 1959; Iyoho and Azar, 1981). Nevertheless, more often than not, the wrong equation of fluid motion in an eccentric annulus was applied, which led to incorrect flow rate predictions. As a follow up and in order to overcome the shortcomings of analytical solutions, several numerical models have been developed. While these mathematical models are mostly ideal for developing flow simulation softwares, the intrinsic computational effort required to predict frictional pressure drops from their final form hinders their general application in making undemanding hydraulic program calculations. Indeed, a search of technical literature, and the few models put forward by past investigators did not provide any explicit correlation for accurate prediction of Fanning friction factors in an eccentric annulus. Notably, some researchers have developed empirical correlations from laboratory experiments that allow us to make practical predictions of annular friction pressure losses for laminar and turbulent flows. However, these correlations are not ideal, i.e. they come with constraints dealing with applicable Reynolds number range and type of fluid being investigated. Also, the published empirical correlations are mostly dependent on their inherent flow geometry. Subsequently, they are very limited in their ability to capture the effect of arbitrary diameter ratios, which is of great practical interest. Ultimately, these have raised the need to develop an explicit Fanning friction factor correlation for laminar and turbulent flow in eccentric annuli with arbitrary dimensions.

The objective of this study is to investigate the frictional behavior of non-Newtonian polymer fluids commonly used in oilfield applications, using the present day

state-of-the-art technique in fluid flow analysis- computational fluid dynamics (CFD) modeling and experimental techniques, to meet industry need for improved hydraulics design of annular flow operations. The computational investigation of flow in an eccentric annulus, with Newtonian and non-Newtonian fluids, presents a contribution to the understanding of the flow field occurring during fully-developed laminar flow conditions. In addition to the significance of this work for annular flow during coiled tubing operations, the study will be useful in several other processes in the industry that involve the flow of fluids through an annulus consisting of an outer cylindrical casing and inner non-rotating tubing, such as cuttings transport, through casing production, hydraulic fracturing, and mud displacement in cementing and other oilfield operations.

The investigation is described in detail in the following Chapters. Chapter 2 presents a comprehensive review for both theoretical and experimental studies of the annular flow of Newtonian and non-Newtonian fluids, to reveal the current state of research in this area of interest. In Chapter 3, CFD modeling was used to investigate the flow fields for the steady, isothermal, fully developed laminar flow of a non-Newtonian power law fluid through annular sections of varying eccentricities, as well as diameter ratios. The procedures adopted from designing the mesh to running CFD simulations are documented. Essential flow features in eccentric annulus were observed, such as altered velocity profiles due to the presence of secondary flows, and consequently, a shear rate profile that defines the local fluid viscosities using the modified non-Newtonian power law rheological model of this study. A new friction factor correlation for non-Newtonian laminar flow in eccentric annuli was developed and verified by

comparing with Haciislamoglu et al. correlation and with experimental data. The chapter ends with a summary of the more important findings.

Chapter 4 describes the experimental set up including the equipment and instrumentation in detail. These include an array of eccentric annular sections, fluid mixing and pumping equipment as well as data acquisition and rheological measurement systems. In Chapter 5, the experimental results of flow test of guar polymer fluids in eccentric annulus are presented. Based on the analysis, several important observations have been made concerning the turbulent flow of non-Newtonian polymeric fluids in fully eccentric annuli. An empirical Fanning friction factor correlation was developed based on the flow test data. The final Chapter deals with the conclusions drawn from this work and recommendations for future research studies.

1.1. Scope of Study

The main contributions of this work include the following:

- A study of the effects of eccentricity on friction pressure losses for Newtonian and non-Newtonian fluids by gathering field scale experimental data in laminar and turbulent flow regimes through 3½-in. by 2 3/8-in., 3½-in. by 1¾-in., 5½-in. by 4-in. and 5-in. by 3½--in. eccentric annuli.
- Computational Fluid Dynamics (CFD) simulation studies of Newtonian and non-Newtonian power law fluid flow in eccentric annular geometries. This will add to an understanding of the fundamental flow behavior and frictional

pressure for fully eccentric annular flow using state-of-the-art computational grids. Numerical predictions of friction pressure drops will be compared with experimental data.

- Development of an explicit Fanning friction factor correlation for pressure drop calculations in eccentric annular geometries with arbitrary dimensions for Newtonian and non-Newtonian fluids in laminar flow regimes.
- Development of an empirical Fanning friction factor correlation for pressure drop calculations in fully eccentric annuli with arbitrary dimensions for non-Newtonian fluids in turbulent flow regimes.

CHAPTER 2

LITERATURE REVIEW

Fluid flow through an annular space is a frequently encountered engineering problem that has been under investigation for many decades (Lamb, 1945; Tao and Donovan, 1955; Frederickson and Bird, 1958; Redberger and Charles, 1962; Guckes, 1974; Iyoho and Azar, 1981; Haciislamoglu, 1989; Escudier et al., 2002; Akgun and Jawad, 2007). If the annular space is concentric, the flow can currently be analyzed without much difficulty by applying the equivalent diameter concept in corresponding pipe equations. For an eccentric annular space (i.e., the axes of the inner and outer tubes do not coincide with each other), a greater effort is required due to the complex geometry that is involved.

This chapter presents critical literature reviews on fluid flow through eccentric annulus, both theoretical and experimental. This is essential for understanding the complex flow phenomenon of fluid flow in eccentric annulus and taking the right approaches for the present study. It also serves as a tool for identifying technical challenges and industry needs, and make sure our research is of interest to the industry. Only those works which are closely related to the present work are mentioned. Theoretical studies are first considered, followed by a discussion of some experimental studies on Newtonian and non-Newtonian fluids. Finally, the review is concluded with a brief discussion of reported studies on the applications of computational fluid dynamics (CFD) simulation, with emphasis on oilfield operations.

2.1 Studies of Fluid Flow in Eccentric Annulus

2.1.1 Equation of Motion

The general form of the equation of motion for a fully developed flow in a Cartesian coordinate system is:

$$\frac{\Delta P_f}{\Delta L} + \frac{\partial}{\partial x}\left(\mu \frac{\partial v}{\partial x}\right) + \frac{\partial}{\partial y}\left(\mu \frac{\partial v}{\partial y}\right) = 0 \tag{2.1}$$

The above equation is very similar to a simplified version of the Navier-Stokes equation except that the viscosity term here is not taken out of the derivative since it is only a constant for Newtonian fluids. The pressure drop is constant because of the assumption of fully developed flow.

Cylindrical coordinates cannot be applied due to the asymmetric nature of an eccentric annular geometry (Fig. 2.1). Hence, a bipolar coordinate system is often adopted to describe this complex geometry. In this orthogonal coordinate system the two cylindrical boundaries of the fluid annulus coincide with two surfaces having constant values of ε (ε_i and ε_o, which can be expressed in terms of the annulus radius ratio S and the dimensionless eccentricity ξ as given in the nomenclature). The other coordinate (η) represents a set of eccentric cylinders whose centers lie on the y-axis and which intersect orthogonally the boundaries of the fluid annulus. The transformed geometry for the fluid annulus in the complex ε -η plane is a slab of length ($\varepsilon_i - \varepsilon_o$) and width equal to the limits of η , that is 2π (Figure 2.3). L is the third axis which is perpendicular to ε and η.

The relationships needed to transform from Cartesian coordinates to bipolar coordinates are given by (Speigel, 1968):

$$x = \frac{a \sinh \varepsilon}{\cosh \varepsilon - \cos \eta} \tag{2.2}$$

$$y = \frac{a \sin \varepsilon}{\cosh \varepsilon - \cos \eta} \tag{2.3}$$

$$L = L \tag{2.4}$$

where $a = R_i \sinh \varepsilon_i = R_o \sinh \varepsilon_o$; also, $0 \leq \boldsymbol{\eta} \leq 2\pi$ and $-\infty \leq \varepsilon \leq +\infty$, $-\infty \leq L \leq +\infty$

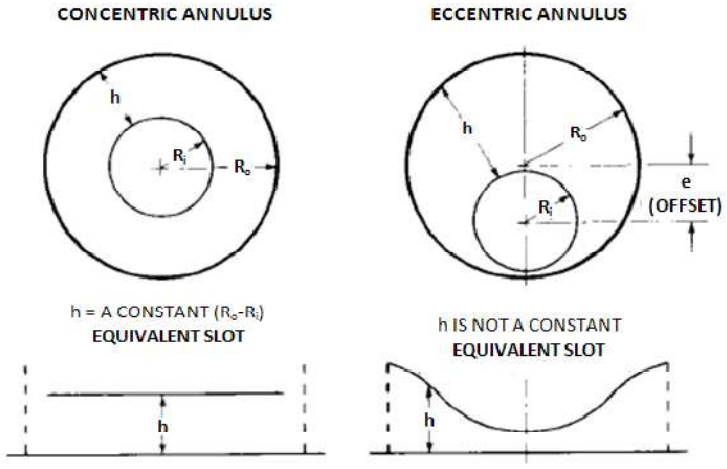

$$\frac{\partial \tau_{yz}}{\partial y} = -\frac{\partial p}{\partial z} \qquad \frac{\partial \tau_{xz}}{\partial x} + \frac{\partial \tau_{yz}}{\partial y} = -\frac{\partial p}{\partial z}$$

Figure 2.1 Slot equivalent of concentric and eccentric annuli (Haciislamoglu, 1989)

The expressions to compute ε_i and ε_o are (Guckes, 1973):

$$\varepsilon_i = \cosh^{-1}\left[\frac{(1+k)-\xi^2(1-k)}{a\xi k}\right] \tag{2.5}$$

$$\varepsilon_o = \cosh^{-1}\left[\frac{(1+k)-\xi^2(1-k)}{a\xi}\right] \tag{2.6}$$

where ξ = eccentricity, dimensionless and k = pipe radius ratio, r_i/r_o

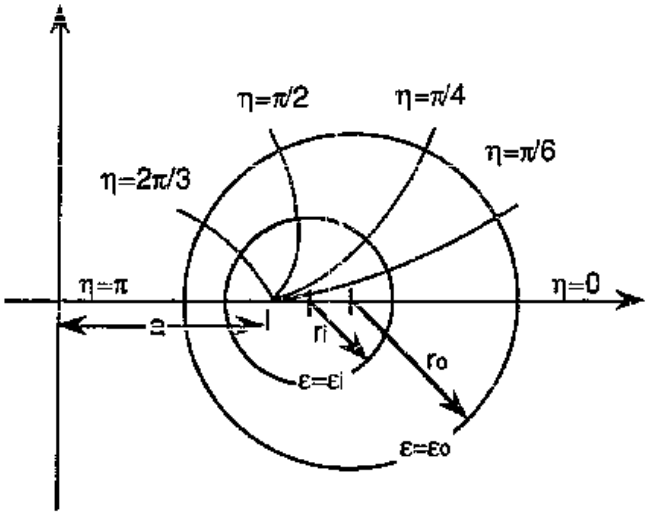

Figure 2.2 Eccentric Annulus in Bipolar Coordinates (Haciislamoglu, 1989)

The final form of the transformed equation of motion in bipolar coordinates is (Haccislamoglu, 1989):

$$\left(\frac{a}{\psi}\right)^2 \frac{\Delta P_f}{\Delta L} + \frac{\partial}{\partial \varepsilon}\left(\mu \frac{\partial v}{\partial \varepsilon}\right) + \frac{\partial}{\partial \eta}\left(\mu \frac{\partial v}{\partial \eta}\right) = 0 \qquad (2.7)$$

where $\psi = \cosh \varepsilon - \cos \boldsymbol{\eta}$ $\quad (\varepsilon_o \le \varepsilon \le \varepsilon_i, \quad 0 \le \boldsymbol{\eta} \le 2\pi)$

At this point mention should be made of other sets of computational grids that have recently found significant application in the analysis of heat and fluid flow in eccentric annular geometries. Notable amongst them is the "boundary conforming, natural coordinates," which is a non-orthogonal, boundary-fitted, and curvilinear coordinates system, with inbuilt ability to handle complicated geometries. For an eccentric annulus, a two-boundary technique of grid generation can be used to build such non-orthogonal curvilinear grid in physical space as shown in Figure 2.3a. Two types of orthogonal grids are also presented in Figure 2.3, the polar orthogonal

coordinate for the concentric annulus (Figure 2.3b) and the bipolar orthogonal coordinate for the eccentric annulus (Figure 2.3c). Most of the recent studies (Chin, 1992; Azouz et al., 1993; Hussain and Sharif, 1998; Escudier et al., 2002) have successfully utilized the non-orthogonal, boundary-fitted, and curvilinear coordinates, to analyze the flow field of non-Newtonian fluids in conduits of arbitrary cross sections, ranging from the simple case of a slightly eccentric annulus to a more tasking case of eccentric annular sections in the presence of cutting beds.

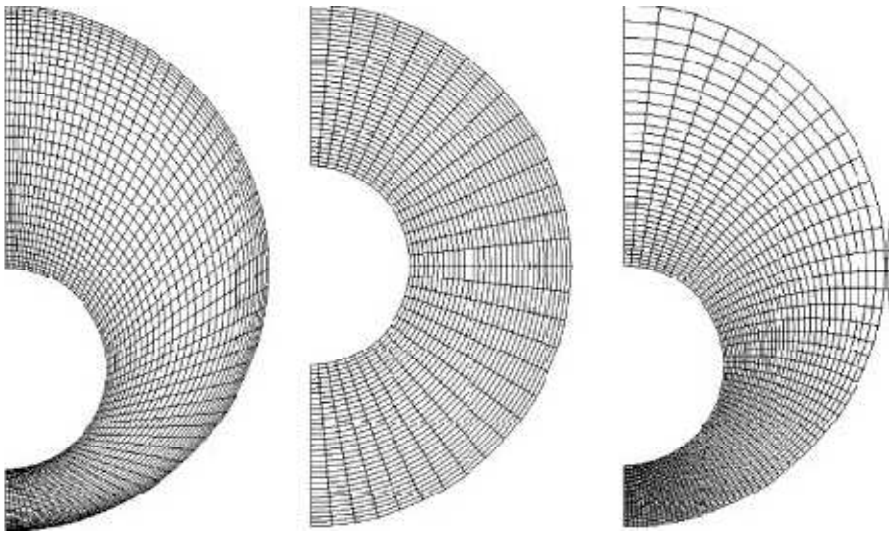

(a) **(b)** **(c)**

Figure 2.3 Typical geometry and meshing of an eccentric annulus (an example of a 32×32) mesh system: (a) non-orthogonal co-ordinates; (b) polar orthogonal co-ordinates; and (c) bipolar orthogonal co-ordinates. (Shklyar and Arbel, 2007)

In almost all industrial problems the descending linear region (the "power law" region) of the log-log plot of viscosity versus shear rate, seen in Figure 2.4, is the most important region. In fact, for many inexpensive viscometers and for many fluids, Bird et

al. (1987) stated that it is almost impossible to obtain data for the horizontal region of the viscosity-shear rate curve. The power law formulation of shear rate-shear stress relationship is the most well known and widely-used empiricism in engineering work, and is given by:

$$\tau = K\dot{\gamma}^n \tag{2.8}$$

where, τ = shear stress, lb/ft^2, K = consistency index, lb$_f$·sec^n /ft^2, n = flow behavior index, dimensionless, $\dot{\gamma}$ = shear rate, sec^{-1}

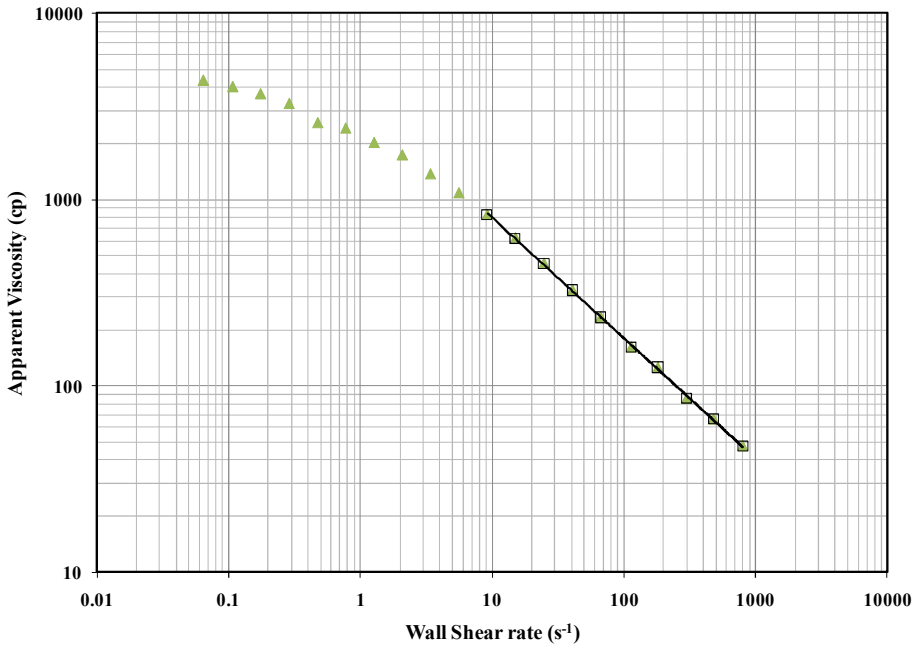

Figure 2.4 Non-Newtonian viscosity of 60 lb/Mgal Guar showing the descending linear region as fitted by the Power-law model.

Viscosity is the ratio of shear stress and shear rate. The non-Newtonian viscosity of the Power-law fluids is defined as:

$$\mu = K\dot{\gamma}^{n-1} \tag{2.9}$$

The definition of shear rate (Bird, 1960), γ , in a Cartesian coordinate system is:

$$\dot{\gamma} = \left| \sqrt{\left(\frac{\partial v}{\partial x}\right)^2 + \left(\frac{\partial v}{\partial y}\right)^2} \right| \tag{2.10}$$

In bipolar coordinates, with a similar transformation technique, it can be written as:

$$\dot{\gamma} = \left| \frac{\psi}{a} \sqrt{\left(\frac{\partial v}{\partial \varepsilon}\right)^2 + \left(\frac{\partial v}{\partial \eta}\right)^2} \right| \tag{2.11}$$

Therefore, the non-Newtonian viscosity in terms of velocity becomes:

$$\mu = K \left| \frac{\psi}{a} \sqrt{\left(\frac{\partial v}{\partial \varepsilon}\right)^2 + \left(\frac{\partial v}{\partial \eta}\right)^2} \right|^{n-1} \tag{2.12}$$

If one substitutes Equation 2.12 into Equation 2.7, the governing equation of motion for Power-law fluids in eccentric annulus is derived. Dimensionless parameters are usually introduced to simplify the equation and make the solution more general (Haciislamoglu, 1989; Azouz, 1993). Introducing dimensionless velocity V_D and dimensionless frictional pressure loss gradient *f*, Haciislamoglu (1989) obtained the final form of the dimensionless form of the governing equation of motion given in Equation 2.13.

$$\left(\frac{\sinh \varepsilon_o}{\psi}\right)^2 f + \frac{\partial}{\partial \varepsilon}\left(\mu_D \frac{\partial v_D}{\partial \varepsilon}\right) + \frac{\partial}{\partial \eta}\left(\mu_D \frac{\partial v_D}{\partial \eta}\right) = 0 \tag{2.13}$$

The above equation needs to be solved for dimensionless velocity and viscosity profiles, and this velocity profile can be numerically integrated to obtain a dimensionless flow rate (Q_D) defined as:

$$Q_D = \int_0^{2\pi} \int_{\varepsilon_o}^{\varepsilon_i} v_D \left(\frac{\sinh \varepsilon_o}{\psi}\right)^2 \partial \varepsilon \, \partial \eta \tag{2.14}$$

Then,

$$Q = \left(\left(\frac{\Delta P_f}{\Delta L} \right) \frac{r_o^{3n+1}}{K} \right)^{\frac{1}{n}} Q_D \tag{2.15}$$

2.1.2 Theoretical Studies

The complexity of flow geometries and the equation of fluid flow through eccentric annuli have attracted many scholars over the years. Various theoretical models have been developed. These theoretical methods are presented under analytical solutions or numerical methods in the sections that follow.

2.1.2.1 Analytical Solutions

To find simple approximations for the velocity profile and the volumetric flow rate, Tao and Donovan (1955) treated an eccentric annulus as a variable-height slot (Fig. 2.1) and developed the analytical solutions for Newtonian fluids. This assumption has been proved to work reasonably well for flows through concentric annuli (Bourgoyne et al, 1987) for certain range of tubular diameter ratio. In their experimental and theoretical work, flow of Newtonian fluids in an eccentric annulus with and without inner pipe rotation was investigated. However, they made several simplifying assumptions that led to incorrect flow rate predictions.

Firstly, they assumed that both the radial clearance and the eccentricity of the annular section are small, limiting the application of the expression (Eq. 2.1) used to define the variable slot height.

$$h_s = c(1 + \xi \cos\theta) \tag{2.16}$$

where $c = R_o - R_i$; h_s = slot height, in.; R_o = radius of the outer pipe, in., R_i = radius of the inner pipe; in. ξ = eccentricity, *dimensionless,* θ = angle of eccentricity, degree. Furthermore, Haciislamoglu (1989) reported that the major setback in this theoretical work is that "the equation of fluid motion used by Tao and Donovan was valid only for concentric annular flow". Figure 2.1 shows the slot flow approach to concentric and eccentric annular flow with the valid equations of motion in each case presented by Haciislamoglu (1989).

Using a bipolar coordinate system and Green's function, Heyda (1959) presented analytical solutions for Newtonian fluid flow in an eccentric annulus in the form of an infinite series. He showed that the velocity profile of Newtonian fluid in laminar flow regime would differ dramatically in an eccentric annulus. Similarly, Snyder and Goldstein (1965), using the bipolar coordinate system, determined the velocity distribution for the fully developed laminar flow of a Newtonian fluid in an eccentric annulus. The analytical expression for the volumetric flow-rate is rather complex and was not presented by Snyder and Goldstein (1965). However, after a lengthy treatment, Tosun (1984) developed expressions for the volumetric flow-rate of Newtonian fluids through an eccentric annulus. Using the expressions for volumetric flow-rate in a concentric annuli developed by Bird et al. (1960), he presented the ratio of the volumetric flow rates in eccentric and concentric annuli in terms of the diameter ratio and the eccentricity, for a given pressure gradient. Their results showed that this ratio increases as the diameter ratio and the eccentricity increases.

In 1965, Vaughn (1965) extended the approach of slot flow approximation to pursue a solution of non-Newtonian Power-law fluids in eccentric annulus. However, he used the same wrong equations for variable slot height (Eq. 2.16) and the equation of motion as Tao and Donovan. Subsequently, Iyoho and Azar (1981) modified Vaughn's approach, developing an accurate technique to calculate the variable slot height by avoiding the latter's simplifying assumptions and developed analytical solutions of the velocity profile and the volumetric flow-rate for power-law fluids. Iyoho and Azar's equation for variable slot height is given by;

$$h_s = (R_o^2 - \xi^2 c^2 sin^2\theta)^{0.5} - R_i + \xi c \cos\theta \tag{2.17}$$

They presented results requiring no mathematical transformation or iterative computations, which they claimed were comparable in accuracy with those obtained numerically by previous investigators using complex bipolar coordinates, and iterative computations. Subsequently, Uner et al. (1988) extended Iyoho and Azar's slot-height model to approximate volumetric flow-rates for both Newtonian and non-Newtonian fluids. They neglected Iyoho and Azar's simplifying assumptions in computing the volumetric flow-rate by accounting for eccentricity ratio while formulating their solutions. However, they also applied the wrong equation of motion.

Furthermore, Luo and Peden (1990) noted that the slot model, because it is in essence a modified model for flow between parallel plates, will result in unrealistic symmetric profiles of the shear-stress/shear-rate magnitudes and the velocity.

Consequently, they treated an eccentric annulus as being composed of an infinite number of concentric annuli with variable outer radii (R_o), which were described as:

$$R_o^{\xi} = \xi \cos\theta + \sqrt{R_o^2 - [\xi \sin\theta]^2} \tag{2.18}$$

Using the velocity profile for the concentric annuli flow, they developed analytical solutions for the shear stress, shear rate, velocity, and volumetric flow rates/pressure gradient for both power-law and Bingham-plastic fluids. However, Yu (1994) reported that Luo and Peden's method failed to give accurate solutions of velocity profiles even for Newtonian fluids flowing in an eccentric annulus, because the equations of motion they used could not correctly describe the flow situation in an eccentric annulus. The error increased as eccentricity increases.

Seemingly unaware or following total negligence of the limitations of the narrow slot approximation for an eccentric annulus, Haige and Yinao (1997) developed expressions for the velocity distribution, flow-rate, and pressure drop for Robertson-Stiff fluids flowing through an eccentric annulus. Though, citing the work of Iyoho and Azar, they still assumed a small clearance and ended up with the same simplified expression for variable height that was first applied by Tao and Donovan. The expression, they developed for the pressure loss is presented in Equation 2.19.

$$\Delta P = \frac{2A}{R_o - R_i}\left\{\frac{2\overline{U} + \frac{3}{4}C\left(2 + \frac{2e^2}{R_o + R_i} + e^2\right)}{\frac{2B}{1+2B}(R_o - R_i)\left[1 + \frac{1}{4}\left(\frac{1+B}{B}\right)\frac{e^2}{R_i(R_o + R_i)}\right]}\right\}^B \tag{2.19}$$

where A = consistency index of a Robertson-Stiff (RS) fluid, $Pa.s^B$

B = Flow behavior index of a RS fluid, dimensionless

C = Shear rate correction index in RS model, s^{-1}

R_o = inner radius of outer cylinder, in.

R_i = outer radius of inner cylinder, in.

e = offset distance between the centre of the two cylinders, in.

$\bar{U}$ = average velocity in an eccentric annulus, ft/sec.

Note that for Power law fluids; n = B, K = A, C = 0 and for Bingham Plastic fluids; PV = A, B = 1, C = Yield Point (YP)/Plastic Viscosity (PV).

Certainly, it seems like an acceptable notion that analytical solutions is not the way to go; hence, no new research have been reported in this area. On the other hand, numerical models continue to attract attention, boosted by the increasing memory available in today's hard drives and the processing speed of computers.

2.1.2.2 Numerical Methods

Using a bipolar coordinate system, Redberger and Charles (1962, 1963) applied numerical methods (finite difference technique) to solve the equations of motion and obtain the velocity profile for Newtonian fluid flow in eccentric annular geometries. This was numerically integrated to develop expressions relating volumetric flow-rates to frictional pressure loss gradients. They obtained a good agreement with Heyda's analytical solution.

In 1973, Mitsuishi and Aoyagi (1973) extended the approach of Redberger and Charles (1962) to non-Newtonian fluids and obtained an approximate solution by using the variational method, while Guckes (1974) presented procedures for calculating the volumetric flow rate for power law and Bingham-plastic fluids. Guckes' equations were

obtained by numerically integrating the velocity profile resulting from a finite difference solution of the equations of continuity and motion after transformation into bipolar coordinates. Although the bipolar-coordinate method may theoretically give exact solutions, the procedure is extremely tedious and involves laborious computations.

Haciislamoglu and Langlinais (1990) first presented studies dealing with fully developed flow of generalized yield-power law fluids in eccentric annuli by adopting a bipolar coordinate system and a finite difference technique. The velocity profiles and the flow-rate versus frictional pressure loss gradient relationship were demonstrated for different eccentricities. In their numerical procedure, a non-uniform grid point distribution in bipolar coordinates was introduced, which could give a more realistic distribution of grid points in physical coordinates. For non-Newtonian fluids in laminar flow, they presented an equation relating the ratio of frictional pressure losses in an eccentric annulus to that of a concentric annulus considering the following factors; pipe diameter ratio (d_2/d_1), power-law index (n), and annular eccentricity (ε). Haciislamoglu and Cartalos (1994) modified the same equation for turbulent flow. The equations used for both flow regimes are expressed as follows:

$$\left[\frac{\Delta P_{ecc}}{\Delta P_{conc}}\right]_{Lami} =$$

$$1 - 0.072\frac{\xi}{n}\left(\frac{d_2}{d_1}\right)^{0.8454} - 1.5\xi^2\sqrt{n}\left(\frac{d_2}{d_1}\right)^{0.1852} + 0.96\xi^3\sqrt{n}\left(\frac{d_2}{d_1}\right)^{0.2527} \quad (2.20)$$

$$\left[\frac{\Delta P_{ecc}}{\Delta P_{conc}}\right]_{Turb} =$$

$$1 - 0.048\frac{\xi}{n}\left(\frac{d_2}{d_1}\right)^{0.8454} - \frac{2}{3}\xi^2\sqrt{n}\left(\frac{d_2}{d_1}\right)^{0.1852} + 0.258\xi^3\sqrt{n}\left(\frac{d_2}{d_1}\right)^{0.2527} \quad (2.21)$$

where ξ = eccentricity (for fully eccentric annulus ξ = 1), and n = flow behavior index. The equations are valid for eccentricities from 0 to 0.95, pipe diameter ratios of 0.3 to 0.9 and flow behavior index of 0.4 to 1.0. To apply Haciislamoglu et al. correlations, it is assumed that the concentric annulus pressure gradient is either known or can be accurately predicted using published or proprietary correlations, which is a major setback.

Chin (1992) obtained numerical finite difference solutions for the problem of non-rotating annular flow of Newtonian and non-Newtonian fluids by utilizing "boundary conforming, natural coordinates" to handle complicated geometries such as boreholes with cuttings beds and washouts, or noncircular drillpipes and casings with stabilizers or centralizers. They presented annular velocity and apparent viscosity profiles for several annular flow configurations ranging from the simple case of a concentric annulus to a more difficult case of a square drill collar in a circular hole. Using a similar approach, Azouz et al. (1991, 1993) reported on an interesting investigation on the numerical simulation of laminar flow of non-Newtonian fluids in conduits of arbitrary cross-section. They utilized non-orthogonal, boundary-fitted, and curvilinear coordinates to investigate volumetric flow-rates at a fixed pressure gradient ($dP/dx = 1.78 \times 10^{-3}$ psi/in.). In their study of the numerical simulation of laminar flow of power law and yield-power-law fluids in conduits of arbitrary cross-section, Azouz et

al. confirmed that high eccentricity can create a zone of no-flow in the narrow gap of the annulus. From the results of their study, the ratio of maximum velocities above and below the drill pipe (at plane of symmetry) for a Yield-Power-law model increased from 3 (at 25% eccentricity) to 50 (at 50% eccentricity), with practically zero velocity below the drill pipe beyond an eccentricity of 75%. Similar results were obtained by Haciislamoglu (1989). Therefore, it is evident that both laminar and turbulent flow conditions can exist across an eccentric annulus at the same time. Such is the complexity that is involved with fluid flow through an eccentric annulus.

Hussain and Sharif (1998) followed the same general non-orthogonal, boundary-fitted curvilinear coordinates approach to conduct a similar study; however, they compared their numerical solutions with available analytical solutions of the axial velocity distribution in a concentric annulus. The constitutive equation for shear stress calculation developed by Papanastasiou (1987), valid for both yielded and unyielded region, was used in their study. Meuric et al. (1998) likewise employed a finite element method to numerically analyze the laminar flow of a yield-power law fluid in vertical annuli. They presented solutions when there is axial or both axial and tangential flows in either a concentric or eccentric annulus. The tangential flow arises from the rotation of the inner cylinder of the annulus. This area of research has been extensively documented for Newtonian (Escudier at al., 2000) and various non-Newtonian fluid models such as Power law model (Roberto, 1994; Chin, 2001; Escudier et al., 2002a), Sutterby model (Batra and Eissa, 1994; Escudier et al., 2002b), and Bingham plastic

(Bittleston and Hassager 1992; Beverly and Tanner, 1992; Locket, 1992). No further discussion is presented on this area of research as it has no bearing on the present study.

Whereas, there have been several numerical annular studies, most of which have considered one value of the flow consistency index, K, and varied the flow behavior index, n, to account for the effect of non-Newtonian behavior on the flow field, our review of related literature did not showcase any study that captures the trend in real field applications where "n" varies with "K". In the present study, four concentrations of Guar gum, a well known water soluble polymer is utilized with their corresponding n and K values to evaluate friction pressure losses during annular flow with eccentricities ranging from 0 to 1. The intent is to develop an improved friction pressure correlation for the flow of drag reducing non-Newtonian Power law fluids in eccentric annuli.

2.1.3 Experimental Studies

Experimental studies on the turbulent flow of water through an eccentric annulus were first reported by Dogde (1963). His research was focused on the measurement of corresponding flow rates and pressure gradients for various diameter ratios, with eccentricities ranging from 0 to 1. He reported friction factor data for the flow of water in eccentric annuli for diameter ratios of 0.875, 0.750 and 0.688 at Reynolds numbers ranging from 20, 000 to 100,000. From his results, probably due to the narrow range of diameter ratio investigated, he erroneously concluded that the diameter ratio was not an important variable for computing friction pressure loses in eccentric annulus. He developed Equation 2.22, which is the first friction factor correlation reported for the turbulent flow of Newtonian fluids in a fully eccentric annulus.

$$f = 0.057\, Re^{-0.25} \tag{2.22}$$

Winkler (1968) successfully applied the Dodge correlation to his data obtained for flow in a fully eccentric annulus; however, he noted that this procedure did not take into account the pipe diameter ratio of the annular sections. Three years after Dodges' experimental study, Jonsson and Sparrow (1966) measured frictional pressure losses and point velocities for the turbulent flow of air in eccentric annuli at various diameter ratios (0.28 - 0.74) and eccentricities. Their results showed that friction pressure decreases with increasing eccentricity for a fixed diameter ratio and Reynolds number. Bourne et al. (1968) investigated the impact of diameter ratio on this phenomenon and presented interesting experimental results on the laminar and turbulent flow of water in annuli of unit eccentricity. Bourne et al reported "for a given Reynolds number, the friction factor is a minimum at a diameter ratio of about 0.750". They also discussed the existence of a gradual change from laminar to turbulent flow, which is a function of the diameter ratio, brought about by the variation in local Reynolds number from zero to a maximum value within an eccentric annulus. As the diameter ratio increases, the sharpness of the transition decreases- and, furthermore, the transition region covers a wider range of Reynolds number. Thus, while at a diameter ratio of 0.373, the transition occurs between a Reynolds number of 2,000 and 3,000, at a diameter ratio of 0.813, the transition occurs between a Reynolds number of 1000 and 3,000. However, the lower critical generalized Reynolds number for most viscous non-Newtonian fluid lies beyond 2,100, which is similar to that encountered in the transition from laminar to turbulent flow in a pipe. This is evident in the experimental data of Ogugbue and Shah (2009).

Reduction in friction pressure due to inner pipe eccentricity was also observed for non-Newtonian fluids (using Sutterby rheological model) through the experimental studies of Mitsuishi and Aoyagi (1973) in small scale eccentric annuli. Mitsuishi and Aoyagi reported that fluids with a stronger non-Newtonian behavior show a slower rate of decrease in pressure drop as eccentricity increases. Nouri et al (1993) conducted experimental studies using Newtonian fluids and a weakly elastic shear thinning polymer at effective bulk flow Reynolds numbers of 1150, 6200 and 9600. The diameter ratio was 0.5 with eccentricities of 0, 0.5 and 1.0, and the use of a Newtonian fluid of refractive index identical to that of the Perspex working section facilitated the point velocity measurements by laser velocimetry. Using the Bragg-cell method, they also captured and presented secondary flow vector distributions of the cross-flow that occurs during fluid flow in eccentric annulus. The vectors suggest transport of fluid from wider to narrower regions and that this transport is stronger along the inner pipe wall, which may explain the distortion of the axial velocity profile in that region.

Subramanian and Azar (2000) conducted experimental studies on friction pressure drop for non-Newtonian drilling fluids in pipe and annular flows. They confirmed that friction pressure losses in eccentric annuli are lower than those for concentric annuli under the same flow conditions for all muds tested.

Moran and Savery (2007) acknowledged the challenging nature of centralizing the inner tubing in highly deviated wells in their research paper. They studied fluid movement through eccentric annuli over a wide range of casing standoffs and flow rates. Nine pipe-in-pipe eccentric annular models were built using standard casing

materials with annular lengths of approximately 7 feet and diameter ratio ranging from 0.7 to 0.82. They monitored and reported the impact of viscosity on the balance between the area weighted velocity of the wide side and narrow side of each eccentric annulus. They observed that highly viscous fluids yields a pronounced imbalance between the wide side and narrow side, an undesired effect that would result in channeling during real cementing operations. Medium viscosity closes this gap, but the wide-side velocity still clearly dominates. However, their result also showed that a low viscosity fluid enables a near perfect balance between the area weighted velocity (i.e. volumetric flow-rates) in the wide side and narrow side of each eccentric annulus. On the other hand, water shows a velocity flip in favor of the narrow side. The second general trend was that the velocity ratio approaches 1.0 as the pump rate increases, at least in the slower pumping region. From their results, they concluded that there exist an optimal combination of viscosity and pump rate that balances annular flow for any given geometry and standoff value. They further argued that a transition to turbulent flow in the wide side may be occurring at high flow rates, boosting the friction pressure and transferring the path of least resistance to the narrow side, hence quickly lowering the velocity ratio.

2.2 Friction Pressure Loss Correlations

Newtonian Fluids: Flow of Newtonian fluids in concentric annulus has been investigated by several authors, such as Meter and Bird (1961), Rothfus et al. (1966), Rehme (1974), Jones and Leung (1981), and of recent, Singhal et al. (2005). Meter and Bird (1961) used the Prandtl mixing length approach to derive the expression for

Fanning friction factor versus Reynolds number for smooth concentric annuli. They modified the Reynolds number using a shape factor, which was a function of radii ratio, R_i/R_o. In 1981, Jones and Leung presented data for smooth concentric annuli and demonstrated that acceptable method of Meter and Bird (1961), and Rothfus et al (1950), deviated substantially from the correct limit for small gaps. They demonstrated that the shape factor approach which provides similarity in laminar flow for round tubes and concentric annuli also provides similarities during turbulent flow conditions. Other criteria often used in determining an equivalent flow area for Newtonian fluids in concentric annuli include the use of equivalent diameter ($d_2 - d_1$) or the slot flow approximation approach, (where the effective diameter is taken as 0.816 of the equivalent diameter) in the correlations available for straight pipes. In order to investigate the commonly used correlations for Newtonian fluids in laminar and turbulent flow regimes in a concentric annulus, Singhal et al. (2005) performed experimental and CFD simulation study on the flow behavior and friction pressure losses of Newtonian fluids using different annular dimensions. Based on the comparison with simulation results, they recommended the use of the correlation proposed by Jones and Leung (1981) for laminar flow of Newtonian fluids in concentric annulus. For Newtonian fluids in turbulent flow regime, the use of equivalent diameter ($d_2 - d_1$) in Reynolds number and Fanning friction factor in Drew correlation for smooth pipes was recommended. An empirical correlation for Newtonian fluid flow in a fully eccentric annulus has been earlier presented in Equation 2.22, however, this was developed using limited experimental data (Dogde, 1963).

Combining the developments of Snyder and Goldstein (1965) and Tosun (1984), Caetano et al. (1992) came up with analytical expression for the friction geometry or flow parameter of a Newtonian fluid in an eccentric annulus. The Fanning friction factor for a fully developed laminar flow of a Newtonian fluid in eccentric annuli was presented as:

$$f = \frac{1}{N_{Re}} \frac{4\left(1-\frac{d_2}{d_1}\right)^2\left(1-\left(\frac{d_2}{d_1}\right)^2\right)}{\emptyset \sinh^4 \mathcal{E}_o} \tag{2.23}$$

where,

$$\emptyset = (\coth \mathcal{E}_i - \coth \mathcal{E}_o)^2 \left[\frac{1}{\mathcal{E}_o - \mathcal{E}_i} - 2\sum_{n=1}^{\infty} \frac{2n}{exp^{(2n\mathcal{E}_i)} - exp^{(2n\mathcal{E}_o)}}\right] + \frac{1}{4}\left(\frac{1}{\sinh^4 \mathcal{E}_o} - \frac{1}{\sinh^4 \mathcal{E}_i}\right) \tag{2.24}$$

which involves an infinite series term. In turbulent flow regime, Caetano et al. (1992), re-arranged the semi-analytical correlations developed by Gunn and Darling (1963) into a Nikuradse-type expression, and the friction factor for concentric and eccentric annuli can be predicted, respectively, from:

$$\frac{1}{\left\{f_{CA}\left(\frac{F_P}{F_{CA}}\right)^{0.45exp[-(N_{Re}-3000)/10^6]}\right\}^{1/2}} = 4.0\, log\left\{N_{Re}\left[f_{CA}\left(\frac{F_P}{F_{CA}}\right)^{0.45exp[-(N_{Re}-3000)/10^6]}\right]^{1/2}\right\} - 0.40 \tag{2.25}$$

and

$$\frac{1}{\left\{f_{EA}\left(\frac{F_P}{F_{EA}}\right)^{0.45exp[-(N_{Re}-3000)/10^6]}\right\}^{1/2}}$$

$$= 4.0\ log\left\{N_{Re}\left[f_{EA}\left(\frac{F_P}{F_{EA}}\right)^{0.45exp[-(N_{Re}-3000)/10^6]}\right]^{1/2}\right\} - 0.40 \qquad (2.26)$$

In these implicit correlations, *f* is the Fanning friction factor and F is the laminar flow friction geometry parameter, given by:

$$F_{CA} = \frac{16\left(1-\frac{d_2}{d_1}\right)^2}{\left[1+\left(\frac{d_2}{d_1}\right)^2 - \frac{1-\left(\frac{d_2}{d_1}\right)^2}{ln\left(\frac{d_1}{d_2}\right)}\right]} \qquad (2.27)$$

$$F_{EA} = \frac{4\left(1-\frac{d_2}{d_1}\right)^2\left(1-\left(\frac{d_2}{d_1}\right)^2\right)}{\emptyset \sinh^4 \varepsilon_o} \qquad (2.28)$$

The friction geometry parameter is constant (F_P=16) for pipe flow, a function of the pipe diameter ratio for a concentric annulus (F_{CA}); and, a function of both pipe diameter ratio and eccentricity for an eccentric annulus (F_{EA}). Notably, both correlations are implicit in *f, while* F_{EA} *i*nvolves an infinite series term as illustrated by *Equation 2.24*.

Non-Newtonian Fluids: The problem of axial laminar flow of power-law non-Newtonian fluids in concentric annuli was first studied by Frederickson and Bird (1958), who presented results obtained by power series expansions for limited values of flow behavior index, n, applied to the arguments of certain integrals which could not be analytically solved. Several authors (Bird, 1965; Vaun and Bergman, 1966) objected to the results of Frederickson and Bird for not being an accurate representation of their

experimental data. However, Russell and Christiansen (1974) used a three-constant rheological model to fit the data which were presented in objection to Frederickson and Bird's analytical solution, showing that they were not well represented by a power-law model. Moreover, Tiu and Bhattacharayya (1973, 1974) presented data which substantiated the results of Frederickson and Bird, showing that they do give an accurate representation of experimental data, when the rheological data are truly power-law. Relying on the valuable theoretical results presented by Frederickson and Bird (1958), Hanks and Larsen (1979) solved the integral and presented a simple algebraic solution for the volume flow rate of power-law fluids through concentric annulus in laminar flow, valid for all values of the flow behavior index, n, and all values of the diameter ratio of the annulus. The analytical expression is shown in Equation 2.25.

$$Q = \frac{n\pi R_o^3}{1+3n}\left(\frac{\Delta P R_o}{2KL}\right)^{\frac{1}{n}}\left[(1-\lambda^2)^{\left(1+\frac{1}{n}\right)} - \left(\frac{R_i}{R_o}\right)^{\left(1-\frac{1}{n}\right)}\left(\lambda - \left(\frac{R_i}{R_o}\right)^2\right)^{\left(1+\frac{1}{n}\right)}\right] \quad (2.29)$$

Where R_i and $R_o$are inner and outer radius, respectively, n is the flow behavior index, K is the consistency index, Δp/L is the pressure gradient, and λ is the dimensionless radial position at which velocity is maximum. Tabulated values of λ as a function of n and radii ratio, R_i/R_o, are also presented in their paper (Hanks and Larsen, 1979).

In 1966, Kozicki et al. investigated the flow of non-Newtonian fluids in ducts of arbitrary cross-sectional shape and reported geometrical factors for circular, slit, concentrically annular, rectangular, elliptical and isosceles triangular ducts. For a

concentric annulus, a modified generalized Reynolds number was developed by introducing two geometric parameters b_1 and b_2, that can be estimated from the ratio of inner to outer diameter of the annular section.

$$N_{Reg}^{*} = \frac{\rho(\bar{u} - u_0)^{2-n} r_h^n}{2^{n-3}\big((b_1 + b_2 n)/n\big)^n K_a} \tag{2.30}$$

where b_1 and b_2 are shape factors, which can be obtained from the following expressions:

$$b_1 = \frac{\left(1 - \frac{R_i}{R_o}\right)^2}{4\left[1 - \frac{1 - \left(\frac{R_i}{R_o}\right)^2}{2ln\left(\frac{R_o}{R_i}\right)}\left\{1 - ln\left[\left(1 - \left(\frac{R_i}{R_o}\right)^2\right)\Big/\left(2ln\left(\frac{R_o}{R_i}\right)\right)\right]\right\}\right]} \tag{2.31}$$

$$b_1 + b_2 = \frac{\left(1 - \frac{R_i}{R_o}\right)^2}{\left[1 + \left(\frac{R_i}{R_o}\right)^2 - \left(1 - \left(\frac{R_i}{R_o}\right)^2\right)\Big/ln\left(\frac{R_o}{R_i}\right)\right]} \tag{2.32}$$

The relation between Fanning friction factor and the modified generalized Reynolds number for annular flow in laminar region remains the same classical equation given by:

$$f = \frac{16}{N_{Reg}^{*}} \tag{2.33}$$

Later, Jensen and Sharma (1987) studied friction factors and equivalent diameter correlations for concentric annular flow of non-Newtonian drilling fluids in turbulent regime. They evaluated four expressions for the effective diameter of a concentric annulus using several Fanning friction factor correlations previously published, such as Jain (1976), Zigrang and Sylvester (1982, 1985), Haaland (1983), , Serghide (1984),

and Chen (1984). From the results of their statistical evaluations, they concluded that annular pressure drop is strongly influenced by the flow behavior index, n, and the hydraulic diameter ($d_h = d_1$-d_2), and proposed a new correlation using these two independent parameters. The expression is given by:

$$f = \pi_1 1\left(N_{Reg}\right)^{-\pi_2} \tag{2.34}$$

where N_{Reg} is the generalized Reynolds number, π_1 and π_2 are constants given by:

$$\pi_1 = \frac{log(n) + 3.93}{(100 - 27d_h)(246 - 236n)} \tag{2.35}$$

$$\pi_2 = \frac{1.75 - log(n)}{7} \tag{2.36}$$

However, Moises and Shah (2000) pointed out that the data range ($2000 < N_{Reg} < 7000$) used in developing this correlation was not large enough, which significantly limits its general application. Over the years, several works have addressed slim-hole drilling hydraulic modeling; these include those of Bode et al. (1991), Delwishe et al. (1992), McCann et al. (1995), Hansen et al. (1999) and Ooms et al. (2000). The importance of the narrow gap, fluid rheology, the effect of eccentricity and inner pipe rotation are generally acknowledged.

Using correlations based on the analytical solution of Frederickson and Bird (1958) which was developed and published by Exlog staff (1985), Reed and Pilehvari (1993) introduced a new effective diameter (d_{eff}) concept for the flow of drilling mud through annuli. It provides a link between Newtonian pipe flow and non-Newtonian concentric annular flow. The relation between Fanning friction factor and generalized

Reynolds number (N_{Reg}) for concentric annular flow in laminar region remains the same classical equation given by:

$$f = \frac{16}{N_{Reg}} \tag{2.37}$$

where,

$$N_{Reg} = \frac{\rho \bar{u} d_{eff}}{\mu_a} \tag{2.38}$$

and the effective diameter (d_{eff}) is given by the following expressions;

$$d_{eff} = \frac{d_2 - d_1}{G} \tag{2.39}$$

$$G = \left(1 + \frac{Z}{2}\right) \frac{[(3 - Z)n + 1]}{[(4 - Z)n]} \tag{2.40}$$

$$Z = 1 - \left\{1 - \left(\frac{d_1}{d_2}\right)^Y\right\}^{\frac{1}{Y}} \tag{2.41}$$

$$Y = 0.37n^{-0.14} \tag{2.42}$$

Moises and Shah (2000) studied flow of non-Newtonian fluids in concentric and eccentric annuli and provided empirical correlations between friction factor and Reynolds number for guar and Xanthan type fluids in both laminar and turbulent flow regimes. Correlations were developed from two sections of 3 ½-in. tubing with 2 3/8-in. 30 ft long tubing placed inside it to form concentric and fully eccentric annuli. The differential pressure is measured across 20 ft with 5 ft entry and exit lengths. For eccentric annuli the equations correlating Fanning friction factor and generalized Reynolds number are given as:

Laminar region: $$f = \frac{7}{N_{\mathrm{Re}g}} \tag{2.43}$$

Turbulent region: $$f = f_{\infty} + \Omega(N_{\mathrm{Re}g})^{-1} \tag{2.44}$$

where f_{∞} and Ω are constant for a particular fluid and depends on the apparent viscosity (μ_a) of the fluid at 511 sec^{-1}. However, the correlation was developed with limited data; hence it does not capture the effect of diameter ratios.

Zamora and Power (2002) proposed a unified rheological model to improve the existing API RP13D recommended practice on drilling fluid rheology and hydraulics. Calculations cover pipe and annular flow and include the impact of pipe eccentricity developed by Haciislamoglu et al. (1990). The pressure loss correlations were validated against an experimental test facility used for a master's thesis study of pressure-loss correlations (Subramanian, 1995). Zamora et al. (2005) also compared annular pressure losses measured at the test facility of McCann et al (1993) using a lab-prepared and a field biopolymer fluid and obtained a good agreement. For annular flow, Bern et al. (2007) stated that the proposed model correlations predicted pressure loss within ±15% (compared with ±20% for the existing RP13D equations).

Later, Singhal, Shah and Jain (2005) reported their experimental and simulation studies to investigate the flow behavior and friction pressure losses of Newtonian and non-Newtonian fluids in concentric annuli. They presented results of CFD simulations for different annular dimensions, with diameter ratios ranging from 0.16 to 0.91 and flow range encompassing both laminar and turbulent flow regimes. Based on the comparison with simulation results, they recommended the use of correlations

developed by Kozicki et al. (1966) and Reed and Pilehvari (1993) for laminar flow of non-Newtonian fluids in concentric annulus. Using limited data, they also proposed correlations, which they claimed could make accurate predictions of friction pressure losses in turbulent regime, for various concentrations of drag reducing fluids, such as guar and Xanthan, in concentric annuli.

Recently, Demirdal and Cunha (2007) reported a new methodology to compute annular pressure losses of non-Newtonian fluids via low shear rate based rheological characterization. They argued that the fluid rheological behavior in annular flow is much more non-Newtonian and viscous compared to its behavior at high shear conditions encountered during pipe flow. However, they neither compared their results with field nor measured data. Similarly, Akgun and Jawad (2007) published a review focused on the friction factor of fluids flowing turbulently through an eccentric annulus. They followed the method of computing friction factors using the concepts of geometric parameters and turbulent hydraulic diameter. Using the proposed method, they evaluated the performance of several correlations, such as, Kozicki et. al. (1966), Kostic and Hartnett (1984), Tam and Tiu (1988), and Hartnett and Kostic (1990), in predicting the friction factors for the flow of non-Newtonian fluids through eccentric annuli. Their results indicated that these correlations, except Kozicki correlation, gave excellent agreement with the experimental data of Newtonian fluid flowing through unit eccentricity annulus. They proposed a new equation for turbulent hydraulic diameter, incorporating the fact that the flow may not be turbulent over the entire eccentric annulus. However, they did not substantiate their turbulent hydraulic diameter

calculations with any experimental data. Moreover, the expressions derived for calculating the geometric parameters requires laborious computational effort; and, hence, can't be easily used to make undemanding hydraulic program calculations. They recommended that experimental studies be performed for turbulent flow of non-Newtonian fluids through an eccentric annulus using fluid of high degree of non-Newtonian behavior and with wide range of radius ratio and eccentricity. These recommendations are within the scope of this study.

While many investigators have studied the flow of Non-Newtonian fluids in annulus and introduced either empirical or analytical solutions, disagreements between calculated and measured pressure losses still exit (Demirdal and Cunha, 2007; Demirdal, 2001). As a matter of facts, no correlation currently exists for making undemanding hydraulic program calculations for the flow of drag reducing polymer fluids through an eccentric annulus. It should be interesting, from the fundamental and applied points of view, to conduct physical and numerical experiments to cover this knowledge gap. In the present work, the annular flow of non-Newtonian fluids is investigated using four concentrations of a widely used oilfield polymeric fluid, varying annular diameter ratios and eccentricities. The rheological and hydraulic properties of the polymer solutions were investigated with equipment available at the Well Construction Technology Center (WCTC), while numerical experiments were conducted using FLUENT 6.3.26, which is a commercial computational Fluid Dynamics (CFD) package developed by ANSYS.

2.3 Computational Fluid Dynamics (CFD)

Computational fluid dynamics (CFD) or the use of computers to solve fluid flow problems has advanced enormously in the last decade. Early computational methods for fluid flow analysis exploited the comparative simplicity of two dimensional simulations, and later advanced to three dimensions, as soon as the computational resources became affordable. Examples of this and its application to significant engineering problems are reflected well in published literature, both in the academic research world (Shah et al., 2004; Ozbayoglu and Omurlu, 2006) and by practicing experts in the field of fluid machinery design (Rosine et al., 2005). The availability of powerful and general purpose CFD software has greatly extended the range of applications to which CFD may be gainfully applied. CFD is especially useful in simulating complex fluid flow geometries. The variety of the available applications requires considerable flexibility in the handling of geometry, and a range of physical (and/or chemical) sub-models. The user can extract a wealth of information through the results of CFD analyses, from complicated unsteady performance parameters to the more fundamental: which way does the flow go? Apart from predicting fluid flow behavior, CFD codes can also be applied to successfully predict heat and mass transfer, chemical reactions, phase change, mechanical movements, as well as stress or deformation of solid structures

As discussed by Roache (1998), the numerical simulation of fluid dynamics is certainly not pure theoretical- if anything; it is closer to be experimental. This statement is especially true when complex geometries are being analyzed, for instance, see results

obtained by Ozbayoglu and Omurlu (2006). However, numerical experiments are as limited as the physical experiments, in that it only gives discreet data for a particular parametric combination. The work is left for the researcher to develop a functional relationship using parameters in the numerical model obtained from simulation results, and possibly, come up with an understanding of the prevailing physical phenomena. Hence, one can easily agree with Roache (1998) that "Computational fluid dynamics is a separate discipline, distinct from and supplementing both experimental and theoretical fluid dynamics, with its own techniques, its own difficulties, and its own realm of utility, offering new perspectives in the study of physical processes".

2.3.1 Applications of CFD in the Oil and Gas Industry

Computational Fluid Dynamics (CFD) is a powerful tool used in many fields of engineering involving the flow of fluids and particulate mixtures (Tu et al., 2008). With the advent of modern powerful computers and sophisticated CFD codes, fluid flow through complex geometries can be modeled and analyzed to an unprecedented level. These could be applied to evaluate frictional pressure losses (Farber, 2008; Pereira et al., 2007; Jain et al., 2004; Zhou and Shah, 2003; Singhal et al., 2005) without entailing significant costs through experimentation. Moreover, through CFD, flow characteristics such as velocity distribution can be visualized to aid in better understanding of the flow phenomenon and can be applied to improve flow characteristics and equipment design. Harnessing these computational capabilities, several investigators have used commercially available CFD codes to study flow characteristics of single phase fluids (Farber, 2008; Jain et al., 2004; Rosine et al., 2005; Bailey et al., 2006; Zhou and Shah,

2003) and multiphase fluids (Chen, 2004; Shah et al., 2004; Park, 2007; Pereira et al., 2007; Mishra, 2007; Manzar and Shah, 2009) using various geometries.

Moreover, Pereira et al. (2007) reported on an interesting investigation on the CFD predictions of drilling fluid velocity and pressure profiles in laminar helical flow using the Cross, three parameter rheological, model (Cross, 1965). They investigated the flow of non-Newtonian fluids through horizontal annuli formed by two tubes in concentric and eccentric arrangements. The study evaluated the performance of the numerical method used in CFD analysis, comparing the results obtained with those in published literature, aiming to validate the simulation strategies adopted. A comparison of the velocity profile results for helical flow of the simulation results with the experimental data of Escudier et al. (2002), for concentric and eccentric annulus cases showed a very good agreement. Thus, validating the numerical method applied in their CFD analysis study.

Recently, Yao and Robello (2008) published the results of their CFD model to predict annular friction pressure loss for various stand-off devices. These devices alter the flow stream and especially the angular bladed type which causes the flow to swirl. Using 3-D CFD modeling, they successfully developed equations and guidelines to calculate the pressure losses due to the stand-off devices, such as stabilizers and other wellbore cleaning devices with similar external profile.

Certainly, the commercial suppliers of general purpose CFD packages have led the developments in software that have enabled all these applications to become common place. These tools are now used extensively throughout the oil and gas

industry, with applications that include annular flow analysis (Hansen and Sterri, 1995; Ozbayoglu and Omurlu, 2006; Yao and Robello, 2008), helical flow (Pereira et al., 2007), cuttings transport (Bilgesu et al., 2002), separator design (Erdal et al., 1996), erosion studies (Edwards, 2000; Shah et al., 2004; Chen, 2004; Rosine et al., 2005; Bailey et al., 2006; Rosine et al., 2008), particle distribution (Manzar and Shah, 2009), bit optimization and design (Watson et al., 1997; De Sousa et al., 1999), design of Frac-Packing tools (Clem et al., 2006), amongst others (Xu et al., 1998; Frankiewicz and Lee, 2002; Ellison et al, 1997, Gregory et al., 1996). Hence, it's no-brainer for Elder et al. (2003) to state that, "there is no doubt that CFD has now come of age and its quite amazing the attribute this science in its early adult life after really quite a difficult adolescence".

CHAPTER 3

CFD MODELING OF NON-NEWTONIAN POWER LAW FLUID FLOW IN ECCENTRIC ANNULAR GEOMETRIES

3.1 Introduction

In this study, computational investigation of annular flow is used to extend our understanding of the flow field occurring during fully-developed laminar flow of Newtonian and non-Newtonian fluids in routine coiled tubing operations. The computational analysis has been performed using FLUENT 6.3.26, which is a commercial Computational Fluid Dynamics (CFD) code developed by ANSYS. FLUENT is one of the most widely used CFD software for modeling fluid flow and heat transfer in complex geometries. Generally, it solves the flow equations in their conservative form and provides complete mesh flexibility that could solve complex flow problems with both structured and unstructured meshes with relative ease.

The software package includes the solver, the preprocessors (such as GAMBIT) for geometry modeling and mesh generation, and translators (filters) for import of surface and volume meshes from CAD/CAE packages. Its solvers are based on the finite volume method, i.e. the flow domain is discretized into a finite set of control volumes or cells. Roache (1998) outlined the advantages of control volume based CFD models to include the fact that it is based on macroscopic physical laws, rather than on the continuum mathematics, i.e. it focuses attention on the actual satisfaction of the physical laws macroscopically, not merely in some never-attained limit as Δx approaches zero.

Following this approach, each of the governing equations are numerically integrated over a control volume, such that the related quantity (mass, momentum, energy, etc) is conserved in a discrete sense. This is achieved by discretizing these equations into algebraic forms which are solved to render the flow field. A finite difference problem represented by a staggered grid is considered solved if the pressure at each node and the velocity in each link between two nodes satisfy the continuity equation and the momentum equations. Although there are many established numerical methods for solution of the partial differential equations governing fluid flow, means of improving accuracy, speed and robustness are still sought. As discussed by Ton-that and Camarero (1987), the pressure correction algorithms (e.g. SIMPLE (Patanker and Spalding, 1972), SIMPLER (Patanker, 1980), SIMPLEC (Van Doormaal and Raithby, 1984), and PISO (Tzabiras et al., 1986)), where the mass conservation constraint is applied to improve the approximated pressure field seem to be the rational choice since there are normally fewer nodes than links in a grid. However, Fluent 6.3.26 provides a measure of control by providing user-selective alternative discretization and solution strategies and care must be taken in choosing discretization and solution methods, considering the complex nature of fluid flow in eccentric annuli.

The following sections cover the development of computational methodologies and mesh synthesis used to obtain the numerical solutions of non-Newtonian Power law fluids in eccentric annuli through the application of the robust non-orthogonal, boundary-fitted, and curvilinear grids. A modified Haciislamoglu et al. (1990) correlation has been developed based on the improved data of CFD analysis.

3.2 Model Geometry and Grid Generation

Generation of the model is the primary step in the simulation process. An accurate model is necessary to obtain good simulation results. GAMBIT® has been used for building the model geometry and meshing the model. More than twenty annular models (with eccentricities: 0, 0.25, 0.5, 0.75 and 0.96; and diameter ratios: 0.3, 0.5, 0.6 and 0.8) have been developed for this study. In each case, the length (120–480in.) was chosen in order to achieve a fully developed flow at the outlet. For a 3D problem, various types of cells can be used including hexahedral, tetrahedral, pyramid, wedge and hybrid cells. Selection of mesh type depends on the setup time, computational expenses, and numerical accuracy (diffusion).

Both structured and unstructured meshes were utilized in this study. For complex geometries, it is advantageous to use unstructured grids employing triangular or tetrahedral cells for saving setup time; however, where applicable, hexahedral structured meshes have been used due to their inherent ability to align the flow with grid cells, and to also ensure that grid cells are parallel to wall surfaces. Below 75 percent eccentricity, hexahedral cells can be utilized with ease, since large aspect ratios could be used in the axial direction without numerical instability. For the unstructured or hybrid mesh scheme, the aspect ratio between grid sizes in the radial and axial directions must be kept low to avoid flow instabilities and also enhance solution convergence. An aspect ratio of 5 is recommended. Because of the symmetrical nature of annular flows, flow simulations were carried out using only a half section of the model. The meshing procedures for the structured mesh are as follows;

- Create straight edges using the dimensions of the model geometry to represent the lines of symmetry.
- Create curved edges using the dimensions of the model geometry to represent the circular edges on the end faces (i.e. tubing and casing walls).
- Create the "inlet" face using the straight and curve edges created above.
- Mesh the circular edges on the end faces with uniform intervals.
- Then, mesh the straight edges representing the lines of symmetry using uniform intervals (or apply a growth factor to create finer cells at the tubing walls).
- The "inlet" face is now ready for complete meshing, specify a mesh size and apply map scheme to finish the meshing (non-orthogonal curvilinear grids are generated).
- Next, create an edge, same length as the model geometry, in the axial direction and mesh into uniform segments by specifying the number of intervals.
- Sweep the meshed "inlet" along the axial direction to create the flow domain.
- Assign appropriate boundary conditions at all zones (velocity inlet, outflow, symmetry, tubing wall and casing wall)
- Finally, export mesh file to Fluent.

In the present study, these procedures have been written as journals files, which can be simply run in GAMBIT, to generate grids for different cases. Samples of these journal

files are shown in Appendix A for both structured and hybrid mesh schemes. Cross-sections of annular geometries with the meshes are shown in Figures 3.1 and 3.2. The figures show the distribution of meshes across the entire cross-section at the inlet and indicate that the mesh density is large enough to successfully simulate the cases under investigation, without requiring finer cells at tubing walls.

3.3 Fluid Rheology

The flow curves (log viscosity versus log shear rate, see Figure 3.3) for guar concentrations studied in this work are linear for a wide range and are modeled well by the power law model (Eq. 2.8). Whitcomb et al. (1980) and Goel et al. (2002) reported extensively on the rheology of aqueous solutions of guar over a wide range of shear rates and concentrations. Data obtained by both authors show that the viscosity curves of guar solutions flatten to a constant value at low shear rates. Similarly, we also expect these solutions to have a Newtonian region at very high shear rates. These constant values, characterizing Newtonian regions, are known as zero shear rate viscosities, η_{max} and infinite shear rate viscosity, η_{min} respectively. The region between these Newtonian plateaus is the shear thinning or pseudo-plastic region. As discussed by Whitcomb et al. (1980) and Bird et al. (1987), the main disadvantage of the power law rheological model is its failure in the regions of very low shear rate, η_{max} or τ_y, and very high shear rate, η_{min}.

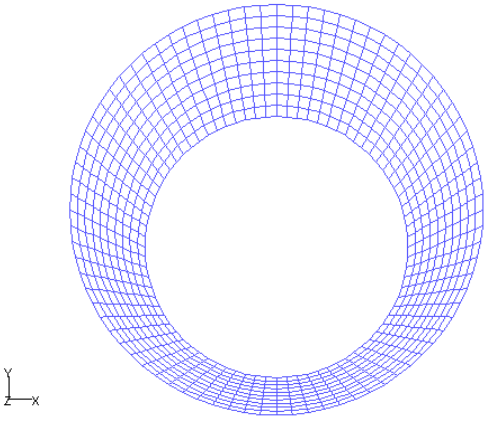

(a) Structured hexahedral mesh for a partially eccentric annulus (ε = 0.5).

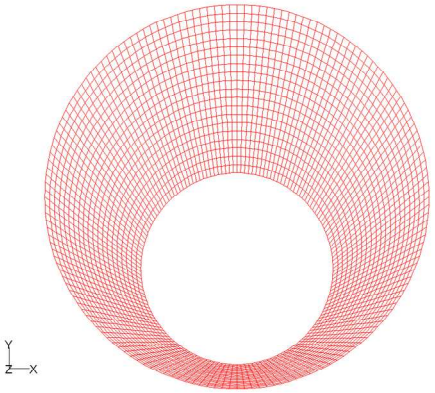

(c) Structured hexahedral mesh for a partially eccentric annulus (ε = 0.75).

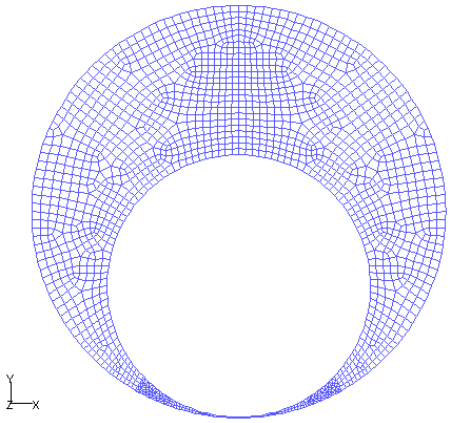

(b) Hybrid mesh for an eccentric annulus (ε = 0.96).

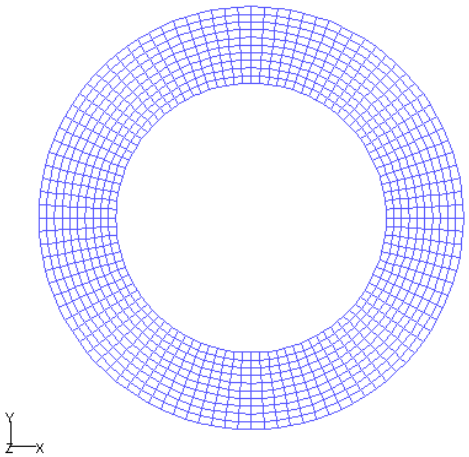

(d) Structured hexahedral mesh for a concentric annulus

Figure 3.1 Mesh distributions at the inlet of annular sections for the case of eccentricity; (a) 0.5, (b) 0.96, (c) 0.75, and (d) zero.

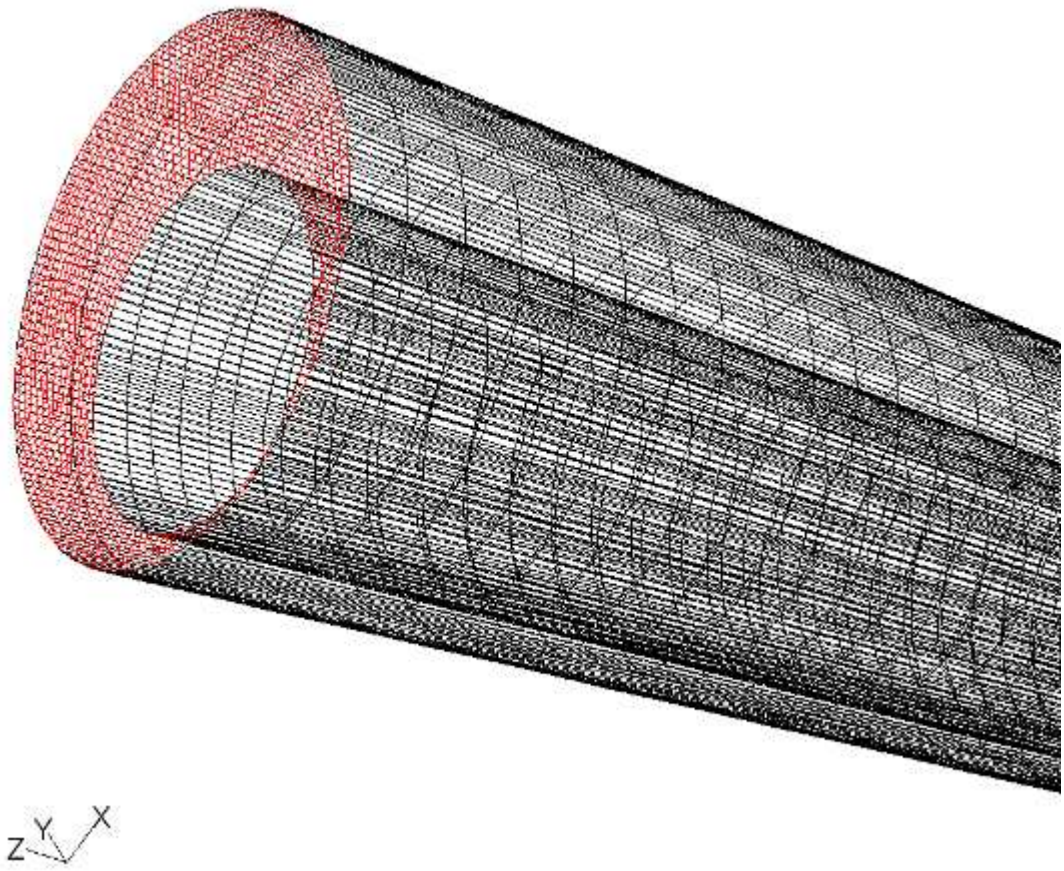

Figure 3.2 Mesh distributions across an eccentric annulus

However, as pointed out by Whitcomb et al. (1980), guar, unlike xanthan or welan gum, has no true yield stress, at least within the concentrations investigated in this study. To overcome other inherent disadvantages, a modified Power law model that accounts for the zero shear rate viscosity, η_{max} and the infinite shear rate viscosity, η_{min} of each fluid is utilized. Figure 3.3 shows the variation of viscosity with shear rate according to the modified non-Newtonian Power law rheological model used in this study. Table 3.1 gives the values for zero shear rate viscosities (η_{max}), infinite shear rate viscosity (η_{min}) and the power law parameters (n and K) measured at various concentrations of

guar. These values are consistent with published data for guar solutions (Whitcomb et al., 1980; Goel, 2001).

Table 3.1 Modified non-Newtonian Power law rheological model parameters for guar fluids

Guar Concentration (lb/Mgal)	n	K (poise-sec^n)	η_{max} (cP)	η_{min} (cP)
20	**0.620**	**1.34**	**62**	**8**
30	**0.550**	**4.00**	**220**	**14**
40	**0.436**	**11.58**	**920**	**18**
60	**0.360**	**38.05**	**5000**	**30**

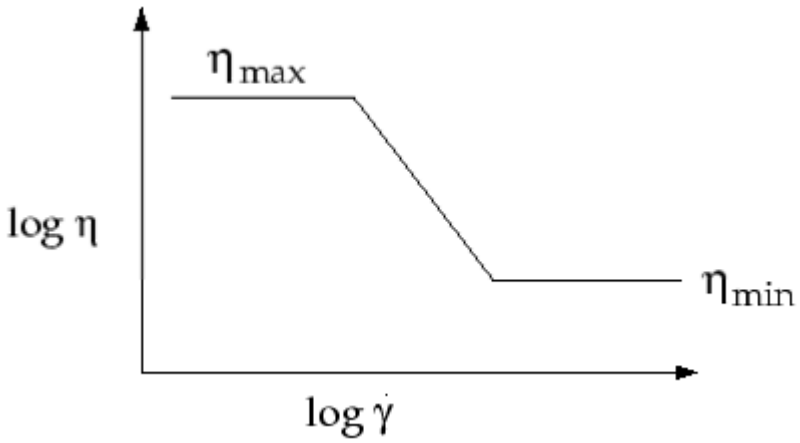

Figure 3.3 Variation of viscosity with shear rate according to the modified non-Newtonian Power law rheological model.

Using modified power law rheological model, the apparent viscosity, μ_a of non-Newtonian fluid is represented by the following expression:

$$\eta_{min} \leq \mu_a = 47880K(\dot{\gamma})^{n-1} \leq \eta_{max} \quad (3.1)$$

where K = consisteny index ($lb_f s^n/ft^2$), $\dot{\gamma}$ = shear rate, s^{-1}, and n = flow behavior index, dimensionless.

3.4 Governing Equations for CFD

If we introduce a general variable ϕ and express all the fluid flow equations, including equations of temperature and turbulent quantities, in the conservative incompressible form, the transport equation for the property ϕ can usually be written as:

$$\frac{\partial \phi}{\partial t} + \frac{\partial (u\phi)}{\partial x} + \frac{\partial (v\phi)}{\partial y} + \frac{\partial (w\phi)}{\partial z}$$

$$= \frac{\partial}{\partial x}\left[\Gamma \frac{\partial \phi}{\partial x}\right] + \frac{\partial}{\partial y}\left[\Gamma \frac{\partial \phi}{\partial y}\right] + \frac{\partial}{\partial z}\left[\Gamma \frac{\partial \phi}{\partial z}\right] + S_\phi \qquad (3.2)$$

Generally, the local acceleration and advection terms on the LHS are equivalent to the diffusion term ($\boldsymbol{\Gamma}$ = diffusion coefficient) and the source term (S_ϕ) on the RHS, respectively. The equation illustrates the various physical transport processes occurring in the fluid flow. Using the basic principles of conservation of mass, momentum, and energy, Tu et al. (2008) was able to formulate the partial differential equations for the three dimensional form of the governing equations by setting the transport property ϕ equal to 1, u, v, w, T, ¥, g, and selecting appropriate values for the diffusion coefficient $\boldsymbol{\Gamma}$ and source terms S_ϕ in Equation 3.2. The expressions for the diffusion coefficient $\boldsymbol{\Gamma}$ and source terms S_ϕ are presented below.

Continuity

ϕ = 1; $\Gamma = 0$; $S_\phi = 0$ (3.3)

Momentum

ϕ = u, v, w; $\Gamma = v + v_T$; $S_\phi = -\frac{1}{\rho}\frac{\partial p}{\partial x} + S'_u, -\frac{1}{\rho}\frac{\partial p}{\partial y} + S'_v, -\frac{1}{\rho}\frac{\partial p}{\partial z} + S'_w$ (3.4)

Energy

ϕ = T; $\Gamma = \frac{v}{Pr} + \frac{v_T}{Pr_T}$; $S_\phi = S_T$ (3.5)

Turbulent quantities

$$\phi = ¥, e;\ \Gamma = \frac{v_T}{\sigma_¥}, \frac{v_T}{\sigma_e};\ S_\phi = P - D, \frac{e}{¥}(C_{e1}P - C_{e2}D) \tag{3.6}$$

where $P = 2v_T\left[\left(\frac{\partial u}{\partial x}\right)^2 + \left(\frac{\partial v}{\partial y}\right)^2 + \left(\frac{\partial w}{\partial z}\right)^2\right] + v_T\left[\left(\frac{\partial u}{\partial y} + \frac{\partial v}{\partial x}\right)^2 + \left(\frac{\partial v}{\partial z} + \frac{\partial w}{\partial y}\right)^2 + \left(\frac{\partial w}{\partial x} + \frac{\partial u}{\partial z}\right)^2\right]$ (3.7)

$$D = g \tag{3.8}$$

Equation 3.2 is usually used as the starting point for computational procedures in either the finite difference or finite volume methods. If flow is laminar, $v_T = 0$, and turbulent quantities are not solved. Dirichlet and Neumann boundary conditions are usually applied in CFD to close the fluid flow system.

3.5 Solution Approach

3.5.1 Simulation Procedure

The basic procedure in a typical CFD analysis involves: (1) problem identification, (2) solver execution, and (3) post-processing. The model geometry and mesh created with GAMBIT is imported into three-dimensional double precision (3ddp) Fluent solver. Within the segregated solver used in this study, appropriate material properties are assigned to the fluid and suitable boundary conditions of pressure and velocity at all the boundary zones are specified. At the entrance, "Velocity inlet" was specified, while an "Outflow" boundary condition, which requires steady state flow for accurate solutions, was chosen at the exit. To start the solver process (iteration), an initial solution has to be provided.

In the present study, the governing equations for laminar three-dimensional flow are solved using the finite volume discretization technique, in which the control volume

cells for velocity components are staggered with respect to the main control volume cells using the SIMPLE (semi-implicit method for pressure-linked equations) pressure–velocity coupling algorithm. In this scheme, a guessed pressure field is used to solve the momentum equations. A pressure correction equation, deduced from the continuity equation, is then solved to obtain a pressure correction field, which in turn is used to update the velocity and pressure fields. These guessed fields are progressively improved through the iteration process until convergence is achieved for the velocity and pressure fields. The salient features of the SIMPLE scheme and the assembly of the complete iterative procedure has been discussed in length by Tu et al. (2008).

The calculations were carried out using the pressure discretization scheme following the PRESTO routine, and for the momentum interpolation, the QUICK (third order scheme) routine was chosen due to its better adaptation to hexahedral meshes. Therefore, the solutions in this modeling study are all third order accurate. The discretized conservation equations are solved iteratively until convergence is reached, i.e., when changes in solution variables (residuals) from one iteration to the next are within convergence criteria, which was set at 10^{-6} for the continuity residual and x-y-z velocities. FLUENT provides useful tools, such as residual plots, to help monitor the convergence process. Proper convergence was achieved using under-relaxation factors ranging from 0.2 to 0.3 for pressure and 0.5 to 0.7 for momentum. A detailed flow simulation procedure is illustrated in the flow chart presented in Table 3.2. If a simulation run fails to converge, the solution parameters, e.g. under-relaxation factors or the grid are modified to achieve convergence. Notably, a converged solution is not

necessarily the correct answer; hence care must be taken to ensure that the results obtained follow known physical laws.

Table 3.2 Basic procedure for CFD Solver execution

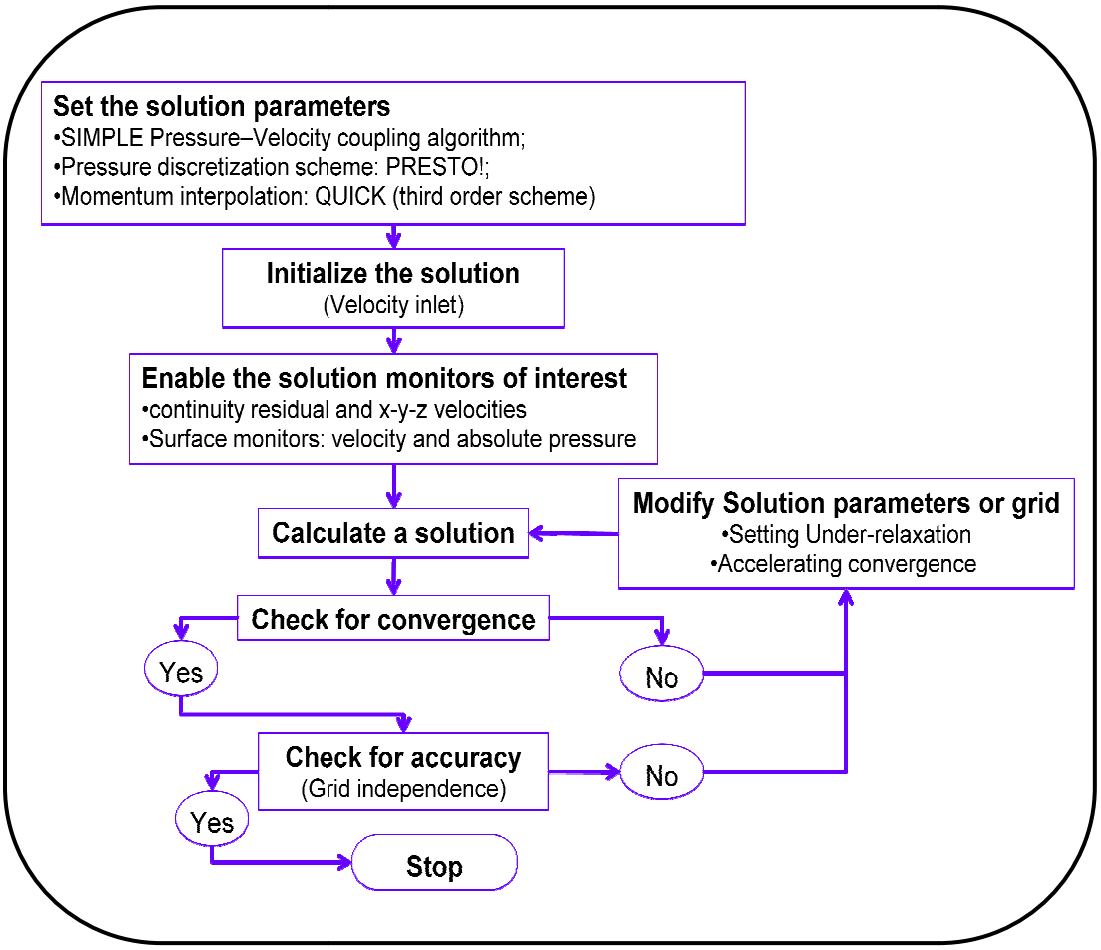

In the post-processing stage, the converged solutions are examined visually and numerically to obtain information on the overall flow patterns, key flow features and to extract useful engineering data. The flow path was divided into three cross-sectional view planes including the inlet and outlet planes to help visualize and inspect the velocity profile at these sections and its transition from the inlet to the outlet. A composite plot of axial velocity and pressure gradient on a streamline originating from

the inlet and terminating at the exit plane of the annular section is used to ensure that steady state flow was achieved across the flow domain.

As seen in Figure 3.4, a constant velocity profile and pressure gradient along the streamline is good evidence that the length of the computational domain was sufficient for the development of the required steady state flow conditions. Revisions to the physical models and modifications to the grid are considered depending upon the solution results.

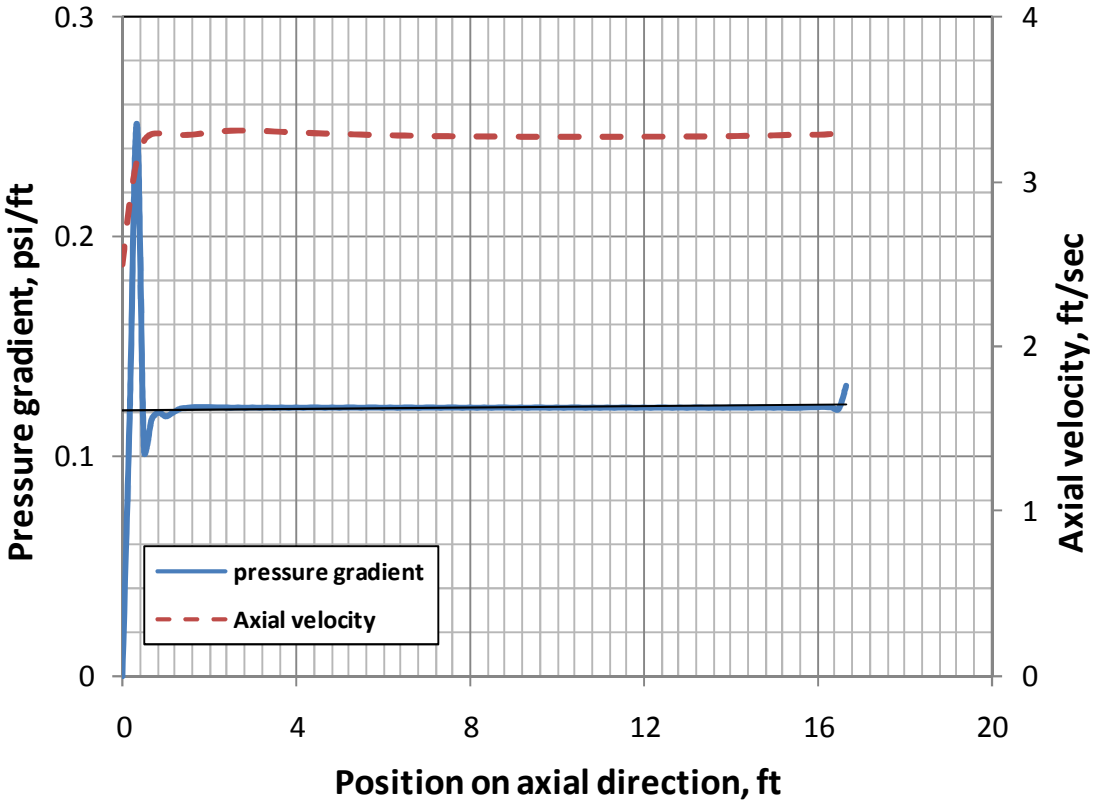

Figure 3.4 Axial velocity and pressure gradient along an eccentric annulus showing steady state flow conditions.

3.5.2 Assumptions and Boundary Conditions

CFD solutions rely upon physical models of real world processes (e.g. laminar, turbulence, compressibility, chemistry, multiphase flow, etc.), so, they can only be as accurate as the physical models on which they are based. In addition to the models and parameters discussed previously, other boundary conditions and assumptions involved in the CFD simulations conducted in this study have been listed below:

- Velocity inlet: a constant velocity is applied at the flow inlet and is calculated from the flow rate and cross sectional area of the physical model.
- All simulations are performed under steady state conditions. This is in line with the application of outflow boundary condition at the flow exit.
- The effect of temperature change on the flow has been ignored and isothermal conditions have been assumed.
- No slip boundary conditions are assumed at the wall of tubing, i.e. velocity at the wall is equal to zero.
- The fluid is considered to be incompressible.

3.5.3 Grid Independence Study

The grid-independence study of numerical results is studied and presented for the three cases specified in Table 3.3. The numerical results using eight (8) different mesh sizes are shown in Table 3.4 and Table 3.5 for case a and case b respectively. It can be seen from both tables that no significant variation is present for all the grid sizes studied, except for the 10(r) x 40(θ) mesh. Similar results were obtained for a hybrid mesh (see Fig. 3.1 (b)) and presented in Table 3.6 for uniform grid sizes 0.0327, 0.049, 0.065, and 0.098. However, an opposite trend is observed here, with lower friction pressure losses

predicted with finer mesh. The maximum deviation obtained was below 2% when pressure gradient values are compared to data obtained using Richardson extrapolation to zero mesh. For a concentric annulus (case b), the numerical deviations when the calculated flow rate versus friction pressure loss are compared with existing analytical solutions of non-Newtonian fluids (Fredrickson and Bird, 1959), are within 0.5%.

Grid independent solutions depend on the complexity of the flow and fluid properties. In order to save computational effort and obtain accurate numerical results, different mesh sizes are used, depending on the values of eccentricity and diameter ratio. Obviously, increasing the number of grid points in the circumferential direction does not have a significant impact on the predicted friction pressure gradients, hence, fewer grid points are used in this direction for flow simulations in concentric and slightly eccentric annuli. For highly eccentric annulus more grid points are needed in the circumferential direction to maintain a reasonable aspect ratio with grid sizes in the axial direction and obtain accurate results, hence the use of hybrid cells. In other studies, Haciislamoglu (1989) recommended a practical minimum of 30 x 20 grids, while Chin (2001) stated that a grid count of 20 in the radial direction is good enough to generate annular data suitable for engineering applications. In the present study, flow simulations were carried out with double precision on a Pentium® 4 CPU 2 GHz computer, having 1 GB RAM and running on Windows XP operating system, and the total computational time varied from 3 to 260 minutes for numerical simulations involving 40, 000 and 500, 000 cells, respectively.

3.6 RESULTS AND DISCUSSION

Due to the amount of grid points and the higher order schemes applied in this study, the computational cost of this analysis is very significant in terms of both CPU effort and in-core storage. It is appropriate to provide some typical values of computational effort. For instance, steady state flow calculations with about 500,000 mesh points require about 100 Mb of memory. The run time, say for 1500 iterations, is about 5hrs on a standard 2GHz intel-CPU PC. Different grid sizes ranging from 30(r) x 80(θ) to 40(r) x 160(θ) for the structured mesh, and 0.02-in. to 0.05-in. for hybrid mesh, were chosen to carry out present simulations. For a particular eccentricity, generalized Reynolds number (N_{Reg}) was varied by changing flow velocity and keeping other fluid and geometric variables constant. Iteration was stopped when difference between two consecutive values for all variables fall below the convergence criteria. For further stabilization of numerical procedure, under-relaxation factors were chosen between 0.2 - 0.7.

Table 3.3 Input data for grid-Independent study

Case a	
Inner pipe diameter, d_1:	0.46 in.
Outer pipe diameter, d_2:	0.726 in.
Eccentricity, ε:	0.43
Flow consistency index, k:	0.0337 $lbfsec^n/ft^2$
Flow behavior index, n:	0.8
η_{max}:	1200 cP
Case b	
Inner pipe diameter, d_1:	1.75 in.
Outer pipe diameter, d_2:	2.75 in.
Eccentricity, ε:	0
Flow consistency index, k:	0.0242 $lbfsec^n/ft^2$
Flow behavior index, n:	0.436
η_{max}:	920 cP
Case c	
Inner pipe diameter, d_1:	1 in.
Outer pipe diameter, d_2:	2 in.
Eccentricity, ε:	0.96
Flow consistency index, k:	0.0242 $lbfsec^n/ft^2$
Flow behavior index, n:	0.436
η_{max}:	920 cP

Table 3.4 Grid-Independent study for case a (v = 0.293 ft/sec)

Mesh size	ΔP/L (psi/ft)	Cells	Computational time (mins)
10(r) x 40(θ) x 100(z)	2.034463	40, 000	3
16(r) x 64(θ) x 100(z)	2.052688	102,400	10
20(r) x 80(θ) x 100(z)	2.057088	160, 000	24
32(r) x 128(θ) x 100(z)	2.062020	409,600	116
40(r) x 160(θ) x 75(z)	2.063198	480,000	230
40(r) x 80(θ) x 100(z)	2.063506	320,000	134
40(r) x 120(θ) x 100(z)	2.063252	480,000	189
50(r) x 100(θ) x 100(z)	2.064117	500,000	260

Table 3.5 Grid-Independent study for case b (v = 2.5 ft/sec)

Mesh size	ΔP/L (psi/ft)	Cells	Computational time (mins)
10(r) x 40(θ) x 100(z)	0.122069	40, 000	2
16(r) x 64(θ) x 100(z)	0.122112	102,400	12
20(r) x 80(θ) x 100(z)	0.122165	160, 000	23
32(r) x 128(θ) x 100(z)	0.122297	409,600	110
40(r) x 160(θ) x 75(z)	0.122460	480,000	230
40(r) x 80(θ) x 100(z)	0.122319	320,000	132
40(r) x 120(θ) x 100(z)	0.122371	480,000	186
50(r) x 100(θ) x 100(z)	0.122469	500,000	256

Table 3.6 Grid-Independent study for case c (v = 2.5 ft/sec)

Mesh size	ΔP/L (psi/ft)	Cells	Computational time (mins)	iterations
0.098	0.15576	61,000	5	100
0.065	0.15442	174,375	15	256
0.049	0.15393	310,000	88	856
0.0327	0.15390	403,560	362	2624

3.6.1 Validation of Present Study

The numerical results generated through CFD analysis are validated in this section through the comparison with available data in the literature. The computed friction pressure gradients by the present approach are compared with the correlation proposed by Jones and Leung (1981) for laminar flow of Newtonian fluids in concentric annulus and the analytical solution of Fredrickson and Bird (1958) using the approach introduced by Reed and Pilehvari (1993) for non-Newtonian power law fluids and the numerical results are in good agreement (within 1%). Similarly, the numerical predictions of friction pressure gradients in the case of a power law fluid in an eccentric

annulus (Table 3.2, case a) are compared in Figure 3.6 to the experimental data published by Mitsuishi and Aoyagi (1973). The rheological behavior of the fluid (3.92 wt. percent HEC polymer solution) used by this authors is a best fit by the Sutterby model which approaches a constant limiting viscosity at low shear rates. The equivalent power law model parameters were determined by Haciislamoglu (1989) and are used here to verify the model predictions in eccentric annulus. Note that for the results in Figure 3.5, the mesh size of 40(r) x 160(θ), eccentricity = 0.43, K = 0.0337 lbfsec^n/ft^2, k= 0.5, n= 0.8, and $\eta_{max} = 1200$ cP were used. It can be seen from Figure 3.5 that the present result agrees well with those of the experimental data of Mitsuishi and Aoyagi (1973).

As illustrated in Figures 3.6 and 3.7, we also obtained a satisfactory agreement between the experimental data (velocity profile) of Nouri and Whitelaw (1994) for a concentric annulus, the experimental data (velocity profile of widest gap) of Escudier et al. (2002a) for the case of an eccentric annulus, and the numerical calculations of this study. The data of Nouri and Whitelaw (1994) is for 0.2% CMC, a power-law fluid with only a modest shear-thinning index (n=0.75), and the agreement between the experiments and the calculations are clearly satisfactory. On the other hand, the data of Escudier et al. (2002a) is for 0.1% CMC/0.1% Xanthan gum fluid for eccentricity = 0.8 (Fig.3.7). There is almost perfect agreement in the region between the outer wall of the annulus (**$\delta = 1$**) and $\delta = 0.3$. Some discrepancies ensue as the inner tubing is approached ($\delta = 0$), which is probably due to the limitations of the experimental set-up. The discrepancy was also observed by Escudier et al. (2002a) in comparing the results of

their numerical model with the experimental data**.** This simply shows that the approach adopted in this study is valid.

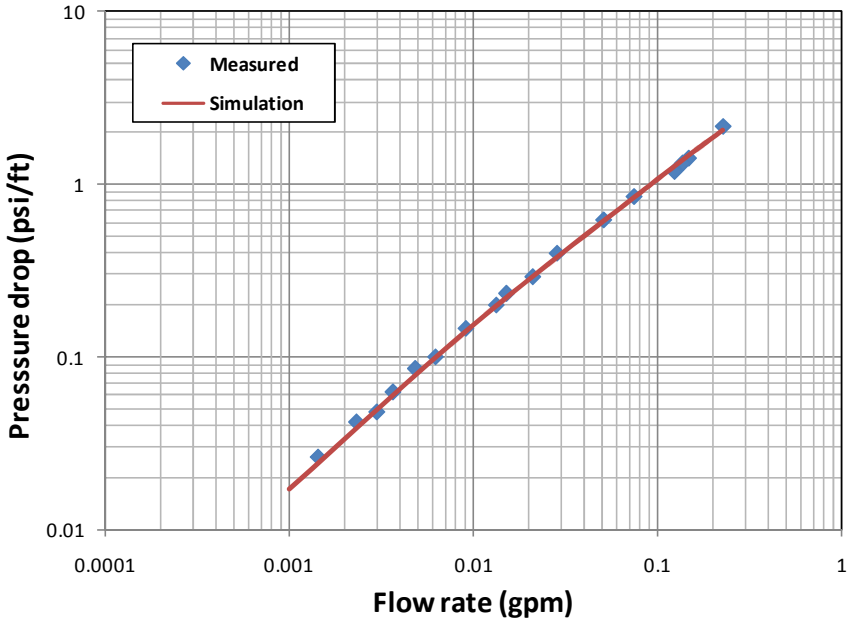

Figure 3.5 Model predictions and measured pressure gradient versus flow rate for power law fluid (Table 3.2, case a)

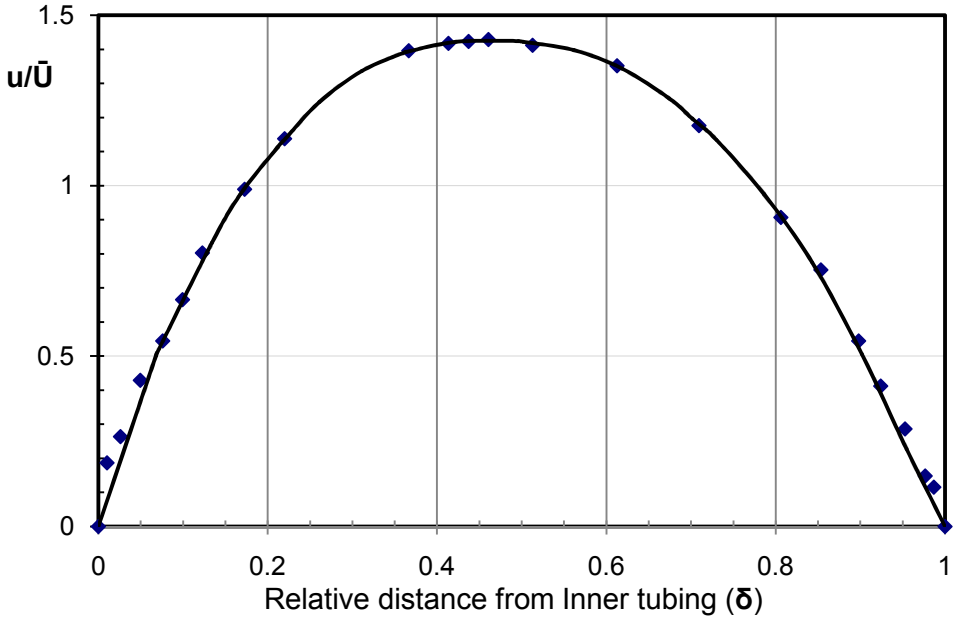

Figure 3.6 Data of Nouri et al. (1994) for 0.2% CMC, k = 0.5, ε = 0, N_{Reg}=600

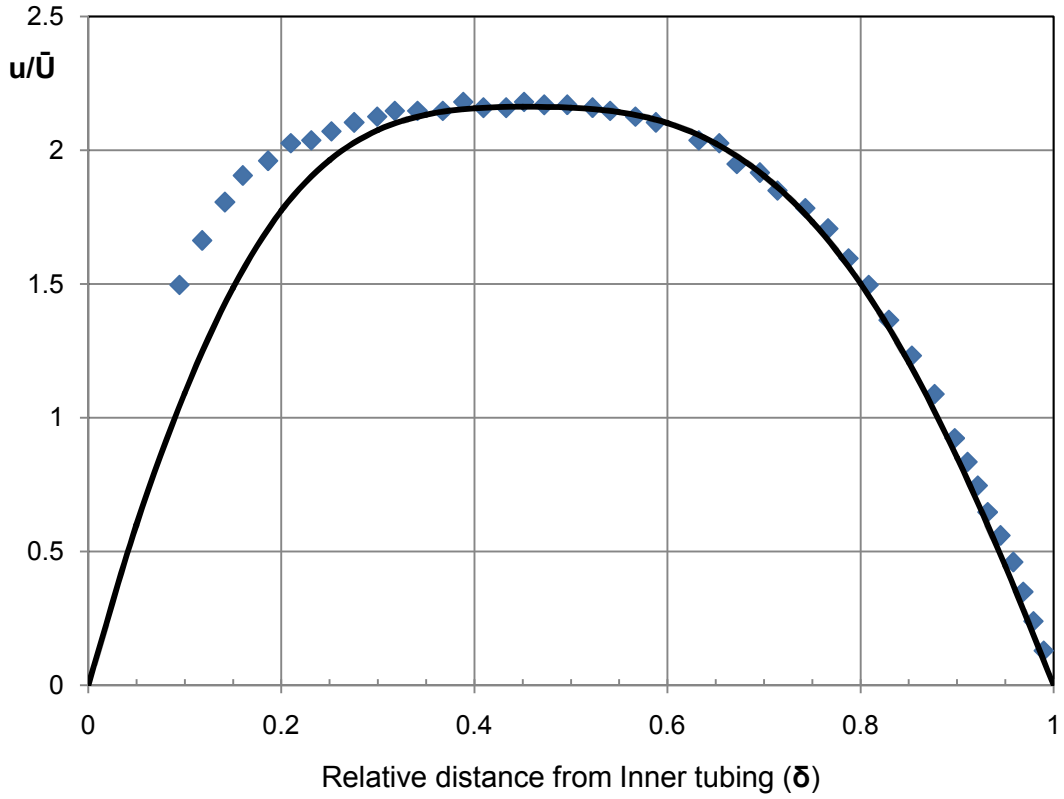

Figure 3.7 Data of Escudier et al. (2002) for 0.1% CMC/0.1% Xanthan gum, k=0.506, ε = 0.8, widest gap, N_{Reg} = 263

3.6.2 Velocity Profiles

For an eccentric annulus, the coordinate system was centred at the inner tubing axis and used to define the conventional planes for velocity profile analysis. A cross section of the annular geometry and the grid arrangement for a typical numerical calculation are shown in Figure 3.8. Following established conventions, sector A of the annulus is referred to as the widest gap, C as the narrowest gap, and B as the widening gap across the centre of the inner tubing (see Figure 3.8).

The velocity profiles calculated for Newtonian and non-Newtonian fluid flow in a concentric annulus are shown in Figures 3.9 to 3.11, as dimensionless plots of the ratio of local velocity (u) to the bulk-velocity (Ū) versus the relative distance from the

inner tubing, **δ**. As expected for a concentric annulus, the velocity profile calculated at planes A, B and C are equal; hence, only one plot is presented for each annular configuration. The velocity profile for non-Newtonian fluids are slightly flattened compared with that for a Newtonian fluid (i.e. peak velocity 1.30Ū (n =0.36) compared with 1.51Ū (n = 1) in Figure 3.9). The polymer tends to suppress fluctuations in the directions normal to that of the bulk flow. One feature of note is that the point of peak velocity is not centrally located, but slightly shifted towards the wall of the inner tubing. The shift is more pronounced at lower values of the diameter ratio than at high values (i.e. peak velocity at **δ** ≈ 0.455 (k = 0.33) compared with **δ** ≈ 0.467 (k = 0.64) and **δ** ≈ 0.492 (k = 0.64).

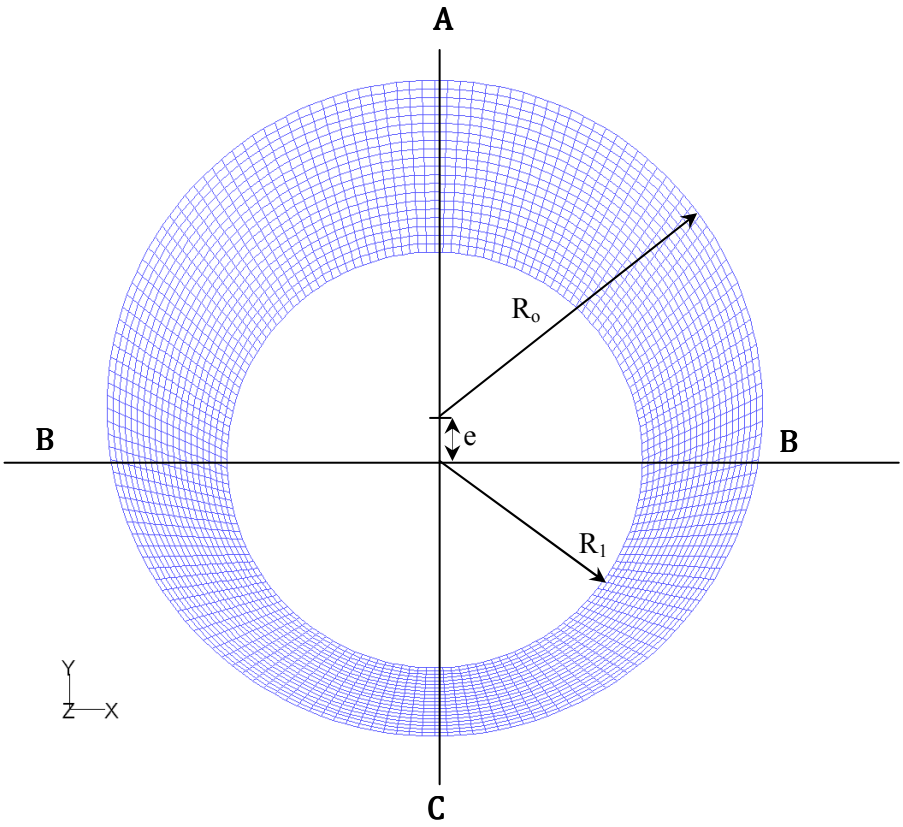

Figure 3.8 Annulus geometry and computational grid (20 x 80 cells)

For an eccentric annulus, the velocity profile changes considerably (Figures 3.12 to 3.16), as the flow field is significantly influenced by secondary flows. A general reduction in the magnitude of the flow velocity as the gap between the cylinders is reduced is observed, i.e. the velocity in sector C of the annulus is reduced, as more fluids seek to flow through zones of least resistance (sector A), thereby increasing the peak velocity in sector A to 2.41Ū while the peak velocities are 1.01Ū and 0.28Ū for sectors B and C respectively for a Newtonian fluid (Figure 3.12).

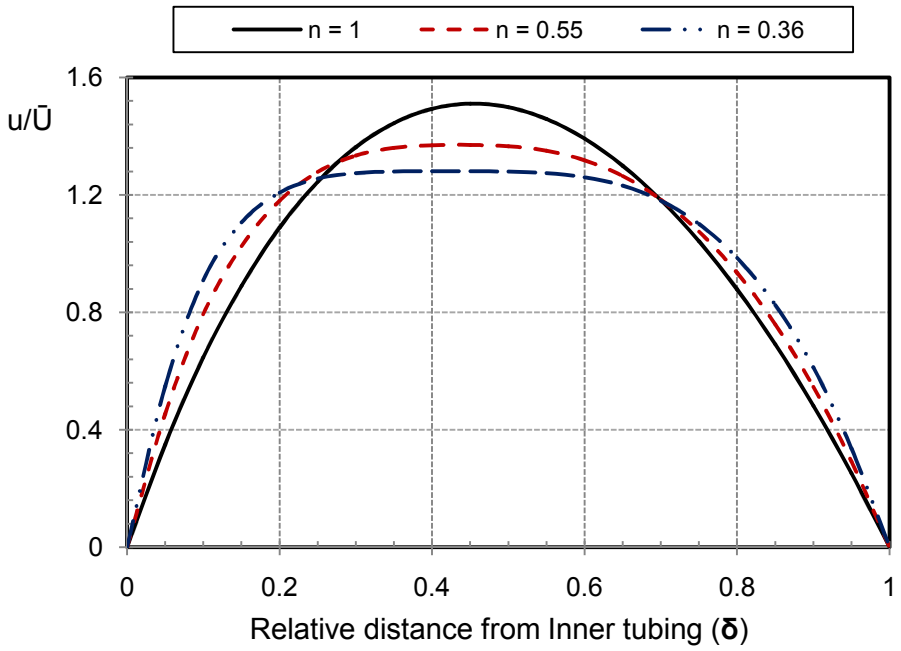

Figure 3.9 Axial velocity profile of Newtonian and non-Newtonian fluids, N_{Reg}= 800, ε = 0, k = 0.33.

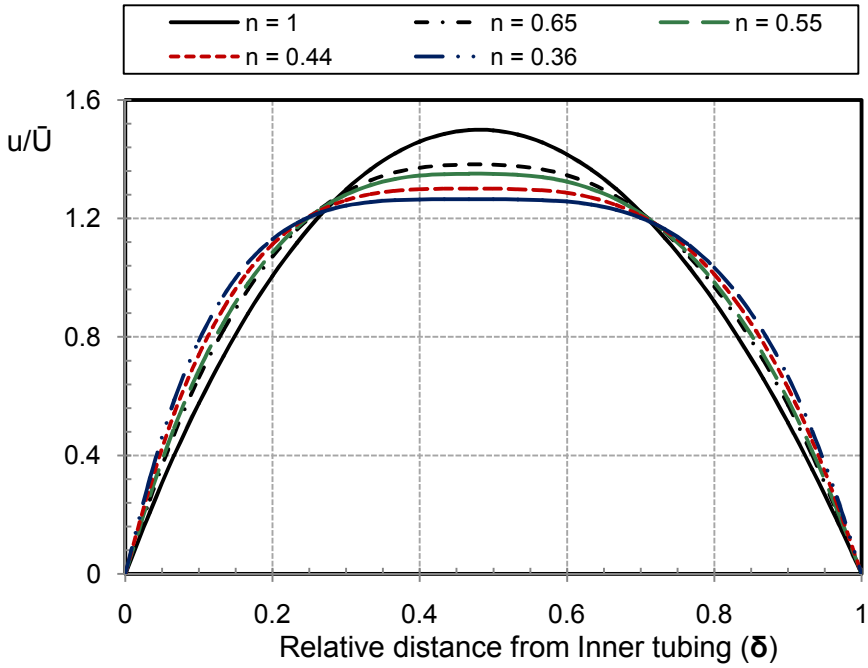

Figure 3.10 Axial velocity profile of Newtonian and non-Newtonian fluids, N_{Reg} = 800, ε = 0, k = 0.64.

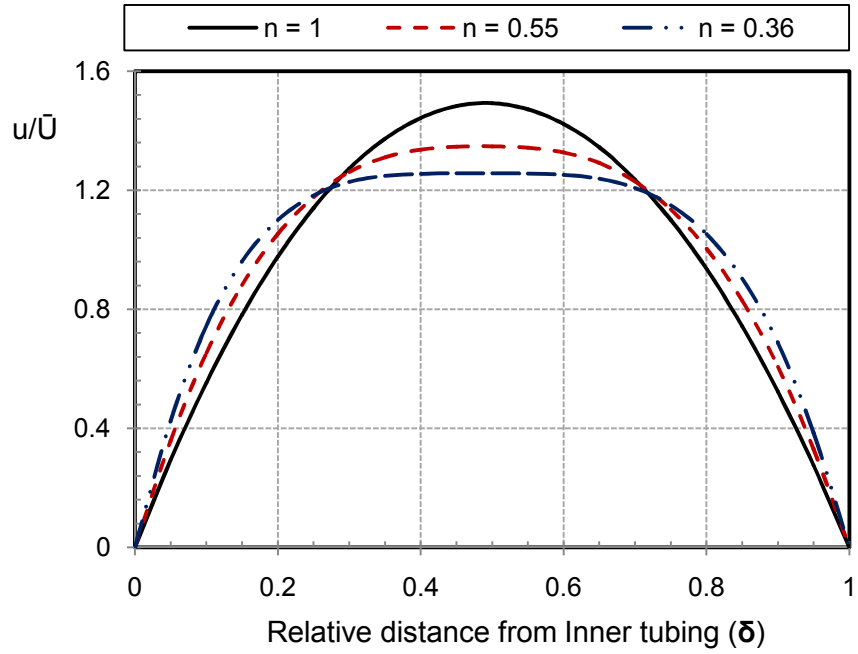

Figure 3.11 Axial velocity profile of Newtonian and non-Newtonian fluids, N_{Reg} = 800, ε = 0, k = 0.8.

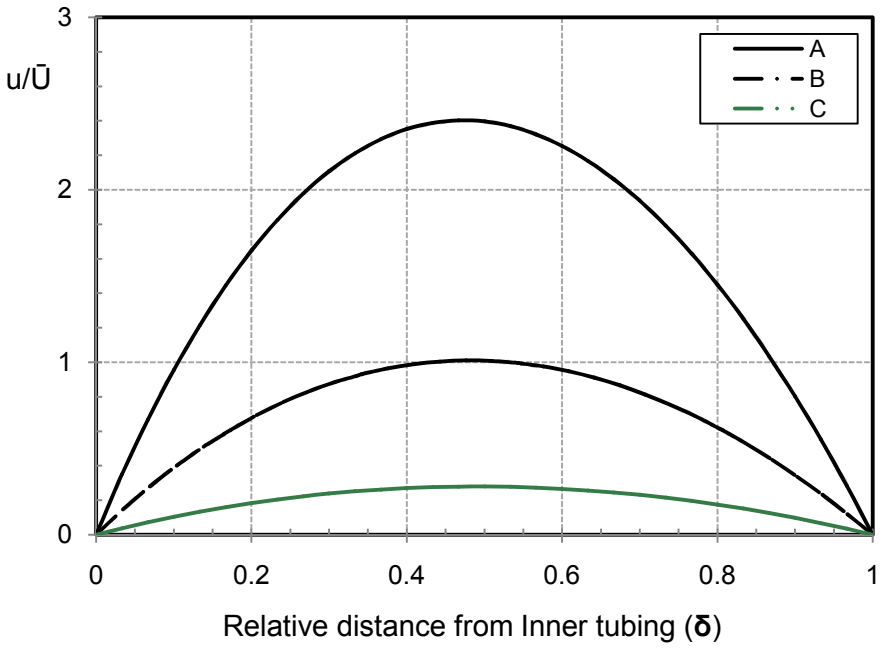

Figure 3.12 Axial velocity profile of a Newtonian fluid for sectors A, B, and C; N_{Reg} = 800, ε = 0.5, k = 0.64.

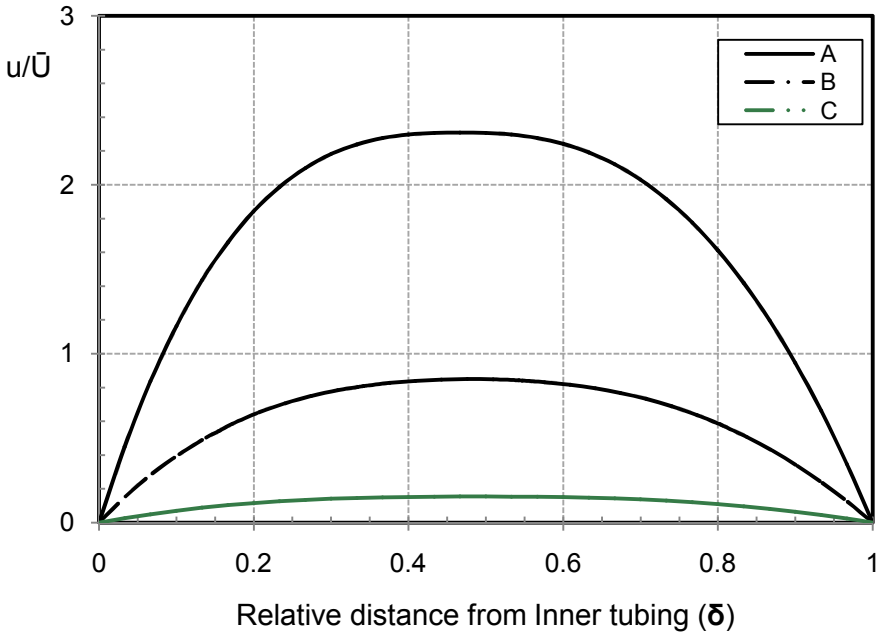

Figure 3.13 Axial velocity profile of a non-Newtonian fluid (20 lb/Mgal guar, n= 0.62) for sectors A, B, and C; N_{Reg} = 800, ε = 0.5, k = 0.64.

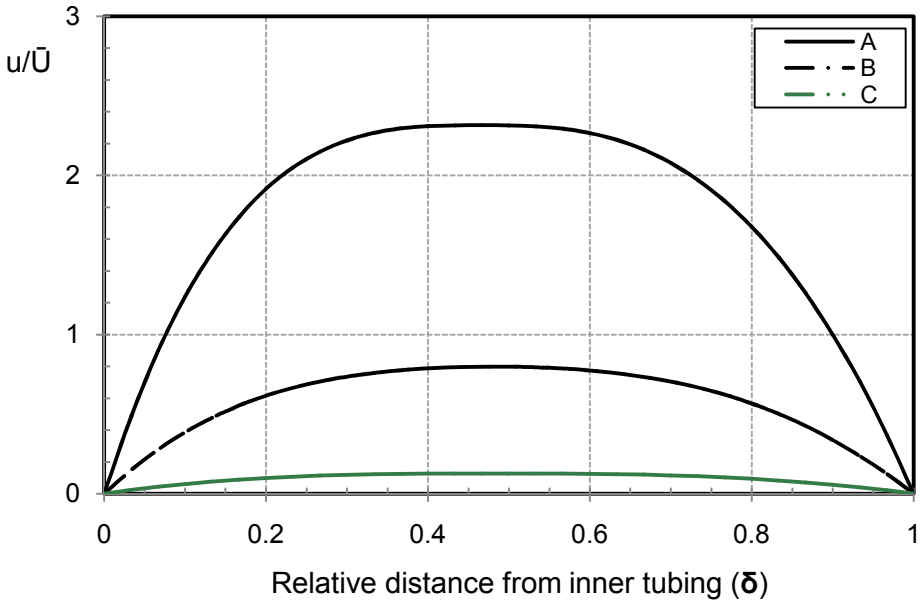

Figure 3.14 Axial velocity profile of a non-Newtonian fluid (30 lb/Mgal guar, n= 0.55) in laminar flow regime for sectors A, B, and C; N_{Reg} = 400, ε = 0.5, k = 0.64.

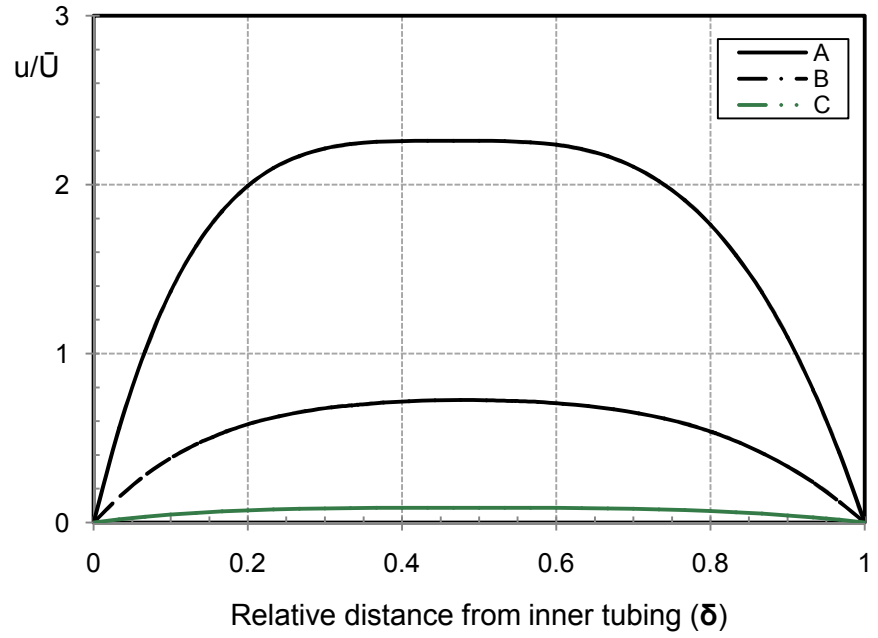

Figure 3.15 Axial velocity profile of a non-Newtonian fluid (40 lb/Mgal guar, n= 0.46) for sectors A, B, and C; N_{Reg} = 265, ε = 0.5, k = 0.64.

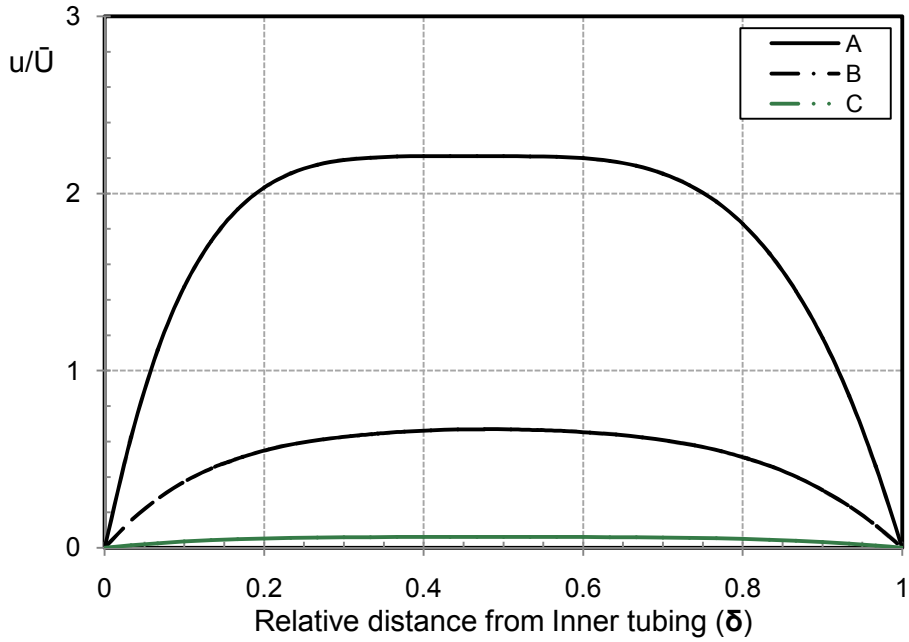

Figure 3.16 Axial velocity profile of a non-Newtonian fluid (60 lb/Mgal guar, n= 0.36) for sectors A, B, and C; N_{Reg} = 124, ε = 0.5, k = 0.64.

Figures 3.17 to 3.22 present composite plots of the velocity profiles calculated for Newtonian and non-Newtonian fluid flow in a 50% eccentric annulus, with k = 0.33, 0.64 and 0.8. It is evident from Figures 3.17 and 3.20 that the difference in maximum velocities for Newtonian and non-Newtonian fluids decreases with increasing value of the diameter ratio. This is due to the reduction in the effect of secondary flows as the flow domain approaches that of flow through parallel plates, i.e. k □ 1.

Furthermore, as eccentricity increases (Figures 3.23 to 3.26), a high velocity zone persist in sector A while a no flow region is created in sector C. Therefore, it is evident that both laminar and turbulent flow conditions can exist across an eccentric annulus at the same time. Such is the complexity that is involved with fluid flow through an eccentric annulus. As discussed by Hacisslamoglu et al. (1989), an accurate prediction of the velocity profile is needed for a successful design of mud displacement

in cementing operations, cuttings transport in directional drilling, and to correctly estimate the travel time of a kick from the bottom of the hole to the surface. Velocity profile plots for various diameter ratios are also presented in Appendix B.

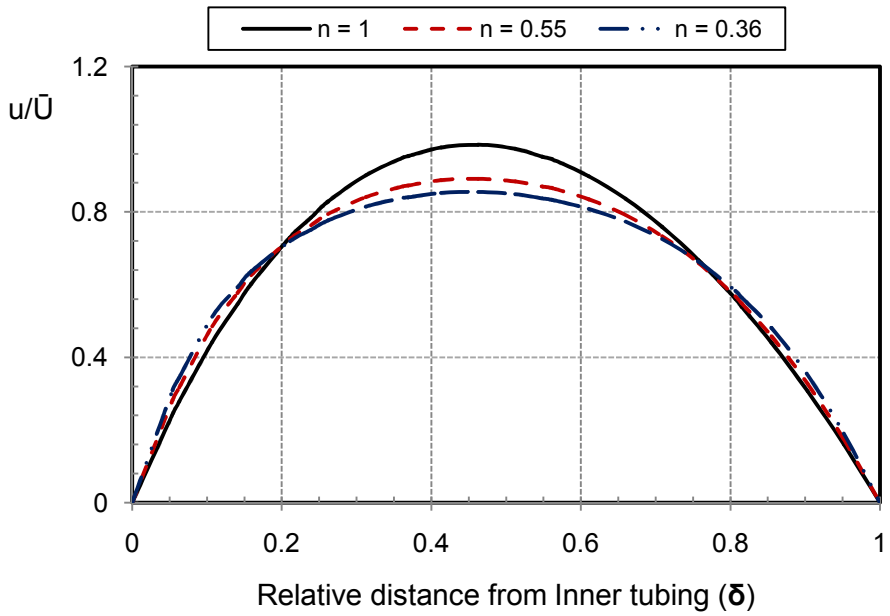

Figure 3.17 Axial velocity profile of Newtonian and non-Newtonian fluids, N_{Reg} = 800, ε = 0.5, k = 0.33, sector B.

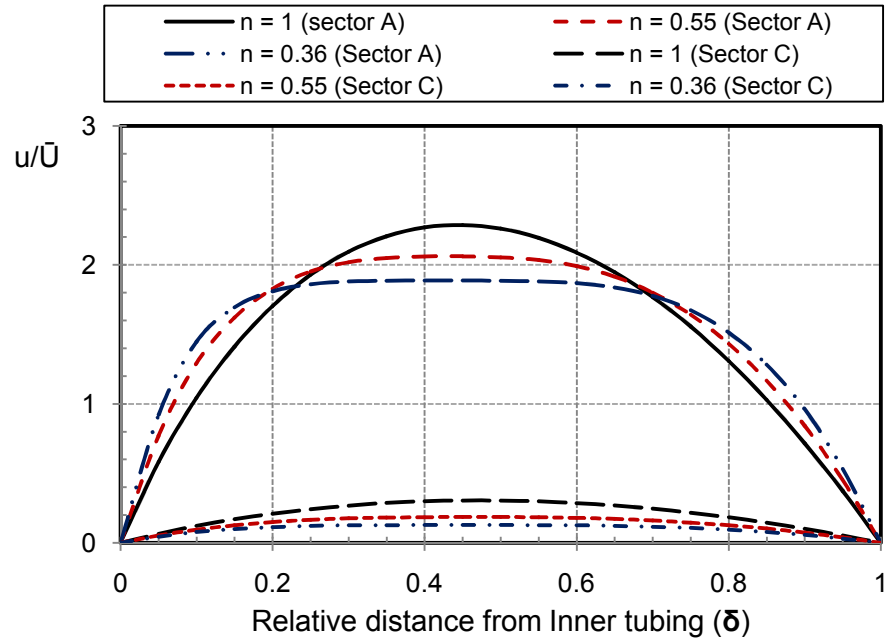

Figure 3.18 Axial velocity profile of Newtonian and non-Newtonian fluids (sectors A & C), N_{Reg} = 800, ε = 0.5, k = 0.33.

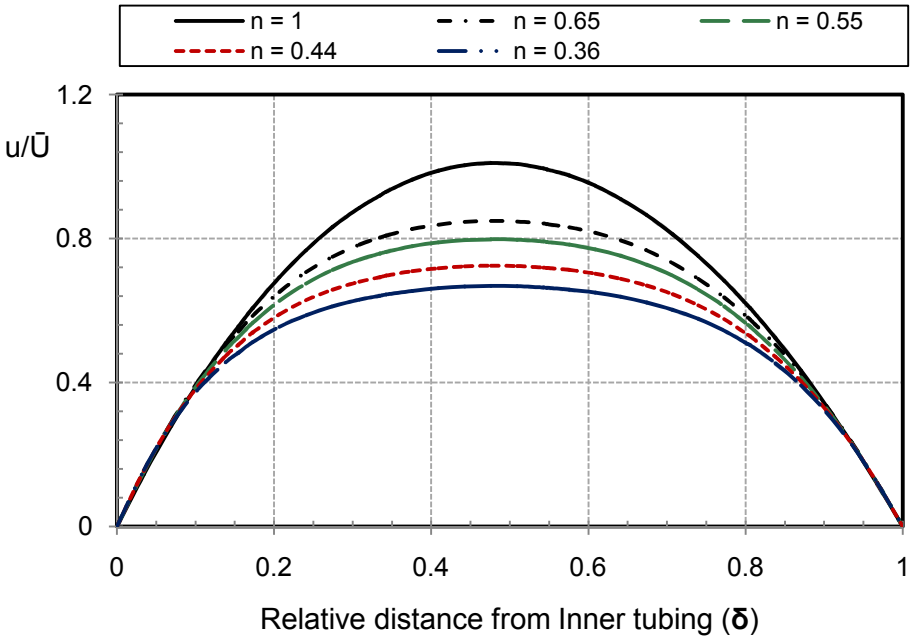

Figure 3.19 Axial velocity profile of Newtonian and non-Newtonian, N_{Reg}=800, ε = 0.5, k = 0.64, sector B.

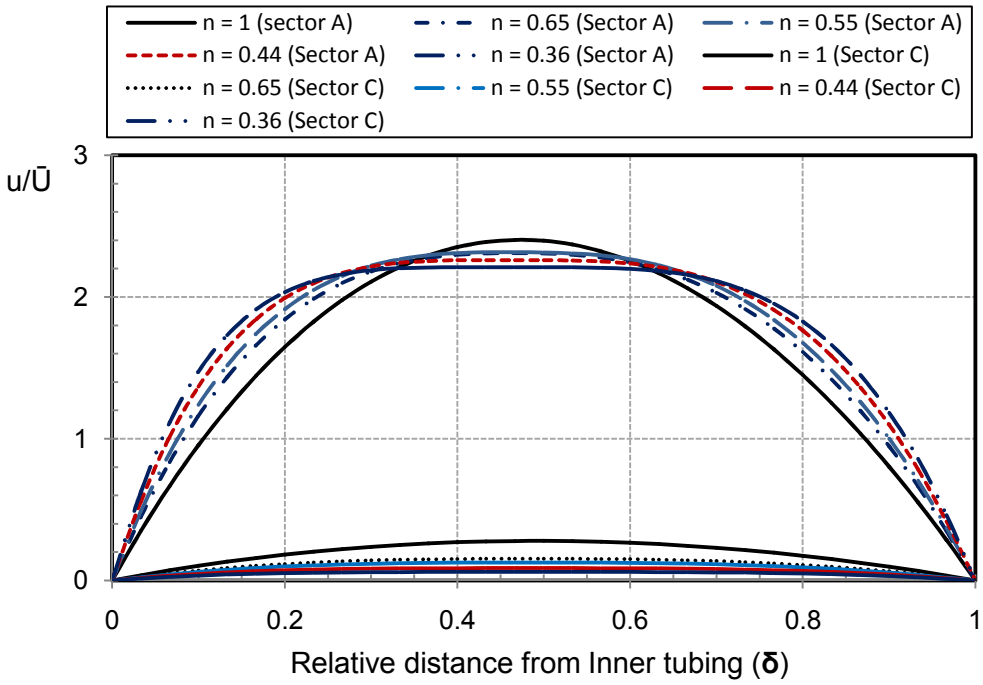

Figure 3.20 Axial velocity profile of Newtonian and non-Newtonian fluids, N_{Reg} = 800, ε = 0.5, k = 0.64.

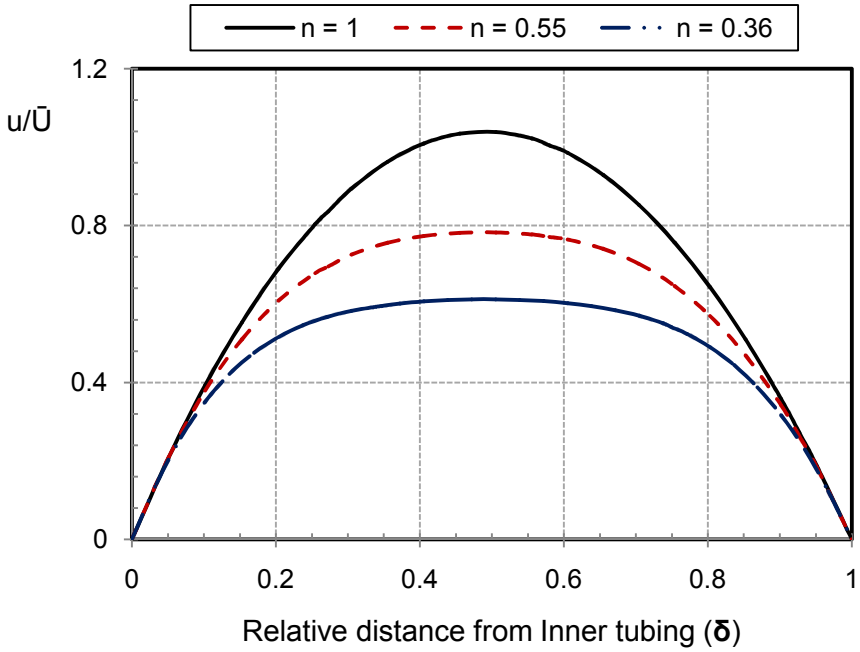

Figure 3.21 Axial velocity profile of Newtonian and non-Newtonian fluids (sector B), N_{Reg} = 800, ε = 0.5, k = 0.8.

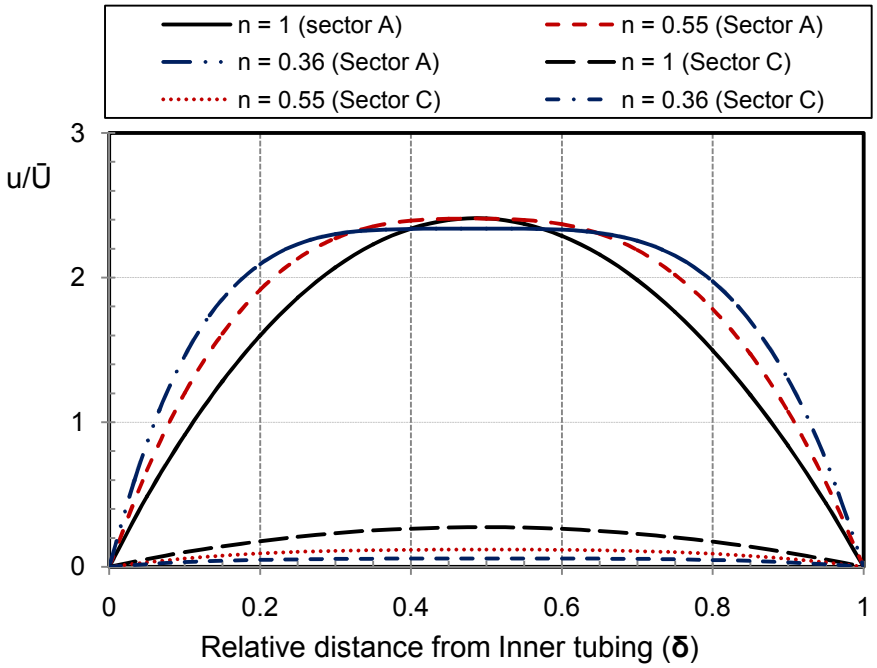

Figure 3.22 Axial velocity profile of Newtonian and non-Newtonian fluids, N_{Reg}= 800, ε = 0.5, k = 0.8.

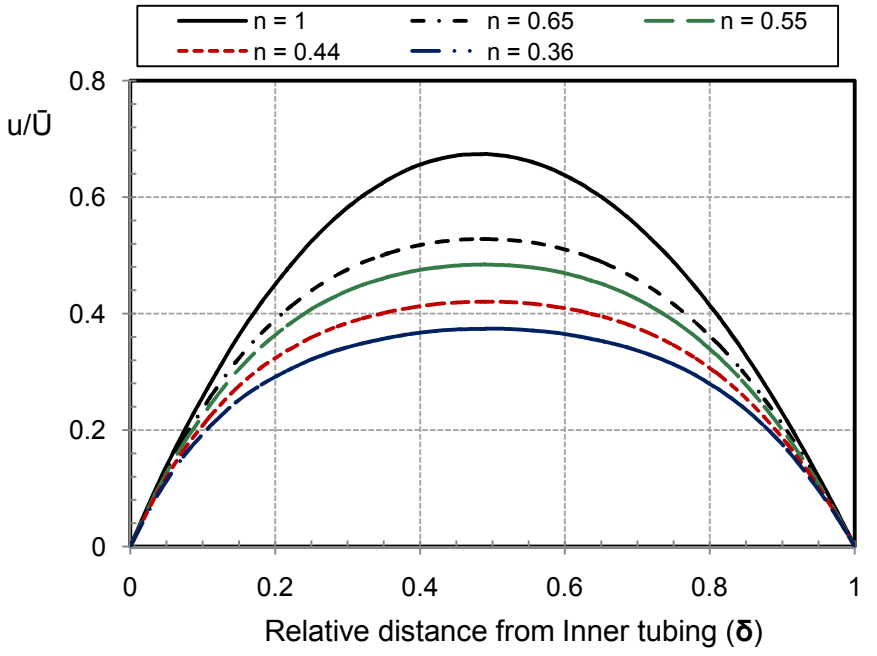

Figure 3.23 Axial velocity profile of Newtonian and non-Newtonian fluids (Sector B), N_{Reg} = 800, ε = 0.75, k = 0.64.

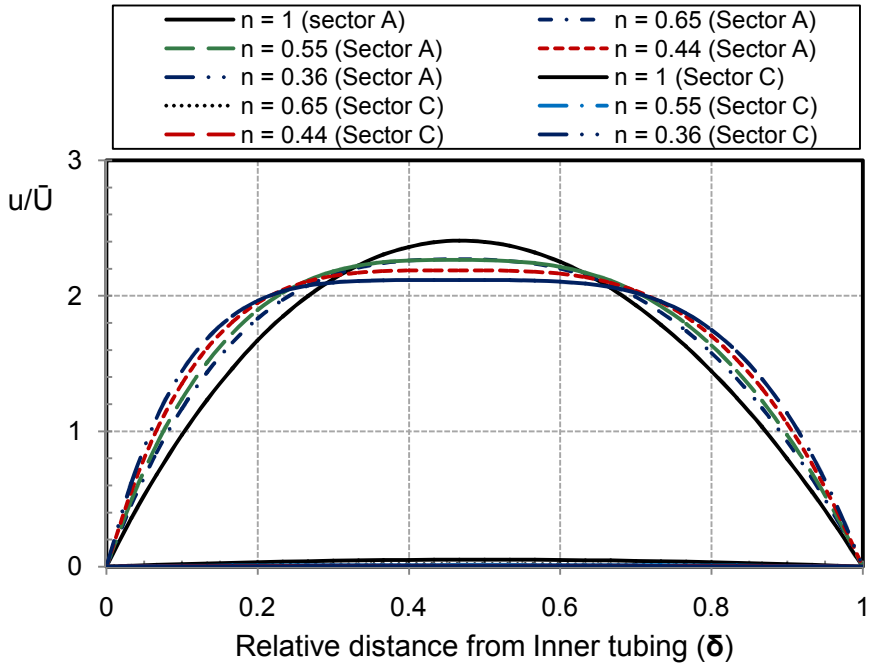

Figure 3.24 Axial velocity profile of Newtonian and non-Newtonian fluids (Sector A & C), N_{Reg} = 800, ε = 0.75, k = 0.64.

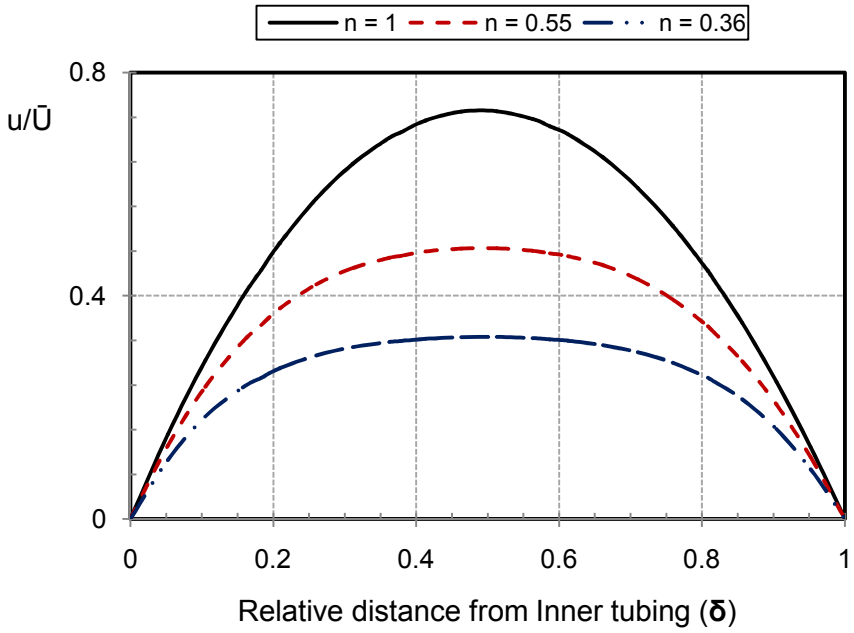

Figure 3.25 Axial velocity profile of Newtonian and non-Newtonian fluids (sector B), N_{Reg} = 800, ε = 0.75, k = 0.8.

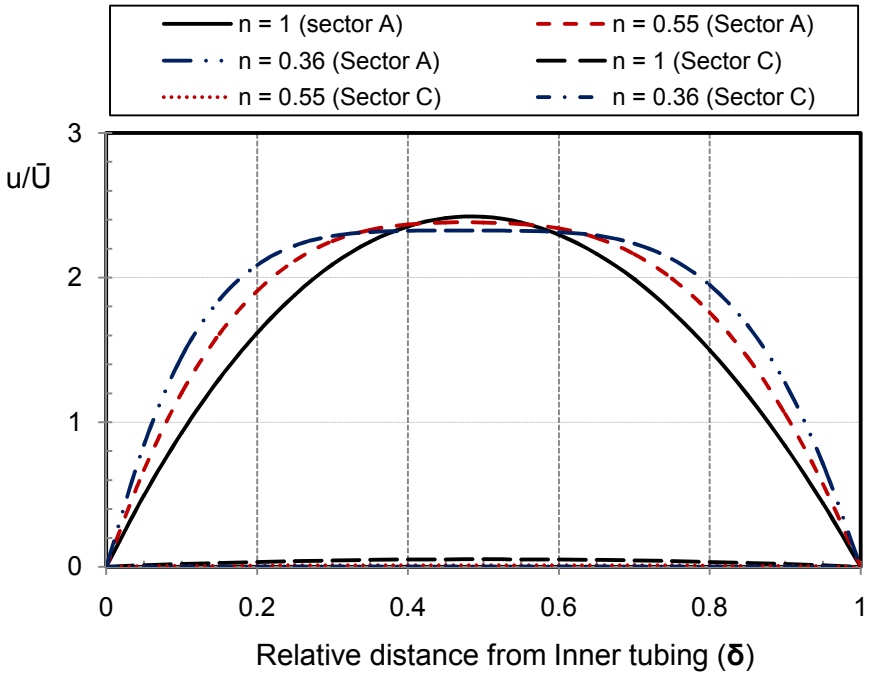

Figure 3.26 Axial velocity profile of Newtonian and non-Newtonian fluids (sector A & C), N_{Reg} = 800, ε = 0.75, k = 0.8.

3.6.3 Viscosity Profiles

Fluid viscosity is an important parameter for most oilfield operations, especially when there is need to transport solid particles (drill-cuttings or proppants) up or down the wellbore annulus. The local value of the viscocity is essential in quantifying the ability of a particular fluid to effectively alter the slip velocity of particles, and prevent wellbore problems that could result from the settling of particles. We have already shown that the Non-Newtonian fluids (Guar polymer solutions) investigated in this study exhibit shear thinning behavior, hence, the existence of a velocity profile implies that there is also a shear rate profile, and consequently, a viscosity profile. Figures 3.27 and 3.28 present the viscosity profile (sector A and B) for 20 lb/Mgal Guar fluid at various values of eccentricity. One feature of note is that the viscosity profile in a concentric annulus is the same for all sectors (A, B and C), while it is considerably

reduced in sector B, as soon as the annulus becomes slightly eccentric. Similar trends are observed for 30 lb/Mgal Guar fluid (Figures 3.29 and 3.30), 40 lb/Mgal Guar fluid (Figures 3.31 and 3.32) and 60 lb/Mgal Guar fluid (Figures 3.33 and 3.34). Compared to the maximum fluid viscosities calculated for the wide (A) and narrow (C) gaps in an eccentric annulus, about 42, 60, 78 and 90% reductions in the maximum fluid viscosity were observed in the widening gap (B) for 20, 30, 40 and 60 lb/Mgal guar gels respectively. This explains the cuttings transport disparity that exist between concentric and eccentric annuli, where significant amount of cutting beds are observed for an eccentric annulus while operating with non-Newtonian fluids that produced effective cuttings transport in corresponding concentric annular geometries.

Figure 3.35 shows the molecular viscosity profile (sector A and C) for the laminar flow of non-Newtonian fluids in a 50% eccentric annulus. The maximum viscosity calculated for both sectors A and C were the same. However, they are lower near the walls and higher in mid annulus. This is expected behavior of shear thinning fluids, as a steep velocity profile near the walls is an indication of high shearing (lower viscosity) while a flattened velocity profile in the mid annulus means low shearing (higher viscosity). It is evident that the often utilized apparent viscosities, which are usually calculated near the pipe walls, are much lower than the prevailing viscosity profile in the flow area. This is in agreement with the results obtained by Haciislamoglu, (1989).

The importance of using four concentrations of guar polymer solution lies in the use of reliable values for the limiting viscosities e.g. $\boldsymbol{\eta}_{max}$ and $\boldsymbol{\eta}_{min}$, as no significant difference was observed as a result of varying the flow consistency index, K with n.

This is the expected behavior, same as the behavior of viscous Newtonian fluids and water, which follow the same trend, i.e. n = 1. Molecular viscosity profile plots for various diameter ratios are also presented in Appendix B.

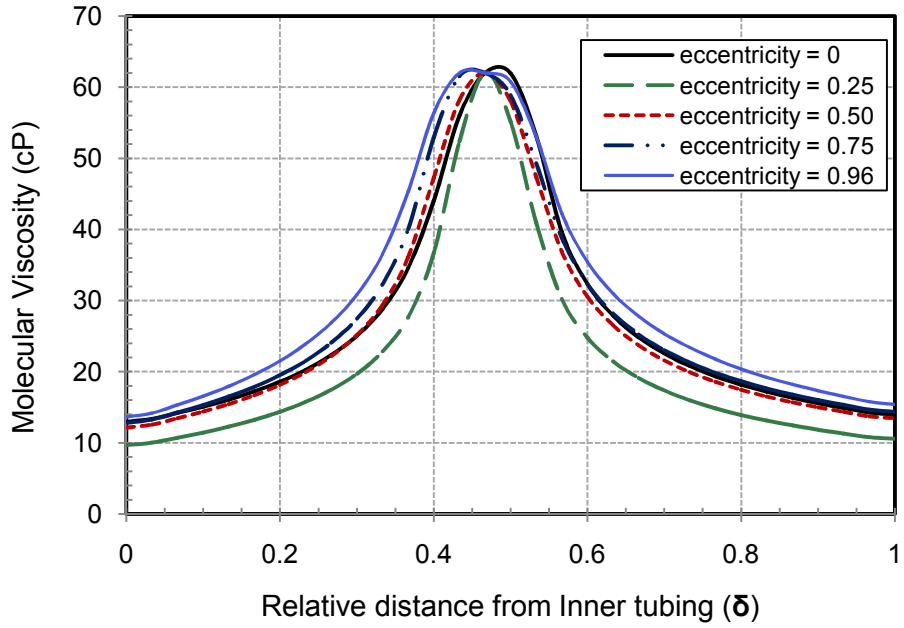

Figure 3.27 Molecular viscocity profile of 20 lb/Mgal guar (n = 0.65) for sector A, N_{Reg} = 800, k = 0.64.

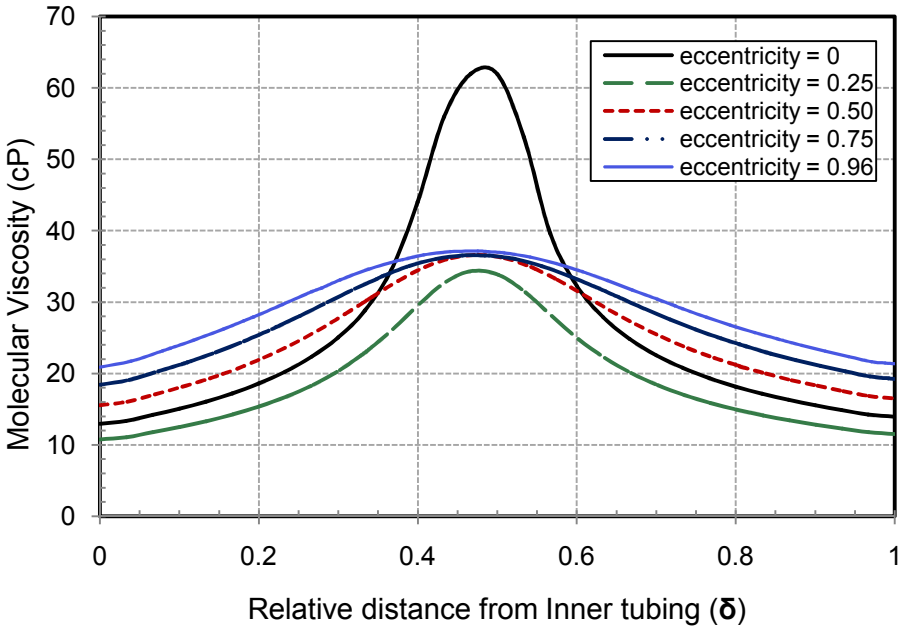

Figure 3.28 Molecular viscocity profile of 20 lb/Mgal guar (n = 0.65) for sector B, N_{Reg} = 400, k = 0.64

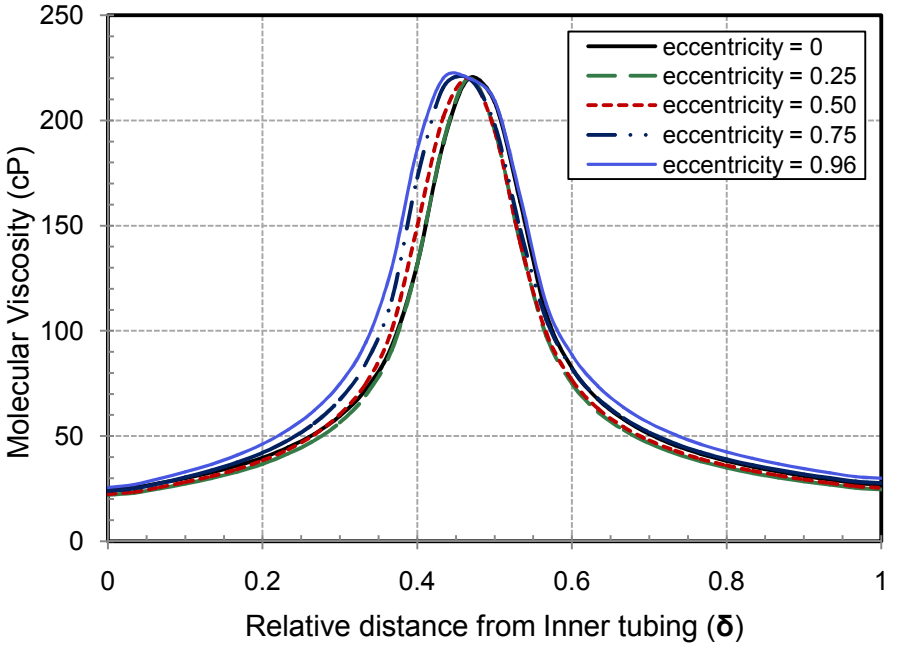

Figure 3.29 Molecular viscocity profile of 30 lb/Mgal guar (n = 0.55) for sector A, N_{Reg} = 400, k = 0.64

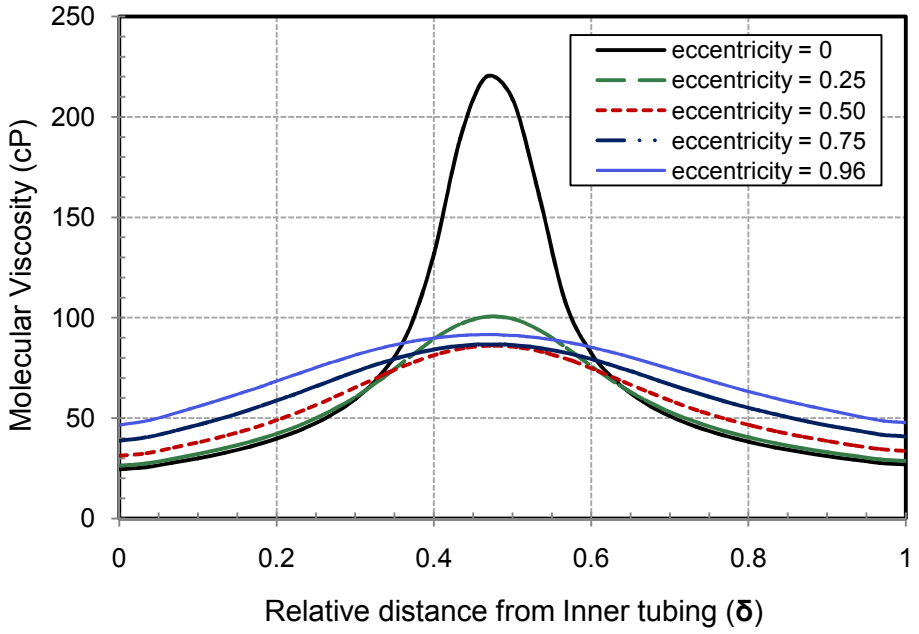

Figure 3.30 Molecular viscocity profile of 30 lb/Mgal guar (n = 0.55) for sector B, N_{Reg} = 400, k = 0.64

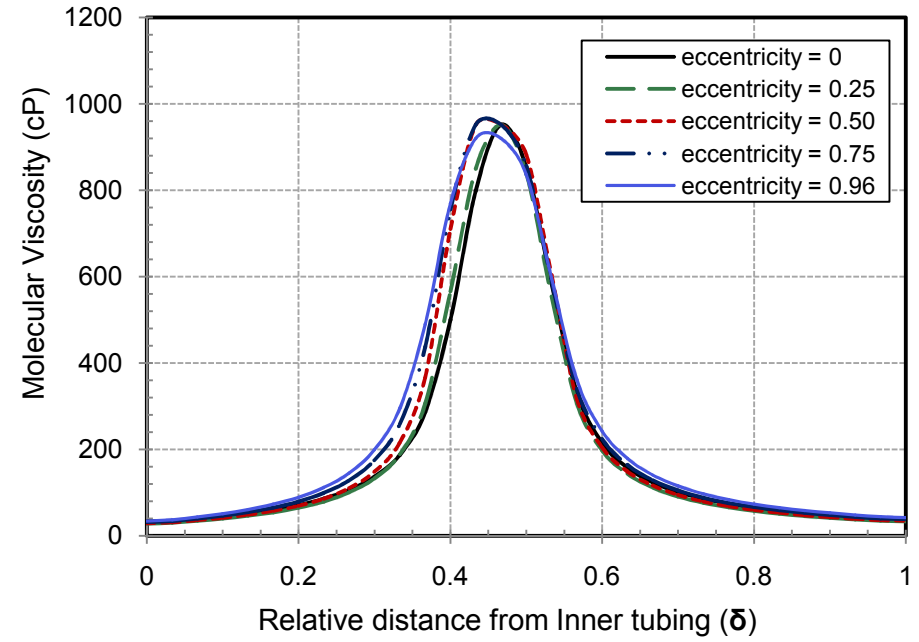

Figure 3.31 Molecular viscocity profile of 40 lb/Mgal guar (n = 0.46) for sector A, N_{Reg} = 265, k = 0.64.

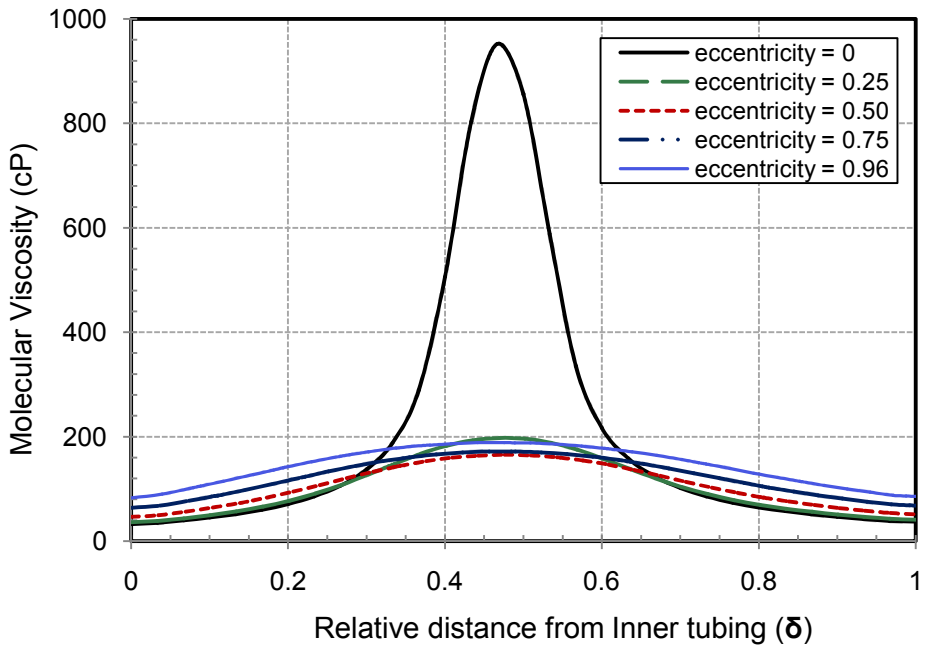

Figure 3.32 Molecular viscocity profile of 40 lb/Mgal guar (n = 0.46) for sector B, N_{Reg} = 265, k = 0.64.

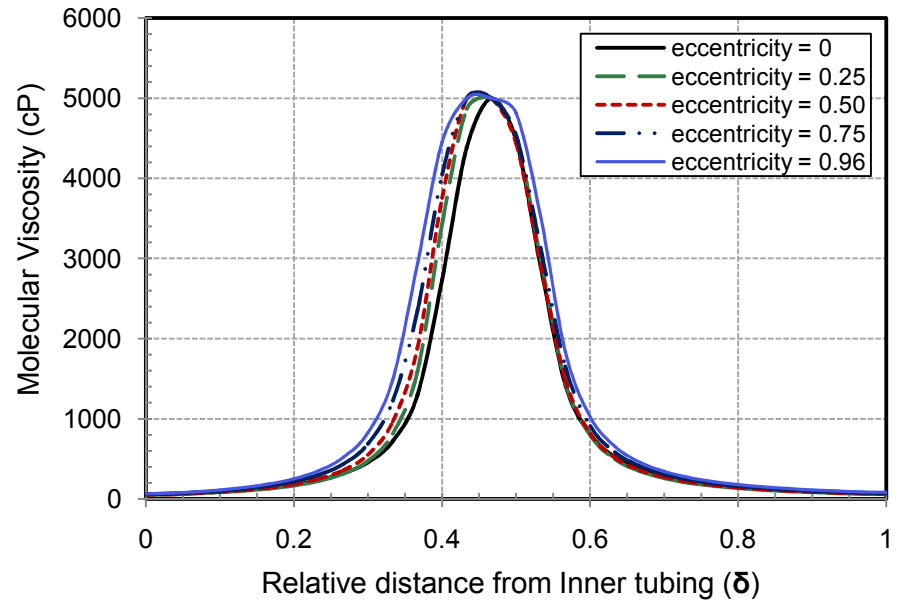

Figure 3.33 Molecular viscocity profile of 60 lb/Mgal guar (n = 0.36) for sector A, N_{Reg} = 124, k = 0.64.

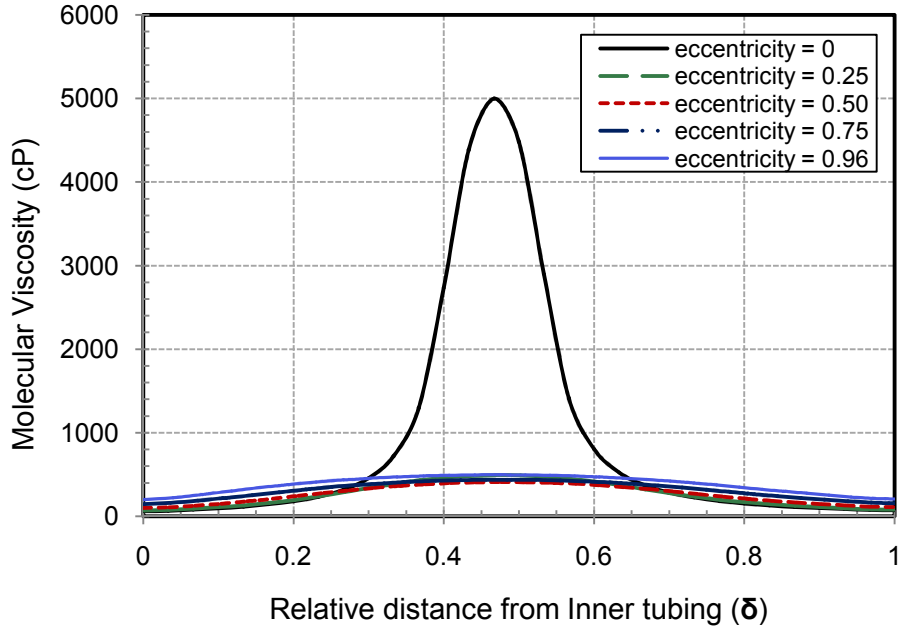

Figure 3.34 Molecular viscocity profile (sector B) for the laminar flow of 60 lb/Mgal guar (n = 0.36), N_{Reg} = 124, k = 0.64.

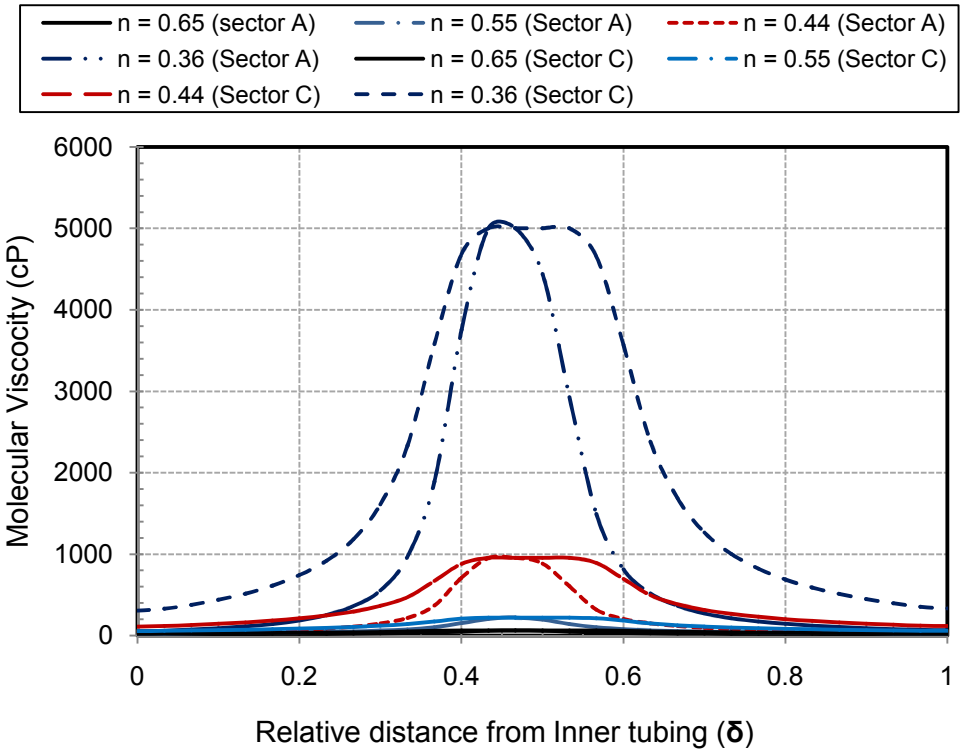

Figure 3.35 Molecular viscocity profile (sector A and C) for the laminar flow of non-Newtonian fluids, N_{Reg} = 800, ε = 0.5, k = 0.64.

3.6.4 Frictional Pressure Losses

For data analysis, the calculated differential pressure gradient versus flow rate data were reduced in terms of Fanning friction factor and generalized Reynolds number. Fanning friction factor, *f*, is a dimensionless variable used to determine friction pressure gradient in pipe and annular flow. This variable is given by the following expression for annular flow:

$$f = 154.6483 \frac{(d_2 - d_1)(d_2^2 - d_1^2)^2 \Delta p}{l \rho q^2} \tag{3.9}$$

The generalized Reynolds number, N_{Reg}, is used for non-Newtonian fluids:

$$N_{\mathrm{Re}g} = \left(\frac{1}{12}\right)^n \frac{7.48052}{32.17 \times 8^{n-1}} \frac{d_{eff}^{\,n} v_a^{2-n} \rho}{K} \tag{3.10}$$

Where n is the power law flow behavior index, K is the fluid consistency index ($lbfsec^n/ft^2$), V_a is the average fluid velocity (*ft/sec*), d_{eff} is the effective diameter of the eccentric annulus. The effective diameter approach introduced by Reed and Pilehvari (1993) for non-Newtonian fluid flow in concentric annulus is used in this study.

At a constant flow rate, the differential pressure gradients for an annulus decreased as eccentricity increases. This is evident on the plots of Fanning friction factor versus generalized Reynolds number for 40 lb/Mgal guar fluids presented in Figures 3.36 - 3.39. The effect of eccentricity is represented by a downward shift of data from the classical Hagen-Poiseuille equation, i.e., the $16/N_{Reg}$ line. To assess the impact of the flow behavior index on frictional pressure gradients in partially eccentric annuli, plots of Fanning friction factor versus generalized Reynolds number for the laminar flow of a Newtonian fluid, and 20, 30, 40 and 60 lb/Mgal guar fluids are

presented in Figure 3.40. As fluids are more shear thinning (decreasing n), their velocity profiles become flatter; thus, increasing their overall viscosity in the narrow and wide parts of an eccentric annulus (Haciislamoglu, 1989). Consequently, these fluids are subject to less reduction in frictional pressure gradients in eccentric annulus. Similarly, Figure 3.41 shows the effect of diameter ratio on the flow behavior of 60 lb/Mgal guar fluid in an eccentric annuli (Table 3.2, case b, eccentricity = 0.96). Notably, at a constant generalized Reynolds number, the Fanning friction factors decreases as diameter ratio increases within the range investigated.

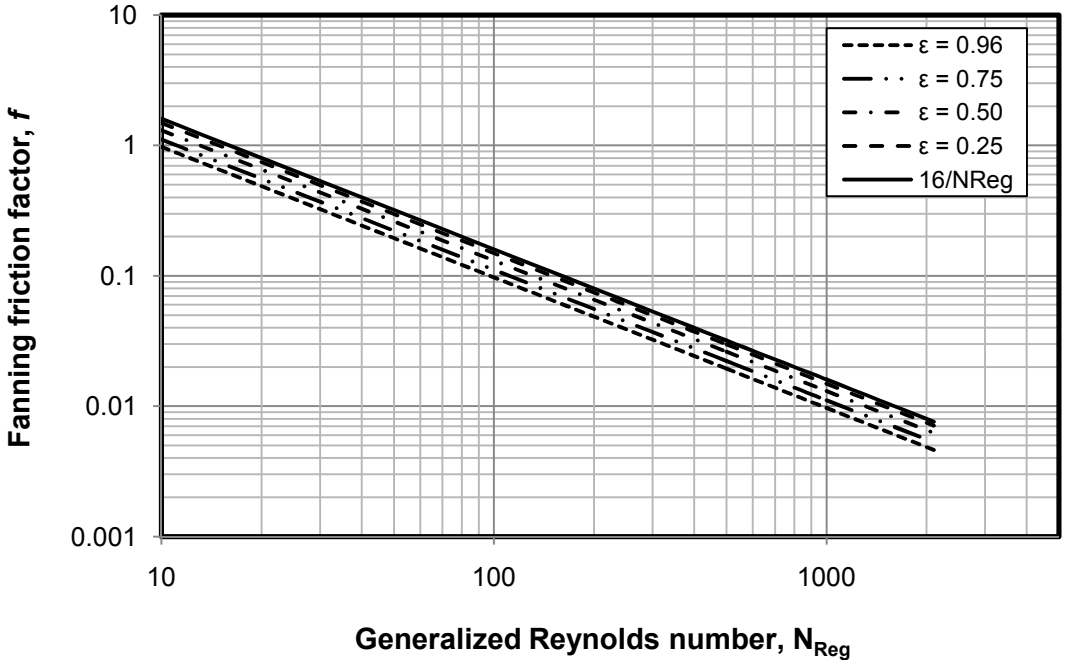

Figure 3.36 Effect of eccentricity on the flow behavior of 40 lb/Mgal guar fluid for the case of k = 0.333.

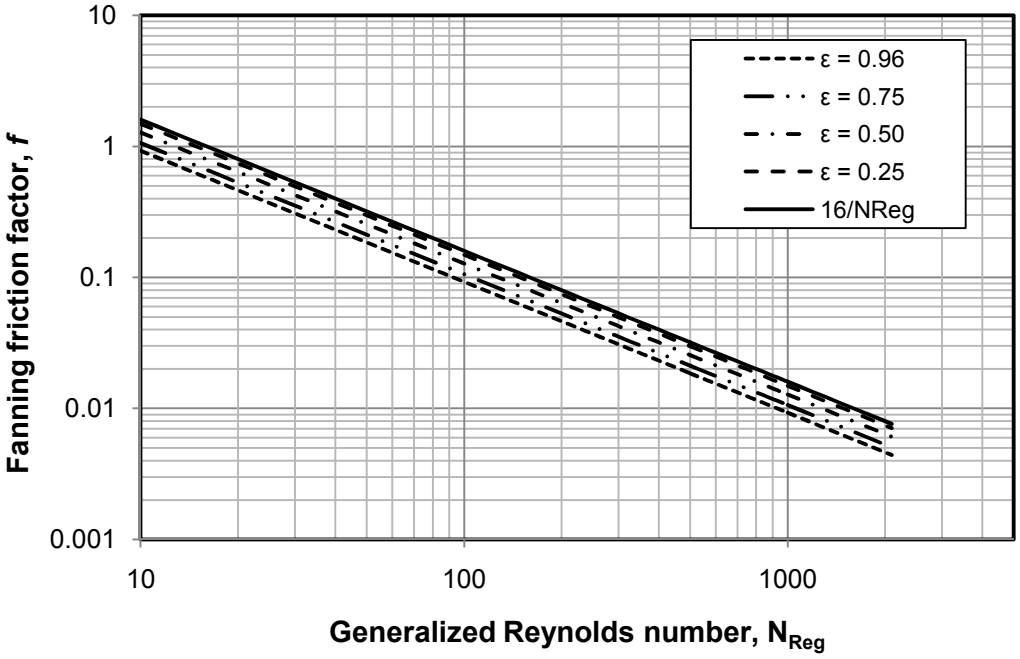

Figure 3.37 Effect of eccentricity on the flow behavior of 40 lb/Mgal guar fluid for the case of k = 0.5.

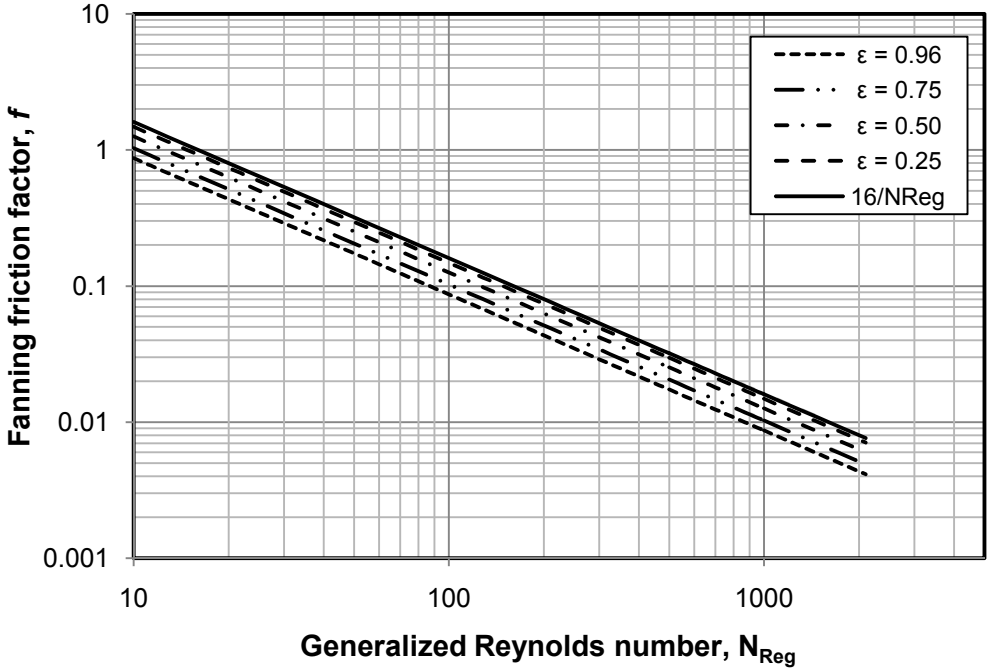

Figure 3.38 Effect of eccentricity on the flow behavior of 40 lb/Mgal guar fluid for the case of k = 0.6364.

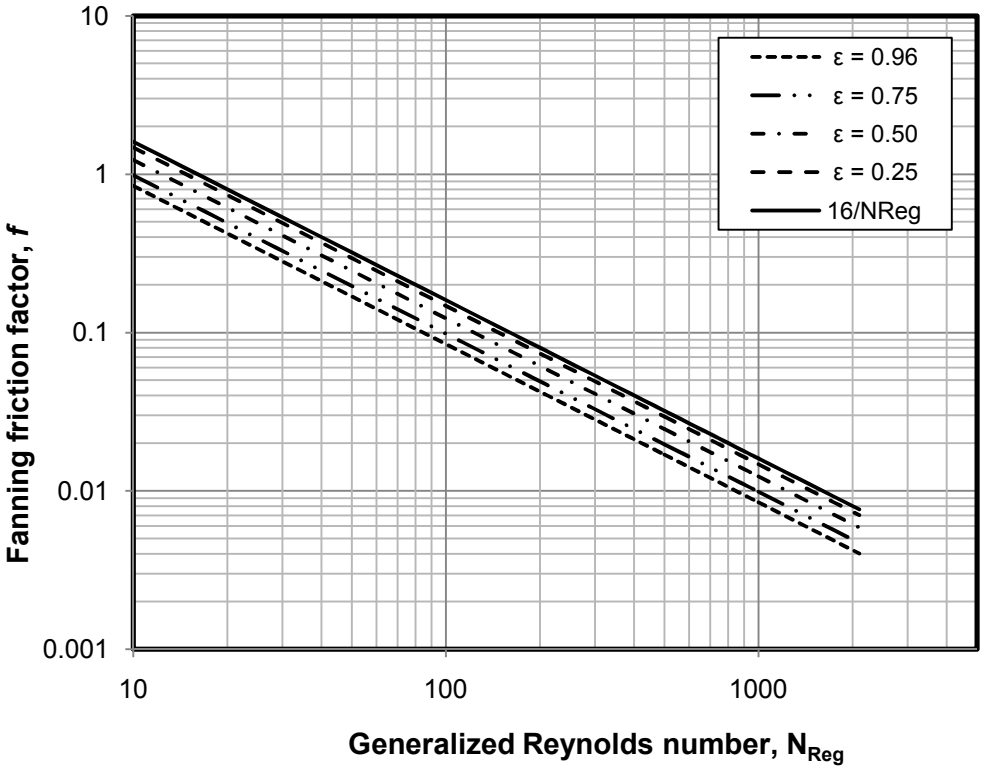

Figure 3.39 Effect of eccentricity on the flow behavior of 40 lb/Mgal guar fluid for the case of k = 0.8.

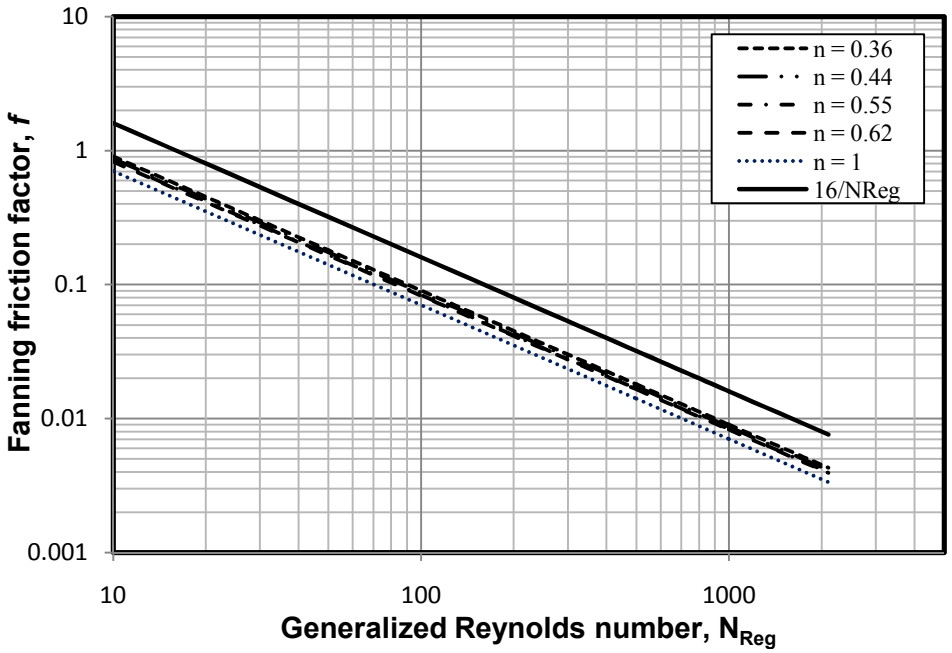

Figure 3.40 Fanning friction factor versus generalized Reynolds number for Newtonian and non-Newtonian fluids flowing through an eccentric annuli (k=0.64, ε = 0.96).

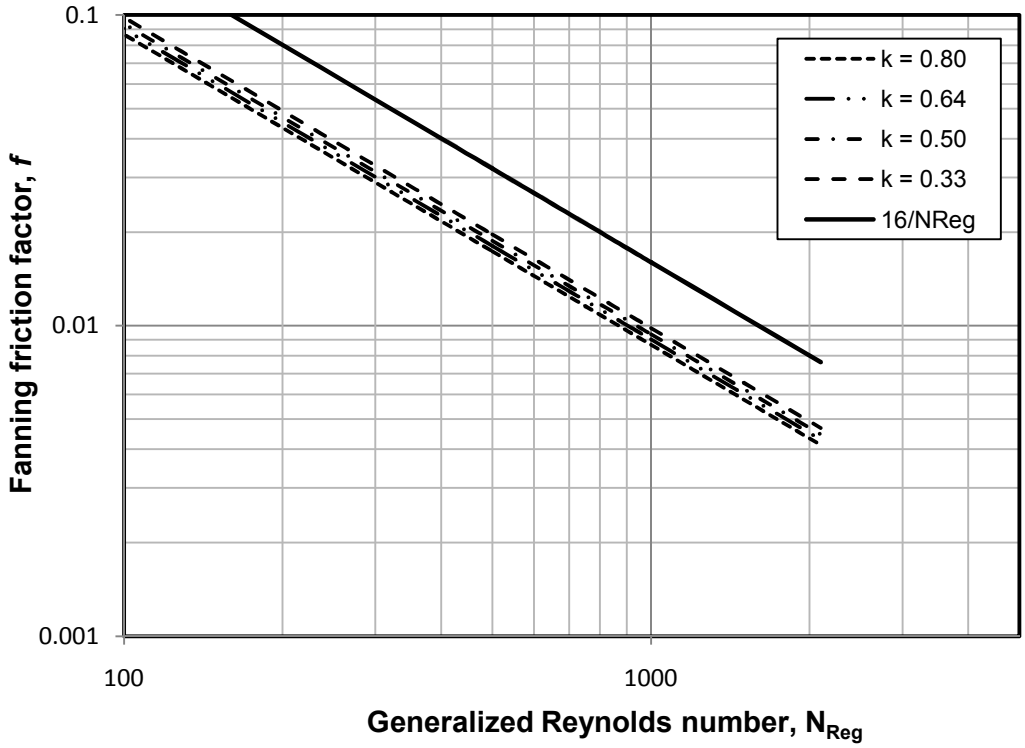

Figure 3.41 Effect of diameter ratio on the flow behavior of 60 lb/Mgal Guar fluid in eccentric annuli (k = 0.64, ε = 0.96)

Comparison with Haciislamoglu et al. Correlation: Several authors (Bern et al., 2007; Bailey and Peden, 2000) have referenced Haciislamoglu et al correlation (*Equation 2.5*), which happens to be the only available explicit friction pressure correlation that accounts for the effect of eccentricity for the annular flow of non-Newtonian fluids. Therefore, it would be useful to compare our result with this correlation. Figures 3.42 and 3.43 show the plots of reduction in friction pressure losses for Haciislamoglu et al. correlation, and the results of this study at diameter ratios of 0.33 and 0.5 respectively. A good agreement is obtained, especially at low values of eccentricity. However, data from the CFD model yields a slightly lower friction pressure, at high eccentricities. The difference is likely due to the complexity of the flow geometry as eccentricity increases and the ability of the model set-up to resolve the flow field accurately. The use of

unstructured mesh (Hybrid) adopted in this study for highly eccentric geometries is very robust; hence, the observed trend is reliable.

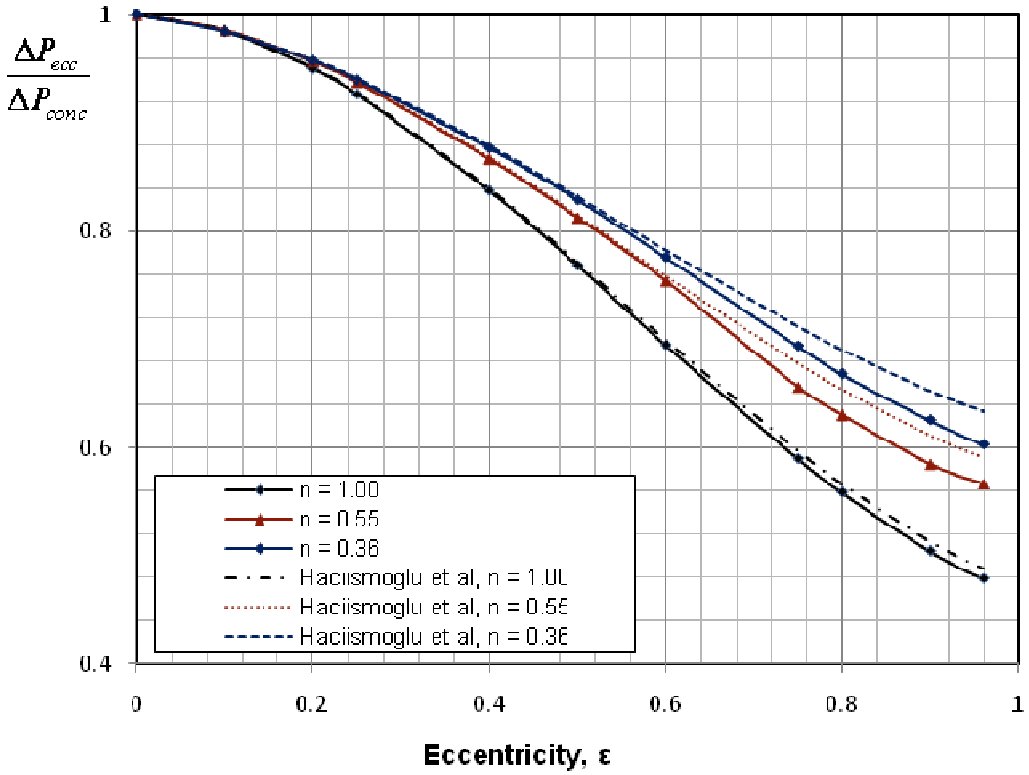

Figure 3.42 Reduction in friction pressure loss in an annulus for the case of k=0.33.

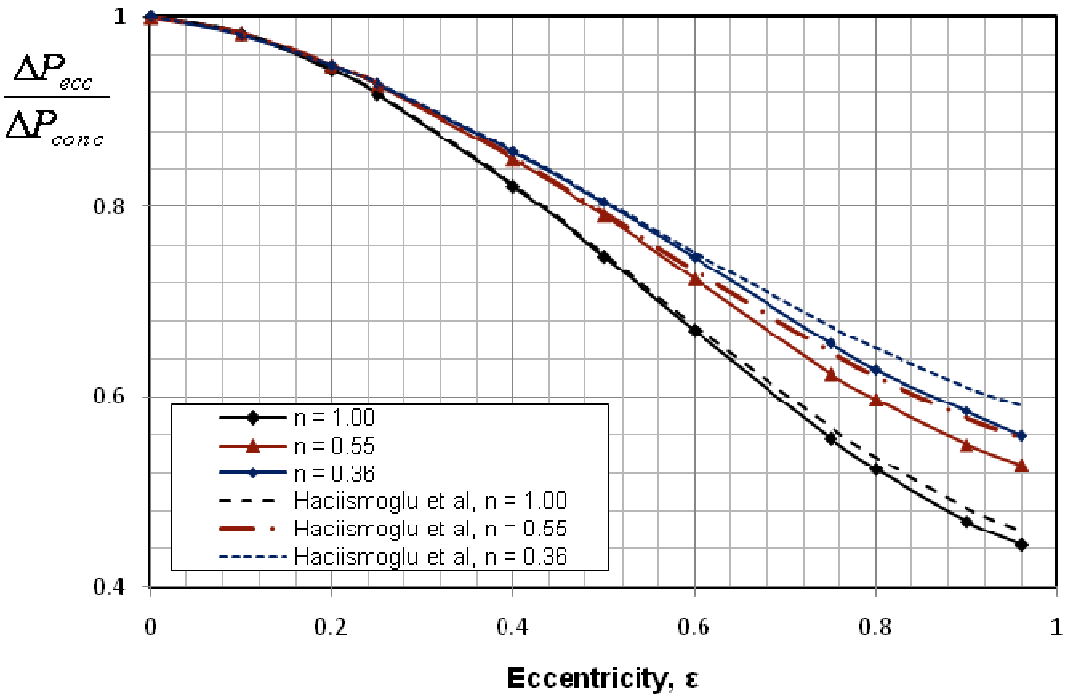

Figure 3.43 Reduction in friction pressure loss in an annulus for the case of k=0.5.

3.6.3.1 Development of Fanning Friction factor correlation

Data obtained for diameter ratios of 0.3 to 0.8, eccentricities from 0 to 0.96, and flow behavior index of 0.36 to 1.0 are reduced to dimensionless Fanning friction factors and generalized Reynolds number. Haciislamoglu et al. correlations were also used at low eccentricity to increase the data bank for improving the existing correlation. Friction pressure data for steady, incompressible, isothermal, fully developed laminar flow of non-Newtonian Power law fluids (20, 30, 40 and 60 lb/Mgal guar fluids) in eccentric annuli from CFD simulations are correlated using the following parameters; Fanning friction factor, f, generalized Reynolds number, N_{Reg}, flow behavior index, n, and diameter ratio, ($k = d_2/d_1$). The data are fitted with a Blasius-type expression using

nonlinear regression analysis. Commercially available curve fitting software, LAB Fit, was used in developing the correlation. The correlation is expressed as:

$$f = \frac{\alpha}{N_{Reg}} \tag{3.11}$$

$$\alpha = 16\left[1 - 0.0597\frac{\varepsilon}{n}\left(\frac{d_1}{d_2}\right)^{0.5077} - 1.557\varepsilon^2\sqrt{n}\left(\frac{d_1}{d_2}\right)^{0.2398} + 0.97\varepsilon^3\sqrt{n}\left(\frac{d_1}{d_2}\right)^{0.3289}\right] \tag{3.12}$$

A cross plot of computed Fanning friction factor from new correlation and CFD data is presented in Fig. 3.44. Majority of the predictions are within ±2%. The ±5% lines are drawn on the plots to show that only a few data points are outside the ±5% lines. This figure further confirms the accuracy of the proposed correlations.

3.6.3.2 Evaluation of New Correlation

Comparison with Experimental data: Figures 3.45 – 3.47 show the plots of Fanning friction factor vs. generalized Reynolds number for guar solutions in 3 ½-in. × 1 ¾-in. eccentric annulus. They compare the experimental data of Ogugbue and Shah (2009) and the predictions by the new correlation and by Haciislamoglu et al. correlation. The rheological properties of guar fluids are given in Table 3.1. Aside from some outliers, esp. at low flow rates, it can be observed that there is good agreement between the experimental data and the predictions by the new correlation of this study. It is found that the deviations between the predicted and the experimental friction factors are

generally within 10% for the new correlation and within 15% for Haciislamoglu et al. correlation.

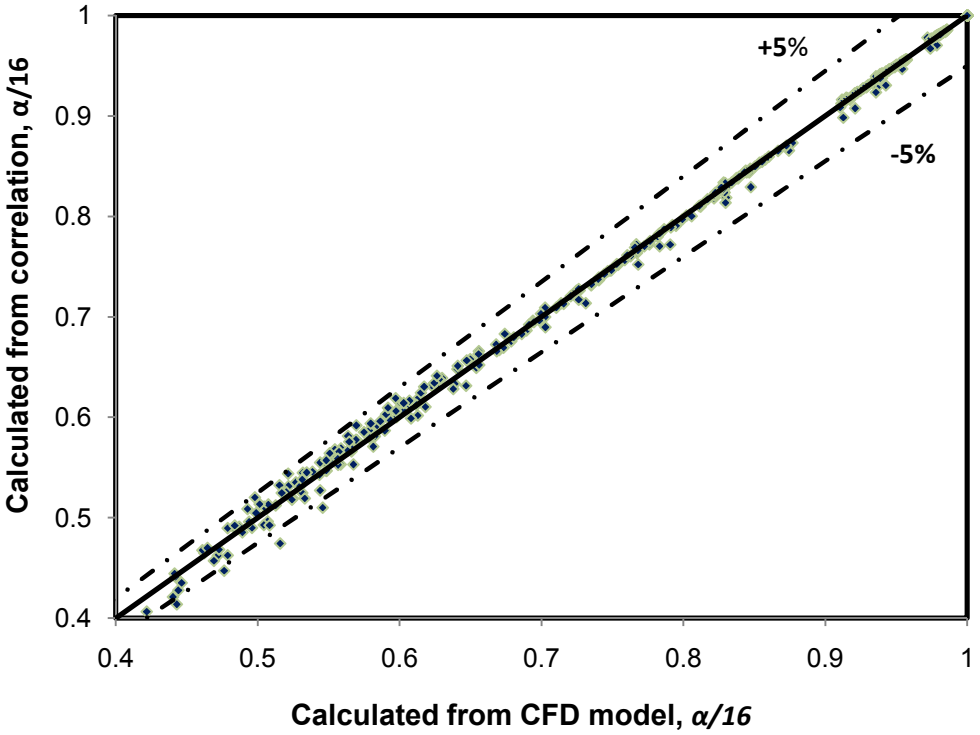

Figure 3.44 Fanning friction factor computed from new correlation and CFD data.

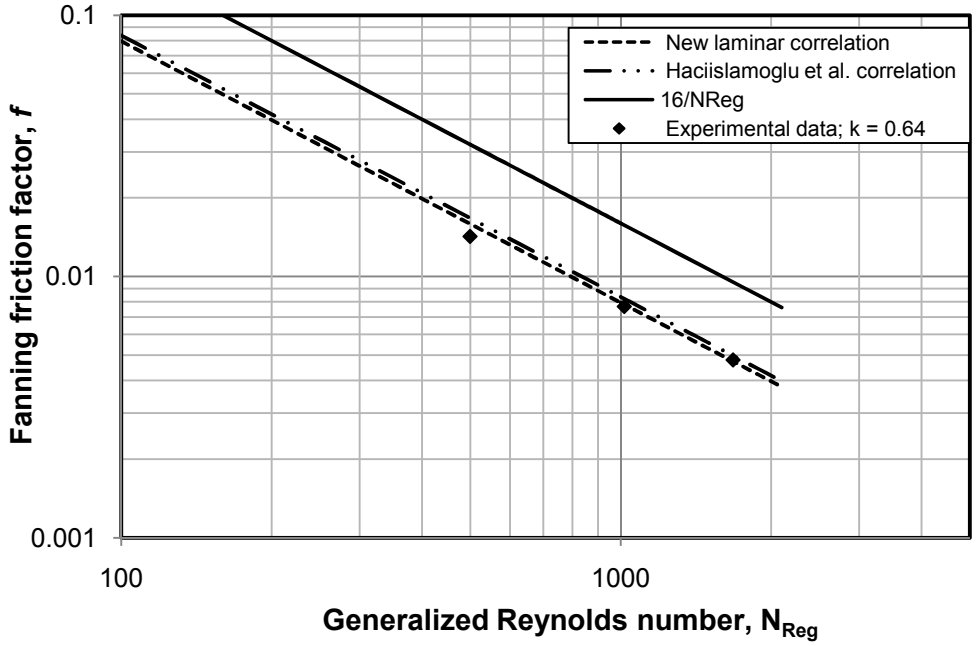

Figure 3.45 Fanning friction factor for 30 lb/Mgal Guar fluid in a fully eccentric annulus.

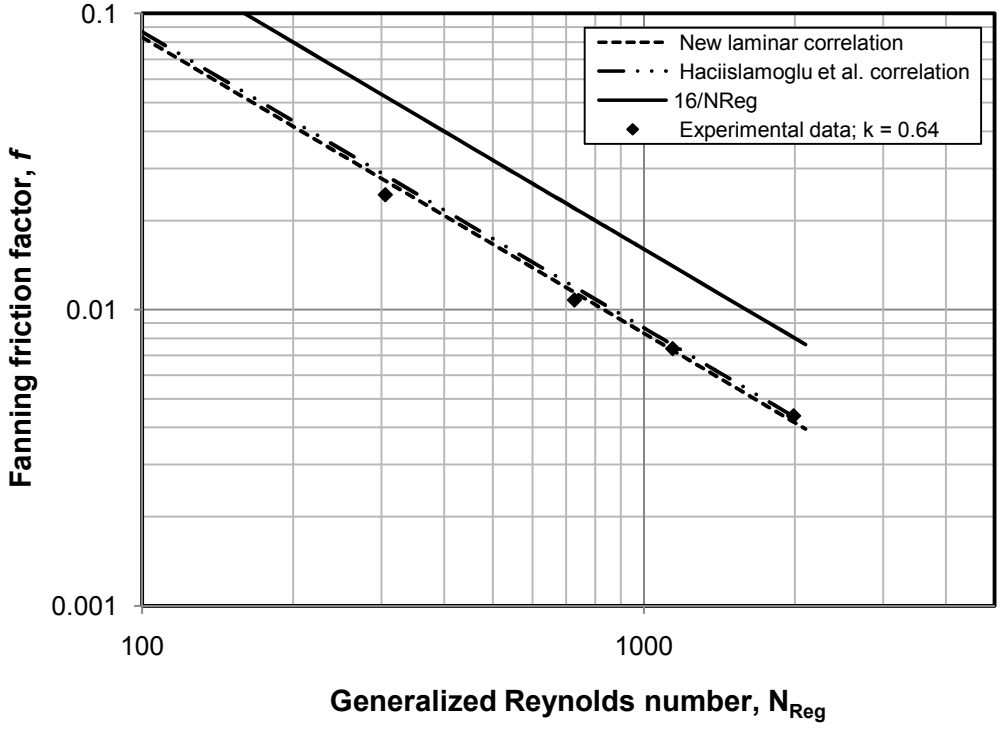

Figure 3.46 Fanning friction factor for 40 lb/Mgal Guar in a fully eccentric annulus.

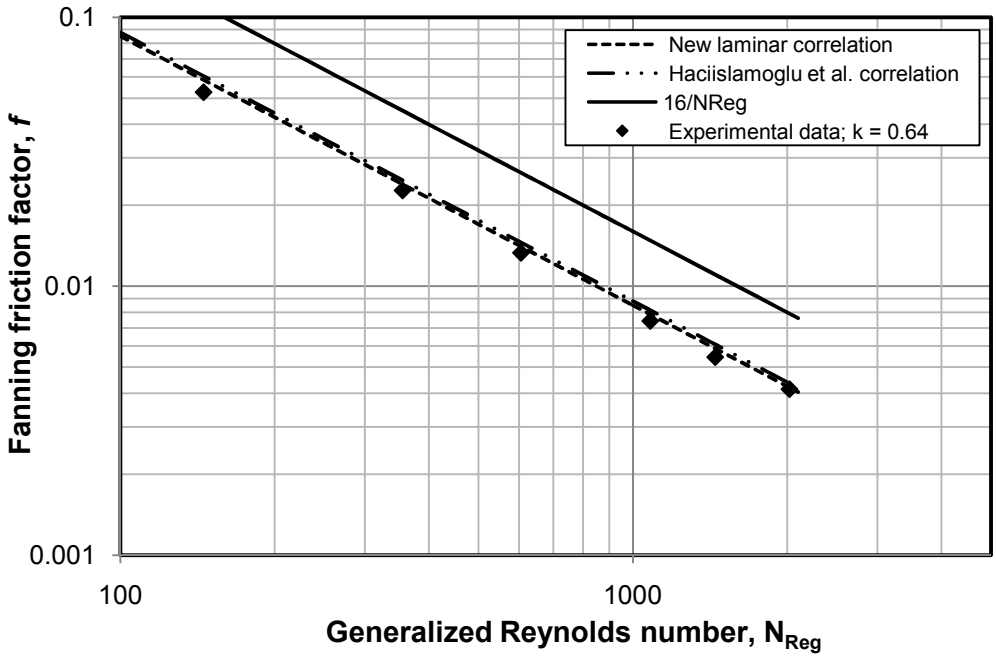

Figure 3.47 Fanning friction factor for 60 lb/Mgal Guar fluid in a fully eccentric annulus.

3.8 Summary

The computational investigation of flow in an eccentric annulus, with Newtonian and non-Newtonian fluids, presents a contribution to the understanding of the flow field occurring during fully-developed laminar flow conditions. The flow patterns revealed by CFD analyses agree well with the previous experimental and numerical studies. First, the velocity profile for non-Newtonian fluids are slightly flattened compared with that for a Newtonian fluid. Second, unlike the uniform velocity profile applicable for every sector in a concentric annulus, the axial velocity profile for an eccentric annulus is distorted and the peak velocities vary with location. A general reduction in the magnitude of the flow velocity as the gap between the cylinders is reduced is observed, i.e. the velocity in the narrow section of an eccentric annulus is reduced, as more fluids rushes to the zone of least resistance (wide section). Moreover, as eccentricity increases

beyond 0.75, a high velocity zone persist in the wide region (sector A) while the velocities near the narrow bottom portions (sector C) are practically zero (Figure 3.24 and 3.26). Therefore, judging from the prevailing local generalized Reynolds number, it is evident that both laminar and turbulent flow conditions can exist across an eccentric annulus at the same time. A virtual inspection of the velocity profiles in an eccentric annulus shows that the zone of highest shear exists across sector B, and noticeably accompanied by a considerable reduction in viscosity (Figure 3.28, 3.30 and 3.32). This is the expected behavior of shear thinning fluids, and if combined with the reduced velocity in the narrow sections of an eccentric annulus, reasonably explains the cuttings transport disparity that exist between concentric and eccentric annuli, where significant amount of cutting beds are observed for an eccentric annulus while operating with shear-thinning non-Newtonian fluids that produced an effective cuttings transport in the corresponding concentric annular geometry.

The friction pressure gradients of non-Newtonian laminar flow predicted by CFD modeling agree well with the flow data of field-scale experiments (Figure 3.45). A new friction factor correlation for Newtonian and non-Newtonian fluid flow in annular sections with varying eccentricity has been developed based on the results of CFD simulation. The simulation result of friction pressure gradients of Newtonian and non-Newtonian laminar flow was also verified with published correlations.

CHAPTER 4

EXPERIMENTAL SETUP

4.1 Introduction

Experimental studies constitute an essential part of the research group at Well Construction Technology Center (WCTC), University of Oklahoma. Over the years, the equipment at this research facility has permitted this research group to carry out several experimental investigations and develop correlations on the characterization of fluid friction and fluid behavior of various fluid systems. Polymer fluids typically used in drilling, completion, and stimulation applications are usually the major, if not the only, subject of interest. Linear polymer solutions, cross-linked fluids, proppant slurries, surfactant based fluids, foam fluids, fracturing fluids and drilling muds have all been investigated one time or the other at WCTC. Basically, the study of friction pressure losses of non-Newtonian fluids in eccentric annulus is an integral part of the present Coiled Tubing Consortium (CTC) established at WCTC. In the present study, guar gum, a water soluble bio-polymer, typically used in oilfield applications is utilized to investigate the flow behavior of non-Newtonian Power-law fluids in a fully eccentric annulus.

In addition to annular flow experiments, characterization of the fluids rheological properties is another important aspect of the experimental investigation. Fann Model 35 viscometers were used for rheological measurements at ambient temperatures. This chapter presents the experimental flow loops, fluid mixing and pumping equipment, measurement instruments, data acquisition system, and rheology measuring system. The functions and capabilities of various components of the

experimental set up are described. The fluid systems and experimental procedures are also discussed.

4.2 Field-Scale Experimental Setup

Figure 4.1 shows the schematic of the field scale flow loop, which is located at the Well Construction Technology Center. The field scale test loop consists of concentric and eccentric annuli, a 200-ft 1 ½-in. (ID=1.188 in.) straight tubing, fluid mixing and storage tanks, fluid pumping equipment and data acquisition system.

4.2.1 Eccentric Annular Sections

In this research, four (4) eccentric annular sections were designed and constructed to study friction pressure losses in fully eccentric annuli. The dimensions of these annular sections are shown in Table 4.1. Figure 4.2 shows the layout of the eccentric annular sections at the Well Construction Technology Center (WCTC). For a fully eccentric annulus, the inner pipe was welded at the bottom of the outer pipe and eccentricity is equal to one.

4.2.2 Fluid Mixing and Pumping System

Two 50-bbl capacity fluid mixing and storage tanks are mounted on a MX-5000 trailer unit, shown in Figure 4.7. Each mixing tank has hydraulically-driven paddles to ensure proper mixing of fluids, which is important in fluid preparation. One of these tanks is used to prepare and store the test fluid while the remaining tank is used to store water either for water test or to flush the system. The mixing tanks have pneumatic control panels to adjust the blending paddle speed and to operate valves for diverting test fluid or water from each tank into the flow loop. A 150-bbl disposal tank is also available for storing spent test fluid for subsequent disposal.

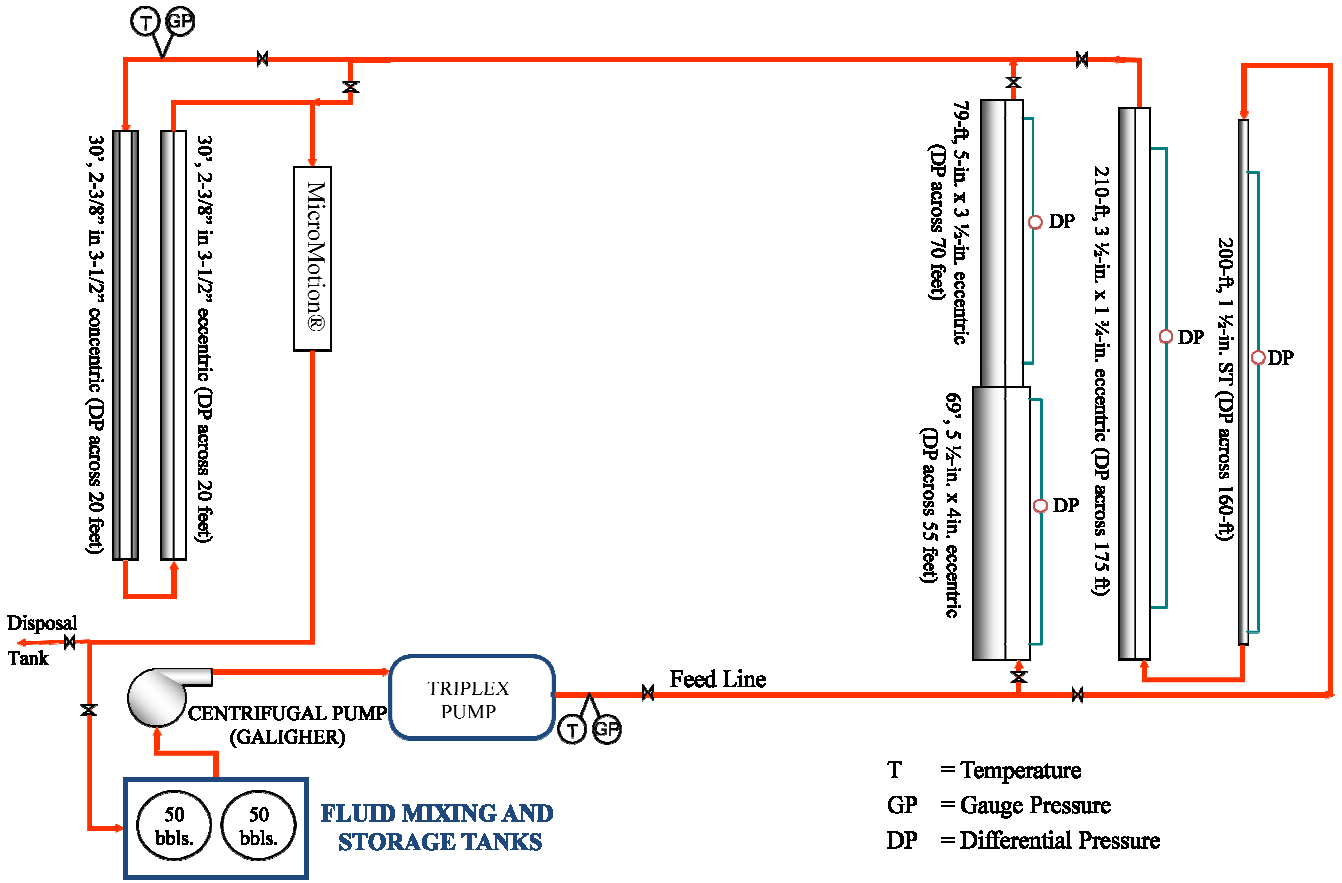

Figure 4.1 Schematic of Experimental Setup.

Table 4.1 Dimensions of Eccentric Annular Sections in Field Scale Flow Loop.

S/N	Casing ID (in.)	Tubing OD (in.)	Length (ft)	Diameter ratio, k
1	3.094	2.375	30	0.77
2	2.75	1.75	210	0.64
3	5	3.5	79	0.82
4	5.5	4	69	0.82

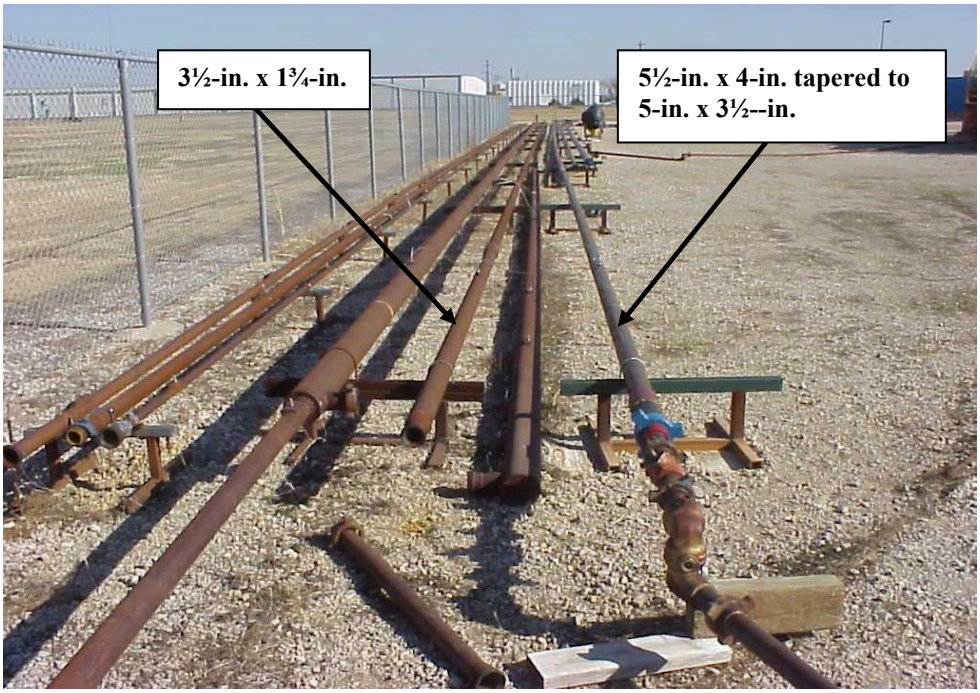

Figure 4.2 Eccentric Annular sections.

Figure 4.3 Two 50-bbl fluid mixing and storage tanks.

The pumping system used for this research is the high pressure Schlumberger B804 triplex plunger pump (Fig. 4.8), which can pump fluid up to 10,000 psi and 290 gpm (6.9 bbl/min) flow rate. A Galigher centrifugal pump, shown in Fig. 4.9, is used to boost the suction of the triplex pump by maintaining a constant supply of fluid to it. The centrifugal pump is also used during test fluid disposal and as an aid in mixing the fluid.

Figure 4.4 Schlumberger B804 triplex plunger pump.

Figure 4.5 Galigher centrifugal pump.

4.2.3 Measurement Instruments

The main data collected during each flow test included: flow rate, differential pressures across eccentric annuli, fluid density, fluid temperature, and system pressure. Standard data reduction methods were employed to establish confidence limits for this

experimental study. MicroMotion flow meters, Honeywell differential transducers, and absolute pressure transducers were among the instruments utilized in this study. Ahmed Kamel (2008) carried out a detailed error analysis and reported that the maximum percentage error for Fanning friction factor and Reynolds number obtained using these equipment were less than 3.6% and 2.4% respectively. The following sections provide a detailed description of the equipment available for data acquisition and measurement system.

4.2.3.1 Micro Motion Flowmeters

Two Micro Motion flow meters that are capable of providing flow data such as mass flow rate, volumetric flow rate, density and temperature have been used in this research study. Specifications for these instruments are shown in Table 4.2.

Table 4.2 Specifications of Micro Motion Flowmeters.

Item	Flowmeter 1	Flowmeter 2
Model	DL200 S228SU	DS300 S157SU
S/N	154891	251696
Flow rate range, gal/min	0 - 420	0 - 840
Flow rate accuracy, %	±0.15	±0.15
Temperature accuracy, ^{o}C	±0.1	±0.1
Density accuracy, g/cm^{3}	±0.0005	±0.0005
Operating pressure, psi	740	740

4.2.3.2 Differential Pressure and Absolute Pressure Transducers

In this research, the differential pressure losses are recorded with Honeywell differential pressure transducers. These instruments are the most important for measuring frictional pressures across various annular sections. The field scale test facility requires that the

differential pressure transducers are capable of working efficiently in high pressure environments with good precision. Table 4.3 lists the differential pressure and absolute pressure transducers used for pressure measurements during this study.

Table 4.3 Differential pressure and absolute pressure transducers used in this study.

No.	Quantity	Model	Max. Span (psi)	Min. Span (psi)	Rating (psi)	Accuracy*	Usage
1	2	STD170V	0 - 3000	0 - 100	6000	±0.15%	200 ft ST
2	1	STD170G	0 - 3000	0 - 100	3000	±0.15%	200 ft ST
3	2	(1) STD130V (2)YSTD130G	0 - 100	0 - 5	6000	±0.075%	Annular sections
4	4	(3) STD130G (1)STD130V	0 - 100	0 - 5	6000	±0.075%	Annular sections
5	2	STG98LC	0 - 6000	0 - 500	9000	±0.10%	System pressure

* expressed in percentage of calibration span.

4.2.4 Data Acquisition System

The measured data from the flowmeters and pressure transducers are collected and transmitted to a computing system, where the data was displayed and saved for later analysis, through a wireless data logger. The wireless logging system consists of a Fluke Hydra data acquisition system, model 2625A, manufactured by Fluke Corporation, Everett, WA. The Fluke Hydra system contains two hydras, each having 21 analog measurement channels. The logging system is also equipped with a wireless

modem radio link in order to communicate with the host computer within a 1200 ft covering radius. Notably, sample rate is up to 10 samples per second.

The software of the data acquisition system provides the option of displaying the data signals graphically. This feature is used to monitor the trends of measured variables and make proper decisions and adjustments during an experiment, e.g. whether data measured is within the prevailing differential pressure span on the transducers. Moreover, through virtual inspection of the signals in real time, the operator can determine when to change from one flow rate to another.

4.3 Rheometers

Figure 4.10 shows the twelve rotor speeds (No. 1/5th torsion spring) Fann Model 35 viscometers used in this study. The viscometer consists of two cylinders: an outer rotating cylinder (rotor) and an inner stationary cylinder (bob). By means of a cup that could be raised or lowered, test sample is introduced into the annular space between the two cylinders. Shear is then applied by rotating the outer cylinder- the rotor. The torque is balanced by a helical wound precision spring where its deflection can be read on a calibrated dial at the top of the viscometer. For a given bob-rotor geometry and given torque spring, the rotational speed of the rotor (measured in rpm) can be converted to shear rate and the torque indicated by the dial reading can be converted to shear stress.

The Fann viscometer used in this study has standard bob and rotor. The bob has a radius of 1.7245 cm and length of 3.8 cm, the rotor has a radius of 1.8415 cm. During each flow loop test, samples were collected from flow loops at the beginning (and end) of each test and their rheological measurements were conducted using the Fann Model

35 viscometer. For highly viscous fluids where the maximum dial readings for the 1/5th spring could potentially be exceeded, the six rotor speeds (No. 1 torsion spring) Fann Model 35 viscometer was used in the rheological test.

Figure 4.6 Fann Model 35 Viscometer.

4.4 Fluid System

In the present study, four concentrations of Guar gum, a well known water soluble polymer suggested by the members of the Coiled Tubing Consortium, is used to evaluate friction pressure losses of non-Newtonian power law fluids during annular flow through conduits with unit eccentricity. The intent is to characterize the laminar and turbulent flow behavior of non-Newtonian Power law fluids in eccentric annuli.

The guar polymer used in this study is WG-19, a product of Halliburton Energy Services, at concentrations of 20, 30, 40 and 60 lb/Mgal in fresh water.

Guar gum is made up of non-ionic polydisperse rod-shaped polymers derived from the seed of the guar plant. The beans are removed from guar bean pod, processed to separate the endosperm from the bean hull and embryo, and ground into powder. Various derivatives have become commercially available, e.g. HPG, to overcome some of the disadvantages of guar gum. HPG is obtained by the reaction of propylene oxide with the guar molecules, creating a more temperature stable polymer. It was developed primarily to reduce the residue obtained from guar gum. The molecular structure of guar gum is shown in Fig. 4.11. Aqueous solutions of guar are non-Newtonian in character and also can be cross-linked by borax (or, other transition metal ion) to give very high gel strength for suspension. Such a structure is easily broken by breakers in fracturing fluids, so it serves as a carrier for placing sand farther into fractures. It is also used as a top-hole drilling fluid. Disadvantages of using guar gum include its lack of thermal stability and sensitivity to high pH and bacterial fermentation.[65] Guar gum and HPG are the most widely used viscosifies for water based facturing fluids. Economides and Nolte (2000) reported that over 70% of all fracturing treatments use guar or HPG based aqueous fluids.

4.4 Experimental Procedure

Fluid preparation was the first step for each flow test. In preparing the test fluids, the procedures from the material provider have been followed. The following briefly describes the general procedure for preparing guar gum fluids;

- Pump 50 bbls (2100 gallons) of water into the mixing tank
- Add the amount of guar needed in the tank while operating the mixer at a moderate speed, e.g., add 84 lbs of polymer to make 40 lb/Mgal guar fluid.
- Add caustic soda to raise the pH of the system to 9 and mix.
- Add guar powder and mix until a homogeneous fluid is formed.
- Add citric acid to lower pH of the fluid system and allow polymer hydration.
- Mixture is allowed to hydrate for one hour.
- Take sample for rheology measurement.
- Check fluid properties to ensure adequate mixing and hydration.

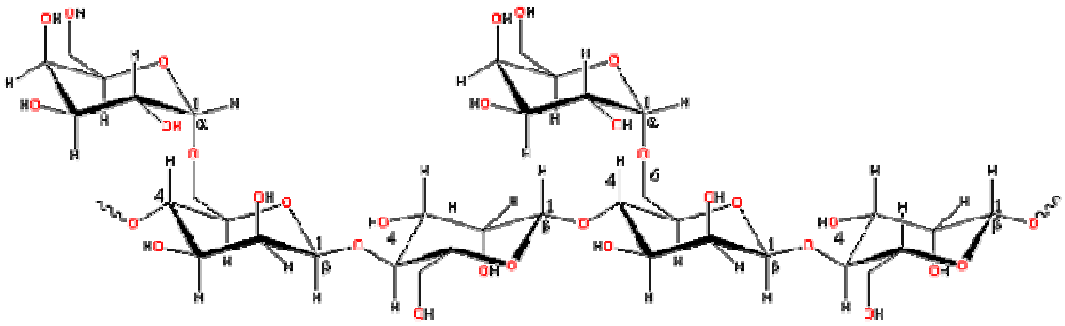

Figure 4.7 Molecular Structure of Guar Gum (Chaplin, 2008).

Before pumping the test fluid, water was pumped through the flow loop at various flow rates for system calibration check. Test fluid was then pumped through the flow loop, and when the system was completely filled with gel, it was switched to recirculation. During each test, the fluid was pumped at various flow rates (30 to 260 gpm) until either the pump rate reached the maximum capacity of the triplex pump or the system

pressure reached a maximum pressure of 5,000 psi. Notably, 2-3 minutes of steady flow data was acquired at each flow rate, i.e., flow rate was set at a desired value and the steady-state pressure drop data across eccentric annuli were recorded. Subsequently, flow rate was increased and corresponding pressure drop was noted. In the beginning and before terminating the test, another fluid sample was collected from a sampling port (located downstream of the MicroMotion flowmeter) in the flow loop and the fluid rheology was again checked with a model 35 Fann viscometer for any possible variation due to degradation, heating or both. Any rheology change is taken into account during the data analysis. At the end of testing, system was flushed by pumping water and displacing the test fluid. It is important to mention that the system was calibrated every time a new test was performed to ensure that reliable data were generated.

CHAPTER 5

EXPERIMENTAL STUDY OF FRICTION PRESSURE LOSS OF NON-NEWTONIAN POWER-LAW FLUIDS IN ECCENTRIC ANNULUS

5.1 Introduction

The majority of the non-Newtonian fluids in oilfield applications exhibit the phenomenon of drag reduction in turbulent flow regimes. As discussed by Nouri et al. (1993), drag reduction with polymer solutions are a direct result of the stretching of the molecules in turbulent flow under the action of high strain rate and low vorticity so that the onset requirement for molecular stretching is fulfilled. The mechanism of drag reduction has been investigated by many scholars; for example, Lumley (1977) and Durst et al. (1982) who explained that the extension of molecules increases the viscosity of the solution in the turbulent region which suppresses the energy containing eddies in the buffer layer to result in a thickening of the sublayer and a reduction of drag. The indications are a reduction in drag coefficient and the suppression of turbulence intensities in the flow field. Due to the phenomenon of drag reduction and the intrinsic nature of fluid flow in an eccentric annulus, with variations in local Reynolds numbers precluding the existence of a specific flow regime (laminar or turbulent), numerical modeling of drag reducing non-Newtonian fluids in turbulent regime is not carried out in this study. To study non-Newtonian fluids in turbulent flow, an experimental approach is adopted. Tests are performed with different concentrations of Guar fluids.

The data were collected both in laminar and turbulent flow regimes and compared with the previously proposed laminar and turbulent flow correlations.

5.2 Data Reduction and Analysis

Data reduction and analysis involved processing and analyzing rheological data from measurements of Fann Model 35 viscometers and the flow data of water and guar polymer solutions through various eccentric annuli.

5.2.1 Rheological Data Reduction and Analysis

Following API RP 13M, standard procedures for evaluation of hydraulic fracturing fluids, shear stress – shear rate data for the Fann Model 35 viscometer with standard (R1-B1) geometry were computed from these equations (API RP 13M, 2004):

$$\dot{\gamma}_w = 1.703 \times N \tag{5.1}$$

$$\tau_w = 0.01066 \times S \times \theta_i \tag{5.2}$$

where, $\dot{\gamma}_w$ = wall shear rate (sec^{-1}), N = Rotor speed (rpm); τ_w = wall shear stress (lb_f/ft^2); S = spring number (=1 for No. 1 spring, 0.2 for $1/5^{th}$ spring); and θ_i = Fann viscometer dial reading at i^{th} rpm.

From the rheology data gathered, the polymer solutions at all concentrations exhibit a non-Newtonian pseudo-plastic (Shear-thinning) fluid behavior and Power law model can adequately describe the behavior of these fluids. Typically, guar solutions do not have a significant yield stress, but they have measurable normal forces, i.e. they are not purely viscous, but exhibit elasticity (Whitcomb et al., 1980). The power law parameters, n and K_v for each gel are determined from the regression of Fann model 35 viscometer data on the log-log plot for high shear rates. Table 5.1 shows the results of

the investigation for test fluid samples taken before flow through different flow loops. The lower the flow behavior index the further away its behavior from a Newtonian fluid. It is found that, the flow behavior index, n decreases and consistency index, K_v increases with concentration.

The consistency index, K_v, obtained from viscometer data, was converted to geometry independent consistency index, K and the consistency index for pipe flow, K_p by using the equation (API RP 13M, 2004):

$$K = \frac{K_v}{\sigma^n} \tag{5.3}$$

$$K_p = \frac{K_v}{\left[\frac{4n\sigma}{3n+1}\right]^n} \tag{5.4}$$

where, σ is a constant defined by:

$$\sigma = \left[\frac{\beta^{\frac{2}{n}}}{n\beta^2}\right]\left[\frac{\beta^2-1}{\beta^{\frac{2}{n}}-1}\right] \tag{5.5}$$

where, β is the ratio of cup to bob radii (R_c/R_b) for the viscometer used in the study. Subsequently, the pipe consistency index, K_p, was converted to annular K_a by using the equation:

$$K_a = \frac{K_p}{\left[\frac{9n+3}{8n+4}\right]^n} \tag{5.6}$$

Using a power law model, the apparent viscosity, μ_a of non-Newtonian fluid is represented by the following expression:

$$\mu_a = K_p(\dot{\gamma}_w)^{n-1} \tag{5.7}$$

Figure 5.1 shows the rheogram for the polymer solutions while Figure 5.2 shows apparent viscosity data as a function of wall shear rate for Guar polymer solutions used for the 3 ½-in. by 1 ¾-in. eccentric annulus flow loop.

Table 5.1 Summary of test fluids and their measured rheological properties

Flow loop	Test Fluid	n	K ($lb_f.sec^n/ft^2$)	K_v ($lb_f.sec^n/ft^2$)	K_a ($lb_f.sec^n/ft^2$)
3.5-in. by 1.75-in.	20 lb/Mgal Guar	0.618	2.86E-03	2.93E-03	3.21E-03
	30 lb/Mgal Guar	0.546	8.60E-03	8.85E-03	9.83E-03
	40 lb/Mgal Guar	0.436	2.42E-02	2.51E-02	2.83E-02
	60 lb/Mgal Guar	0.360	7.95E-02	8.27E-02	9.40E-02
3.5-in. by 2.375-in.	20 lb/Mgal Guar	0.666	1.53E-03	1.57E-03	1.70E-03
	35 lb/Mgal Guar	0.528	9.06E-03	9.34E-03	1.04E-02
	40 lb/Mgal Guar	0.455	2.07E-02	2.14E-02	2.41E-02
	60 lb/Mgal Guar	0.335	9.13E-02	9.52E-02	1.08E-01
5-in. by 3.5-in. & 5.5-in by 4-in.	20 lb/Mgal Guar	0.651	1.82E-03	1.86E-03	2.03E-03
	30 lb/Mgal Guar	0.536	6.74E-03	6.94E-03	7.72E-03
	40 lb/Mgal Guar	0.471	1.62E-02	1.67E-02	1.88E-02
	60 lb/Mgal Guar	0.341	7.48E-02	7.79E-02	8.86E-02

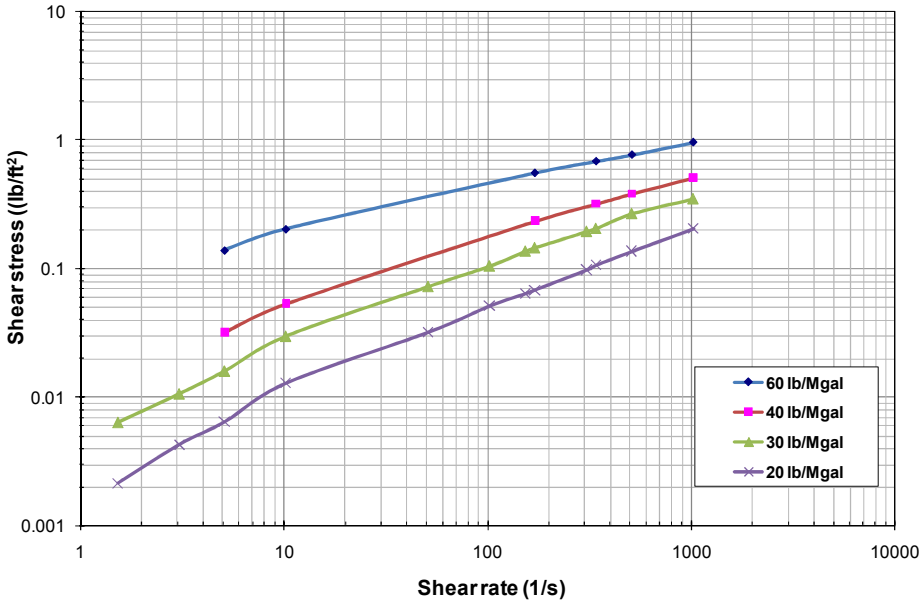

Figure 5. 1 Rheogram of 20, 30 40 and 60 lb/Mgal test fluid samples taken before flow through 3 ½-in. × 1 ¾-in. eccentric annulus

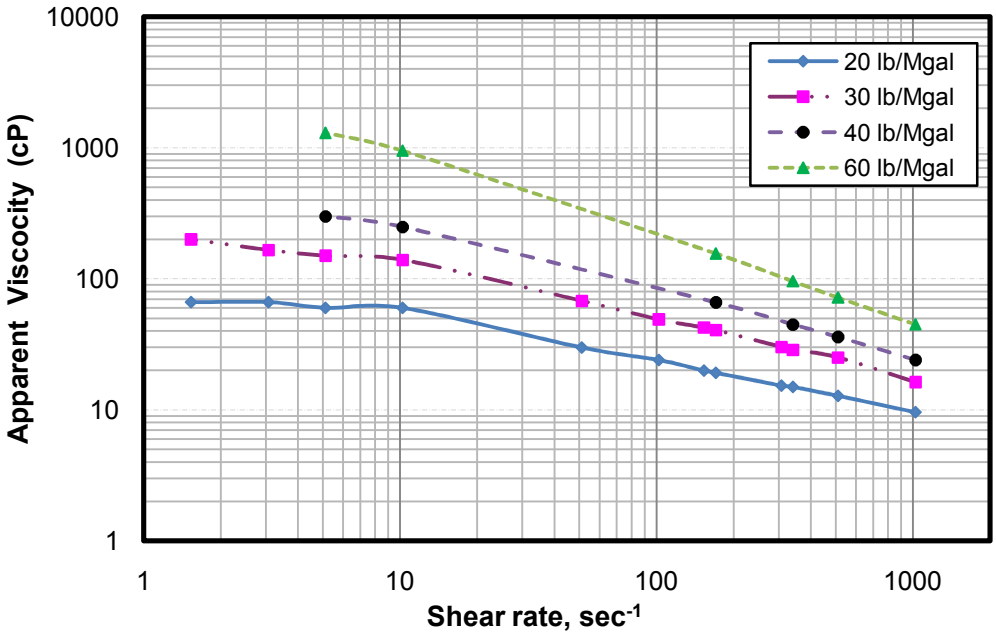

Figure 5.2 Apparent viscosity of 20, 30, 40 and 60 lb/Mgal test fluid samples taken before flow through 3 ½-in. × 1 ¾-in. eccentric annulus

5.2.2 Flow Data Reduction and Analysis

The data recorded during each flow test consist of flow-rate, pressure drop across eccentric annuli, fluid density, and temperature. The transition data points due to flow rate change or due to any operational challenges were removed so that only the steady state data points were used for the data analysis. Figure 5.3 shows an example of the recorded signals after the transient points are eliminated. Going forward, the differential pressure versus flow rate data were reduced in terms of Fanning friction factor and generalized Reynolds number for each test fluid. These two dimensionless parameters were used in characterizing fluid flow through eccentric annulus.

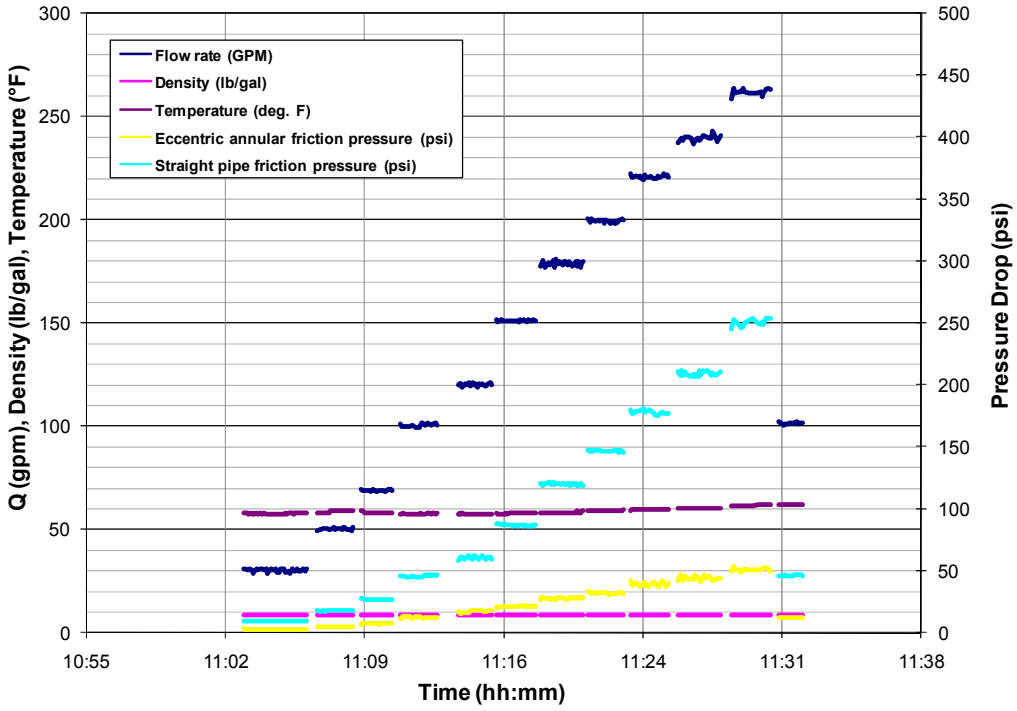

Figure 5.3 Plot of recorded data for 20 lb/Mgal guar fluid flow through 3 ½-in. × 1 ¾-in. eccentric annulus and 1 ½-in. straight tubing after removing transition points.

The Fanning friction factor, *f*, is a dimensionless variable used to determine friction pressure gradient in pipe and annular flow. Using the equivalent diameter concept (d_1-d_2), Fanning friction factor is given by the following expression for annular flow in oil field units:

$$f = 154.6483 \frac{(d_2 - d_1)(d_2^2 - d_1^2)^2 \Delta p}{l \rho q^2} \tag{5.8}$$

where q is the flow rate (*gal/min*), d_2 is the inner diameter of outer pipe (*in.*), d_1 is the outer diameter of inner pipe (in.), Δp is the pressure drop (*psi*) over an annular section of length, *l (ft)*. For annular flow of Newtonian fluid, Fanning friction factor is plotted against Reynolds number, N_{Re}:

$$N_{\mathrm{Re}} = 378.79 \frac{\rho q}{(d_2 + d_1)\mu} \tag{5.9}$$

where μ is the fluid dynamic viscosity (*cP*).

The generalized Reynolds number, N_{Reg}, is used for non-Newtonian fluids:

$$N_{\mathrm{Re}g} = \left(\frac{1}{12}\right)^n \frac{7.48052}{32.17 \times 8^{n-1}} \frac{d_{eff}^n V_a^{2-n} \rho}{K} \tag{5.10}$$

where n is the power law flow behavior index, K_a is the fluid consistency index for annular flow ($lbfsec^n/ft^2$), V_a is the average fluid velocity (*ft/sec*), d_{eff} is the effective diameter of the eccentric annulus.

The effective diameter approach introduced by Reed and Pilehvari (1993) for non-Newtonian fluid flow in annuli is used in this study. It is given by the following expressions;

$$\mathrm{d_{eff}} = \frac{d_2 - d_1}{G} \tag{5.11}$$

where G is given by:

$$G = \left(1 + \frac{Z}{2}\right)\frac{[(3-Z)n+1]}{[(4-Z)n]} \tag{5.12}$$

$$Z = 1 - \left\{1 - \left(\frac{d_1}{d_2}\right)^{Y}\right\}^{\frac{1}{Y}} \tag{5.13}$$

$$Y = 0.37n^{-0.14} \tag{5.14}$$

The expressions were derived from the analytical solution originally obtained by Fredrickson and Bird (1981). The average fluid velocity (*ft/sec*) for annular flow is calculated from the following equation:

$$V_a = \frac{q}{2.448(d_2^2 - d_1^2)} \tag{5.15}$$

5.3 Water Test

To ensure accuracy of the measurement in each annular section and during every experimental procedure, water data were acquired before and after each test. This also helps to get the base line for comparison and calibration. These data have been analyzed and compared with published correlations. The results were compared with the Haciislamoglu et al. correlation, using two classical friction factor correlations published by Drew et al. (1932) (for smooth pipe) and Chen (1979) (for rough pipe)

and the equivalent diameter concept to estimate the Fanning friction factors for the corresponding concentric annulus. Drew correlation for smooth pipe is given by:

$$f = 0.0014 + \frac{0.125}{N_{\mathrm{Re}}^{0.32}} \tag{5.16}$$

where f is the Fanning friction factor, and N_{Re} is Reynolds number. The correlation is valid for Newtonian turbulent flow in smooth pipes, in the Reynolds number range of $2100 < N_{Re} < 3 \times 10^6$. Chen (1979) correlation for rough pipe is given by:

$$\frac{1}{\sqrt{f}} = -4.0 \log\left[\frac{h}{3.7065d} - \frac{5.0452}{N_{\mathrm{Re}}} \log\left\{\frac{1}{2.8257}\left(\frac{h}{d}\right)^{1.1098} + \frac{5.8506}{N_{\mathrm{Re}}^{0.8981}}\right\}\right] \tag{5.17}$$

where h is the tubing roughness projection and d the tubing inside diameter (or equivalent diameter (d_2-d_1) for annular section). The result of the Chen's correlation is identical to the well-known Colebrook (1939) equation for the range of Reynolds number from 4000 to 4×10^8 and (h/d) from 0.05 to 5×10^{-7}. However, Chen's correlation is explicit, thus, eliminating the trial-and-error approach inherent in the implicit Colebrook equation. Using Chen's correlation and the equivalent diameter concept, an estimate of the Fanning friction factors for a concentric annulus was made, so as to compare our experimental results to the Haciislamoglu et al. correlation (Eq. 2.21) for turbulent flow of water in eccentric annulus.

Figure 5.4 shows a comparison between experimentally determined Fanning friction factors for the 3½-in. × 1¾-in. eccentric annulus and the predictions from the combination of Chen's (h = 0.0072-in.) and Haciislamoglu et al. correlations (Eq. 2.21). The agreement between the two is reasonably good. A combination of the Drew equation for smooth pipe and the Haciislamoglu correlation under predicts the

experimental data. This indicates that for the 3½-in. × 1¾-in. eccentric annulus, the effect of pipe roughness is obvious, especially at high flow-rate conditions.

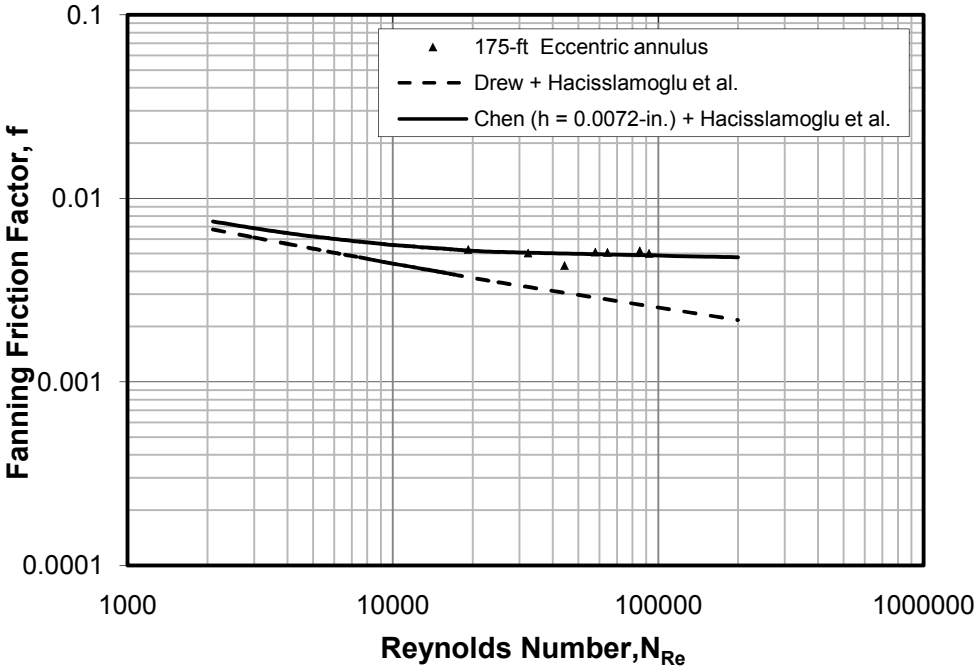

Figure 5.4 Fanning friction factor versus Reynolds number for water in 3½-in. × 1¾-in. eccentric annulus.

Figures 5.5 and 5.6 indicate that the friction factors in the 5 ½-in. × 4-in. and 5-in. × 3 ½-in. eccentric annular sections are higher than the predictions from the combination of Drew and Haciislamoglu et al. correlation (Eq. 2.21). Therefore, tubing roughness effects are evident in both flow-loops. To estimate the magnitude of possible tubing roughness, a combination of Chen (Eq. 5.16) and Haciislamoglu et al. correlations (Eq. 2.21) was applied to match the experimental data of the 5½-in. × 4-in. and 5-in. × 3½-in. eccentric annular sections. From Figures 5.5 and 5.6, it is seen that a combination of Chen and Haciislamoglu et al. correlations (Eq. 2.21), showed reasonably good agreement with the experimental data of 5 ½-in. × 4-in. and 5-in. × 3 ½-in. eccentric

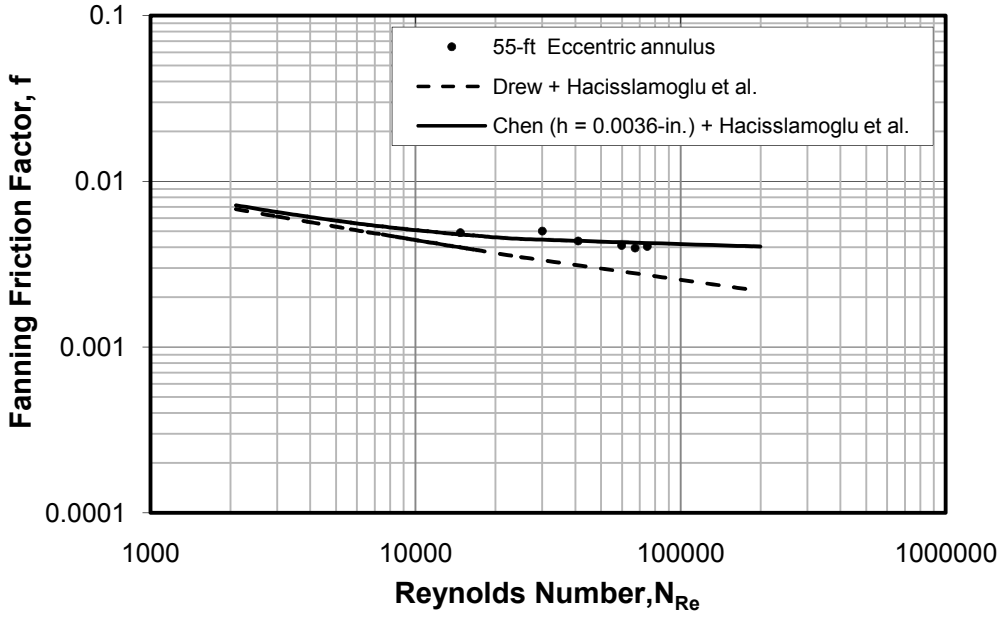

Figure 5.5 Fanning friction factor versus Reynolds number for water in 5½-in. ×4-in. eccentric annulus.

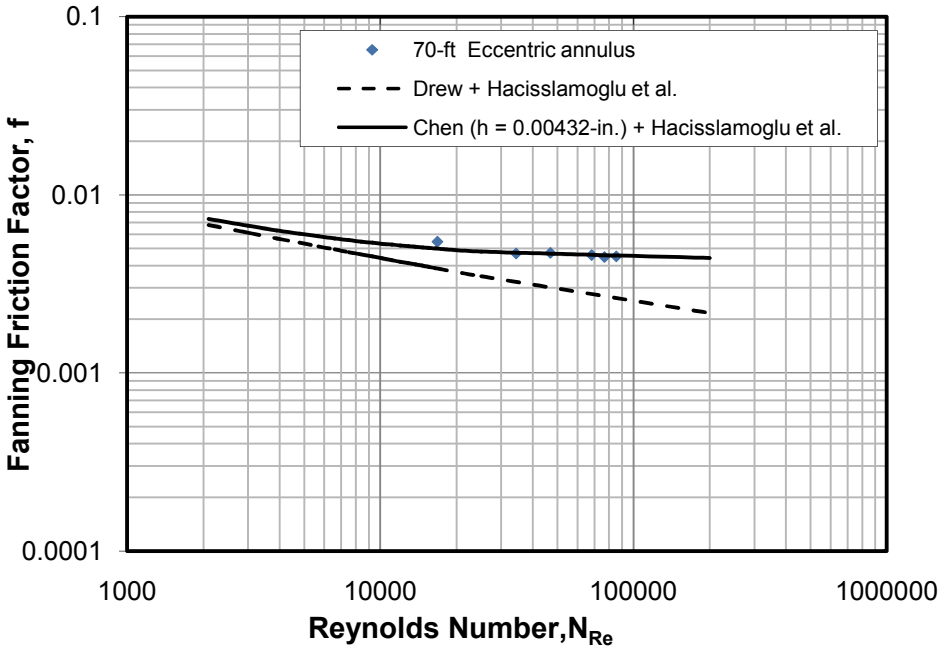

Figure 5.6 Fanning friction factor versus Reynolds number for water in 5-in.×3½-in. eccentric annulus.

annular sections with tubing roughness of 0.0036-in. and 0.00432-in. respectively. Compared to the 3½-in. × 1¾-in. eccentric annulus, the roughness values are lower because these eccentric annular sections are newly constructed.

5.4 Flow Test of Guar Fluids

Guar fluids at several polymer concentrations (20, 30, 35, 40 and 60 lb/Mgal) have been tested using the field scale flow loop. Figures 5.7 to 5.12 show the friction behavior on the traditional plots of Fanning friction factor versus generalized Reynolds number in four eccentric annular sizes respectively. On these plots, we also plotted the classical Hagen-Poiseuille equation ($f = 16/N_{Reg}$) for laminar tubing flow and, a combination of Chen and Haciislamoglu et al. correlations for turbulent Newtonian flow in eccentric annulus. Several features can be observed from these plots and they are discussed in the sections that follow.

5.4.1 Effect of Polymer Concentration

The effects of polymer concentration on friction factor in eccentric annulus are shown in Figures 5.7, 5.8 and 5.9, using composite plots of friction pressure gradients at various polymer concentrations for 5-in. x 3 ½-in., 3½-in. x 2 3/8-in. and 3½-in. x 1¾-in. eccentric annuli respectively. As guar polymer concentration increases from 20 to 60 lb/Mgal, the friction pressures increased significantly for the 5-in. x 3 ½-in. eccentric annulus (Fig. 5.7). The more concentrated Guar polymer solution tends to yield higher friction pressures. The trend is not clearly observed for the 3½-in. x 1¾-in. eccentric annuli (Figure 5.9), which has a significant degree of roughness as compared to the 5-

in. x 3 ½-in. eccentric annulus. Evidently, turbulent flow data for low polymer loading (e.g. 20 lb/Mgal Guar) were significantly affected by tubing roughness for the 3½-in. x 1¾-in. eccentric annulus. However, at all polymer concentrations, the fluids showed significant drag reduction in the turbulent flow regime as compared to the friction pressure data obtained with water for each flow loop. Also, the observed roughness effect is more apparent in the dimensionless plots of friction factors versus generalized Reynolds number presented in Figures 5.10 to 5.13. It is interesting that at concentrations of 30, 40 and 60 lb/Mgal, the friction factor is not very sensitive to the changes in concentration. Therefore, the effect of tubing roughness is not as important beyond a concentration of 30 lb/Mgal, as they are eliminated with incremental polymer loading. Moreover, as generalized Reynolds number increases, the friction factor in a fully eccentric annulus tends to follow the extended line of laminar flow, especially at high polymer concentrations.

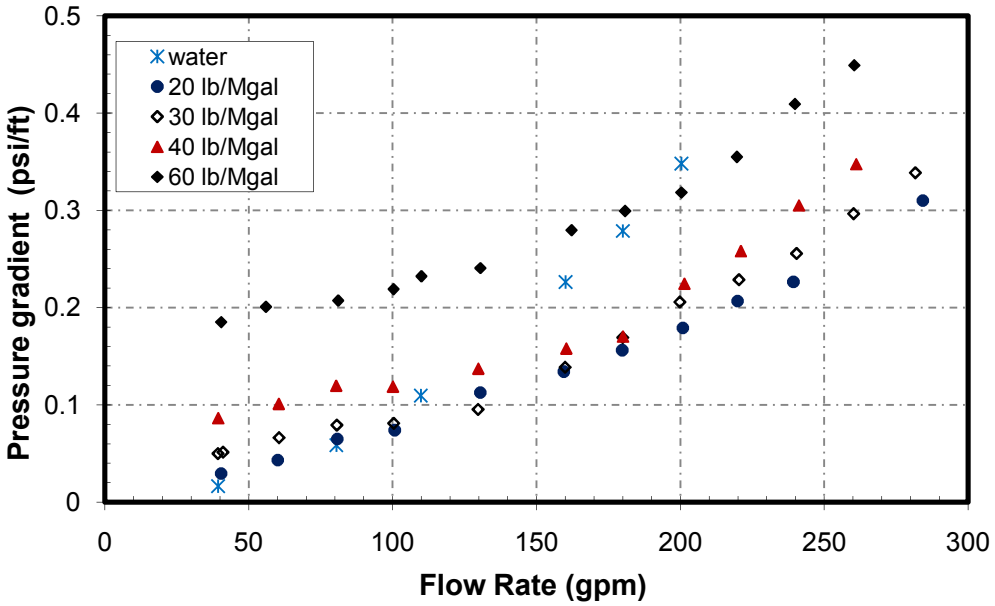

Figure 5.7 Friction pressure loss of Guar polymer solutions in 5-in. x 3 ½-in. fully eccentric annulus.

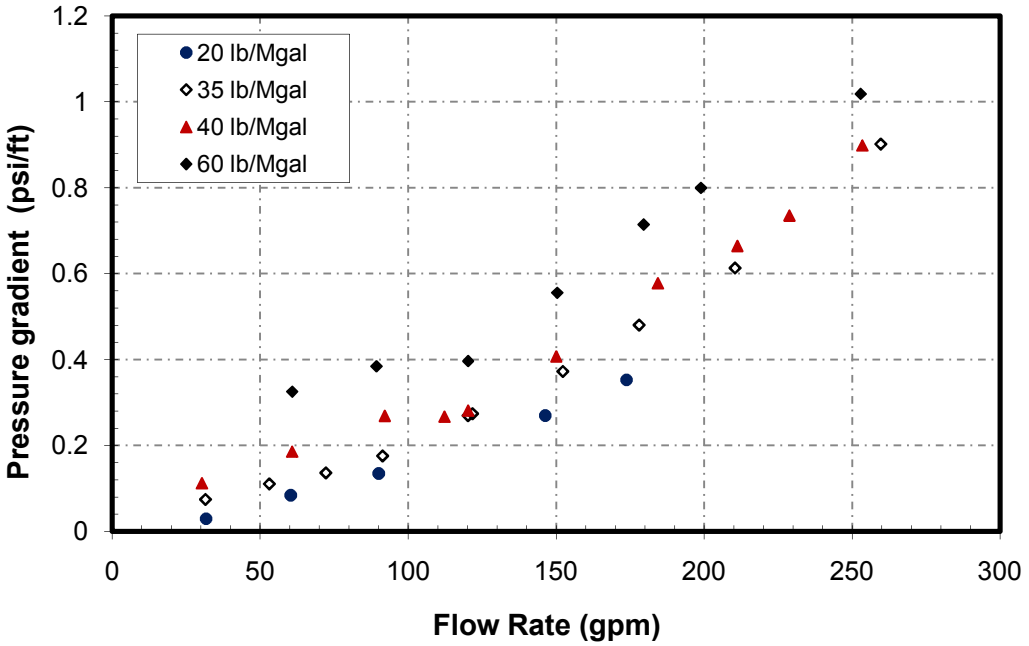

Figure 5.8 Friction pressure loss of Guar polymer solutions in 3½-in. x 2¾-in. fully eccentric annulus.

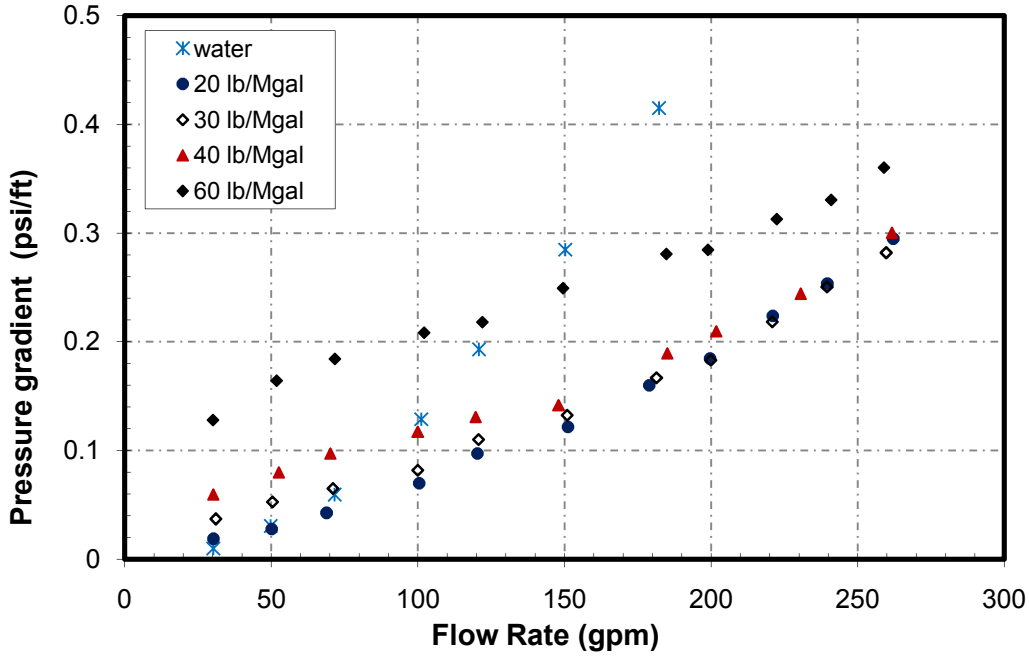

Figure 5.9 Friction pressure loss of Guar polymer solutions in 3½-in. x 1¾-in. fully eccentric annulus.

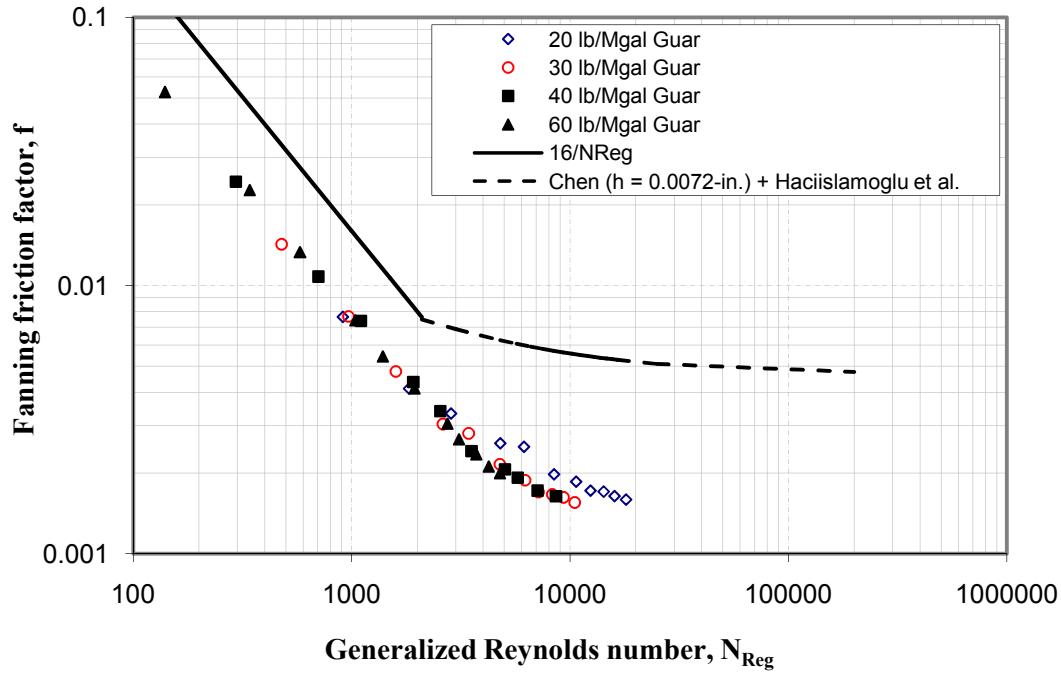

Figure 5.10 Fanning friction factor versus Reynolds number for Guar fluids in 3½-in. × 1¾-in. eccentric annulus.

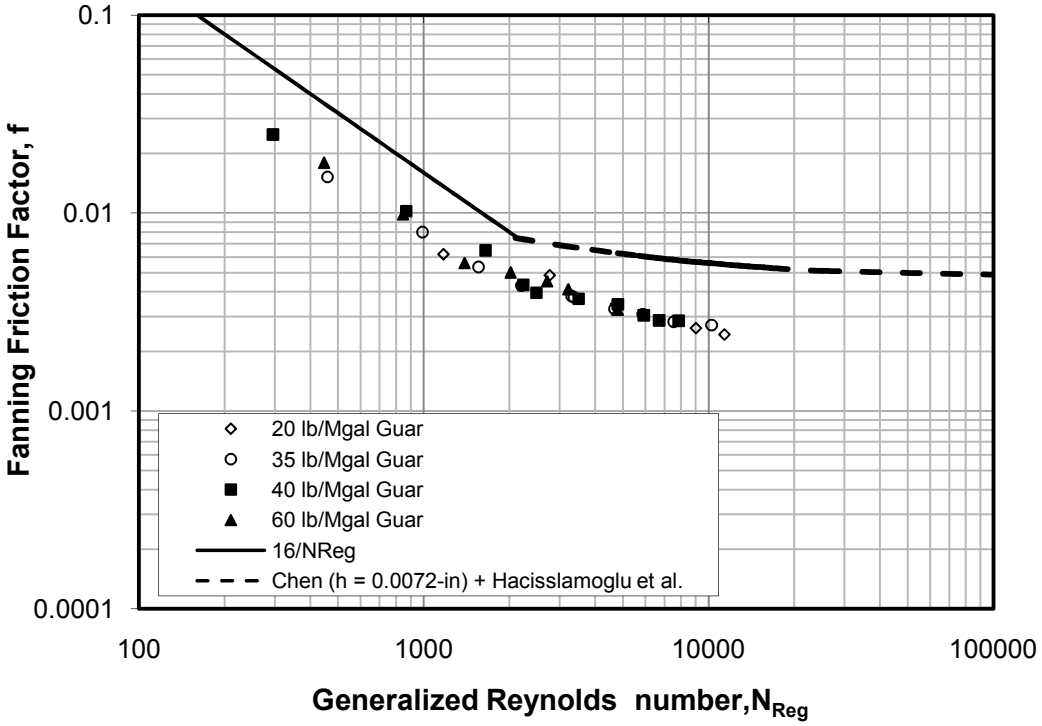

Figure 5.11 Fanning friction factor versus Reynolds number for Guar fluids in 3½-in. × 2 3/8-in. eccentric annulus.

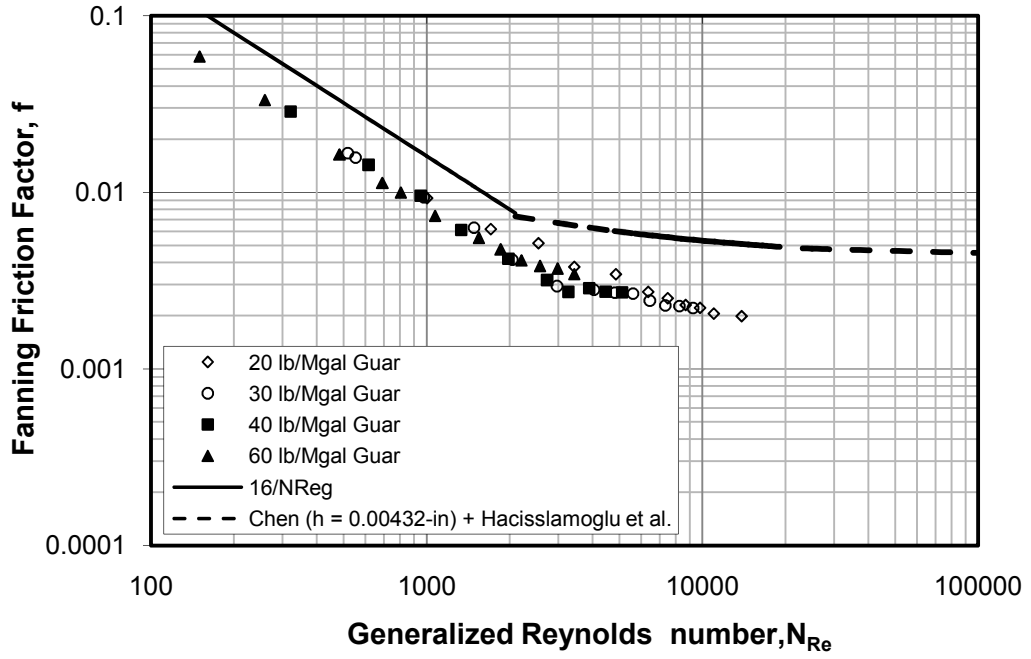

Figure 5.12 Fanning friction factor versus Reynolds number for Guar fluids in 5-in. × 3½-in. eccentric annulus.

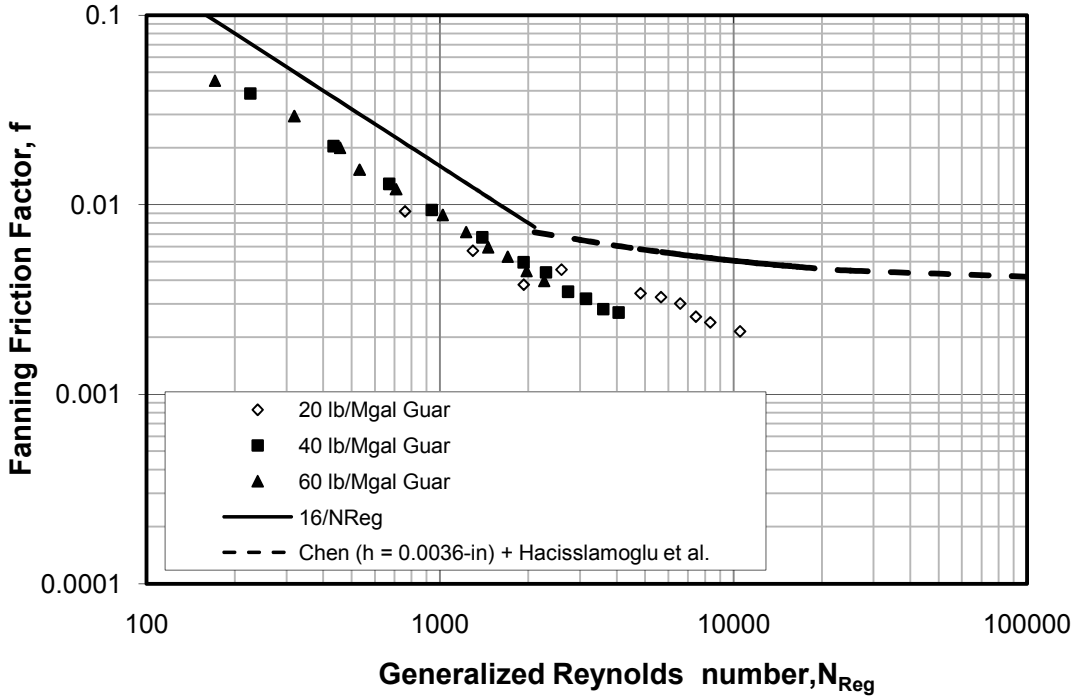

Figure 5.13 Fanning friction factor versus Reynolds number for Guar fluids in 5½-in. × 4-in. eccentric annulus.

5.4.2 Effect of Diameter Ratio

Over the years, several test data for water as reference fluid and Guar (20, 30, 35, 40 and 60 lb/Mgal) have been acquired using four fully eccentric annular sections of dimensions 3 ½-in. by 2 3/8-in. (30 ft long), 3 ½-in. by 1 3/4-in. (200 ft long), 5½-in. × 4-in. (69 ft long) and 5-in. × 3 ½-in. (79 ft long) at the Well Construction Technology Center (WCTC), University of Oklahoma. A comparison of the Fanning friction factors as a function of generalized Reynolds number for these geometries showed that the effect of equivalent diameter or diameter ratio is significant when fully eccentric annular friction pressure losses are estimated. This agrees with results obtained by previous investigators (Bourne et al., 1968; Hacisslamoglu et al., 1990). Typical results are presented in Figures 5.11 and 5.12 for 40 and 60 lb/Mgal Guar polymer solutions respectively. Notably, the effect of pipe roughness is negligible at high polymer concentrations (Shah, 1990). Hence, high polymer loading is utilized to nullify the plausible effect of pipe roughness in each flow loop. The higher frictional losses encountered is as a result of the magnitude of wall shear effects on the fluid system.

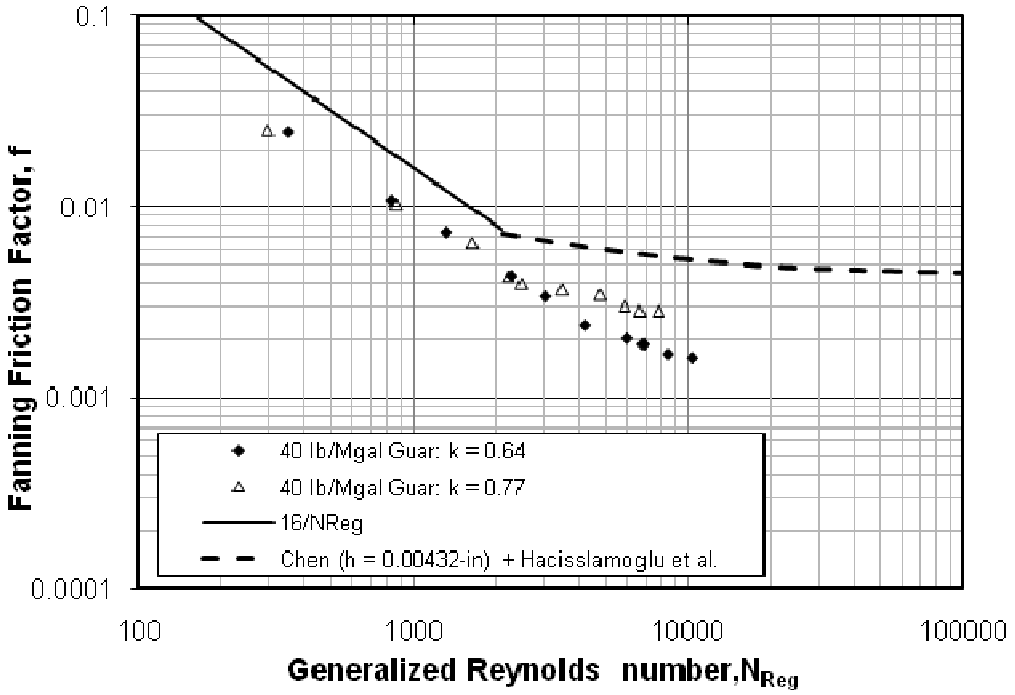

Figure 5.14 Effect of diameter ratio on the friction pressure loss of 40 lb/Mgal Guar fluid in eccentric annulus.

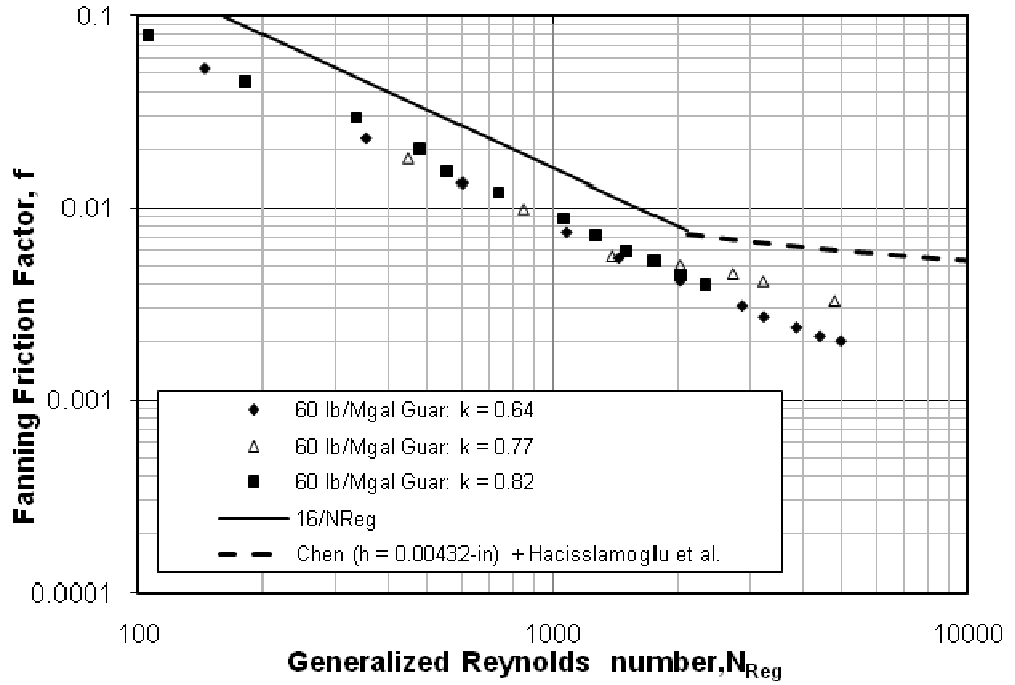

Figure 5.15 Effect of diameter ratio on the friction pressure loss of 60 lb/Mgal Guar fluid in eccentric annulus.

5.4.3 Development of Friction Factor Correlations

To make the above field scale experimental data and observations useful to making undemanding hydraulic program calculations, empirical correlations of Fanning friction factor of Guar fluids have been developed. In developing this correlation, only those data points *(see Figure 5.16)* whose generalized Reynolds number is greater than 2100 were included. Below this critical generalized Reynolds number, we recommend the use of laminar correlations such as the theoretical correlation developed and presented in the Chapter 3 of this study.

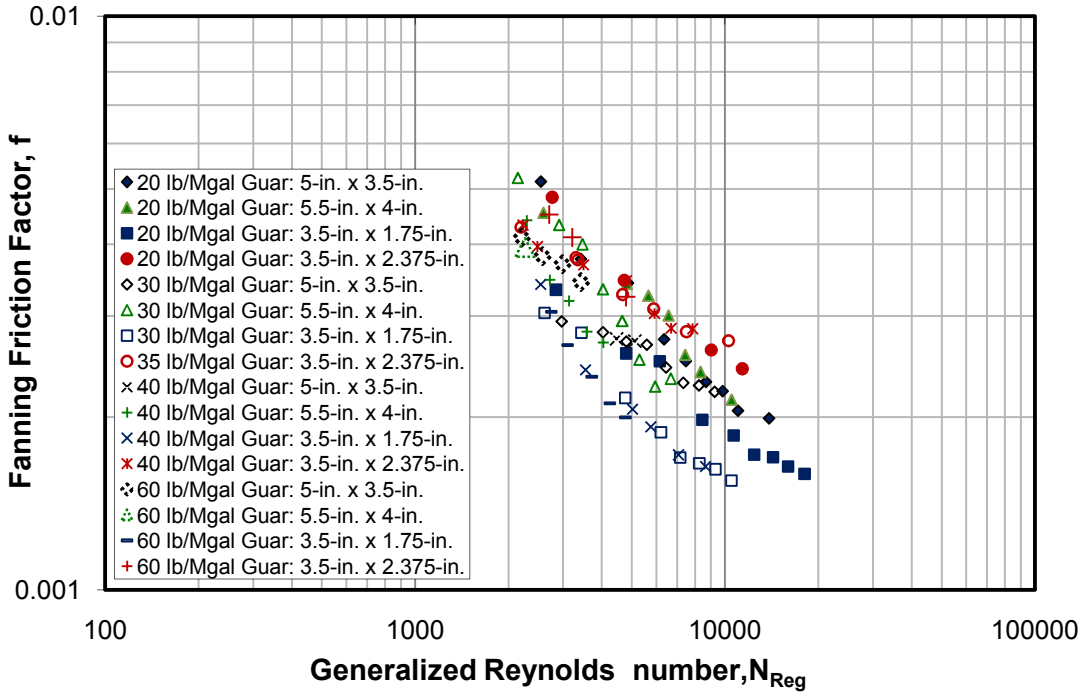

Figure 5.16 Composite plot of Fanning friction factor vs. generalized Reynolds number for guar fluids.

As shown in Figure 5.16, the data of the 5½-in. × 4-in. (69 ft long) eccentric annulus showed large scatter, possibly due to not having enough entry and exit lengths for attaining fully developed flow across the pressure ports. Several other observations can be made and will be useful for selecting the final form of an appropriate correlation. First, all fluids show well behaved data trend when plotted as Fanning friction factor vs. generalized Reynolds number. The data points seem to display certain degree of curvature over a wide range of generalized Reynolds number for each fluid. Second, the vertical separation of the experimental data presented in Figure 5.17 is mainly due to difference in diameter ratios. For clarity, we chose consistent marker convention so that it will be easier to distinguish between different polymer concentrations within each data set of a given flow loop. Each color represents a specific flow loop, hence, within each color band, any minor separation between the sub-sets of data corresponds to the effect of polymer concentration, which is shown to be quite negligible, except for 20 lb/Mgal Guar.

After the outliers are removed (see Figure 5.17), it can be easily seen that the data sets form two distinct groups, apparently representing the variations in diameter ratios. The lower set of data is for the 3½-in. by 1¾-in. eccentric annulus, with diameter ratio, k = 0.64, while the upper sets of data represent the experimental data of 3½-in. by 2.375-in. (k = 0.77) and 5-in. by 3½-in. (k = 0.82) respectively. Within the limits of experimental measurements, it is difficult to effectively separate data for k = 0.77 and 0.82, which are approximately same.

Based on the above observations, friction pressure data for the turbulent flow of Guar polymer solutions in eccentric annulus from experimental observation are correlated using the following parameters; Fanning friction factor, *f*, generalized Reynolds number, N_{Reg}, and diameter ratio, k = d_1/d_2. Commercially available curve fitting software, LAB Fit, was used in developing the correlation. The correlation is expressed as:

$$f = 0.00378\frac{d_1}{d_2} + \frac{3.7374}{N_{Reg}} + \frac{4042}{N_{Reg}{}^2} - 0.00124 \tag{5.18}$$

valid for 2,100 < N_{Reg} < 15,100, k = 0.64 – 0.82 and 0.3 < *n* < 0.7. This four parameter type correlation was found to be sufficient in describing the friction behavior of Guar polymer solutions in eccentric annuli.

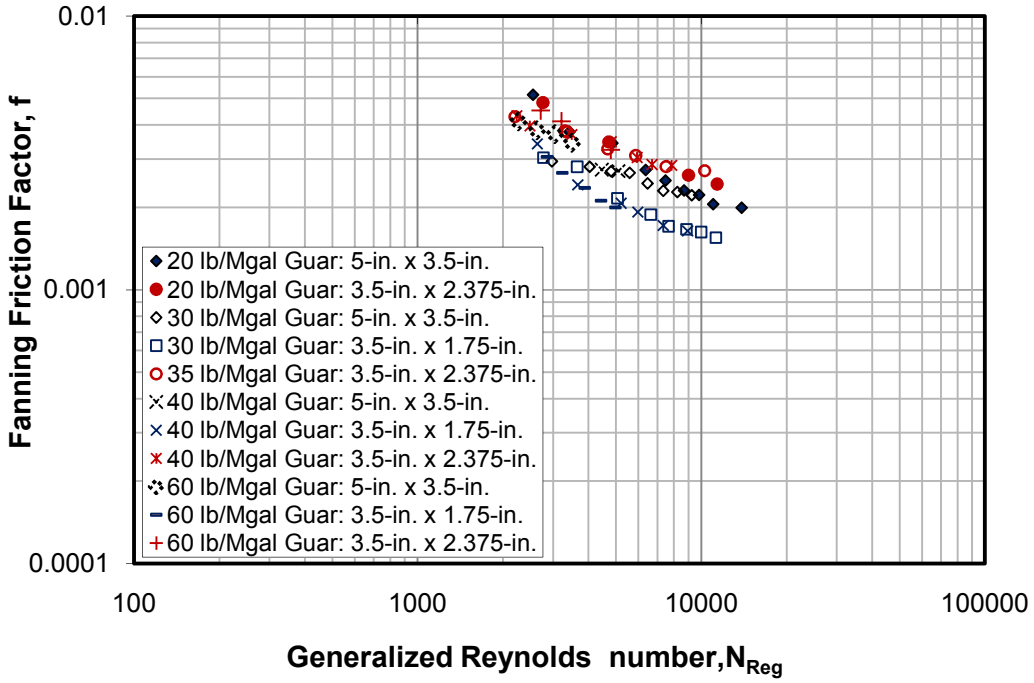

Figure 5.17 Composite plot of Fanning friction factor vs. generalized Reynolds number for guar fluids with outliers eliminated.

5.4.4 Evaluation of the New Friction Factor Correlation

To evaluate the performance of the developed empirical correlations given in Eq.(5.18), the experimental friction factors were compared with the predictions of the above correlation. The results of this comparison are shown in Figure. 5.18. It can be seen that the correlation could adequately match the experimental data. Majority of the predictions are within ±5%. The ±10% lines are drawn on the plots to show that only a few data points are outside the ±10% lines. Percentage deviation was computed using the following expression:

$$\%Deviation = \frac{f_{predicted} - f_{experimental}}{f_{experimental}} \tag{5.19}$$

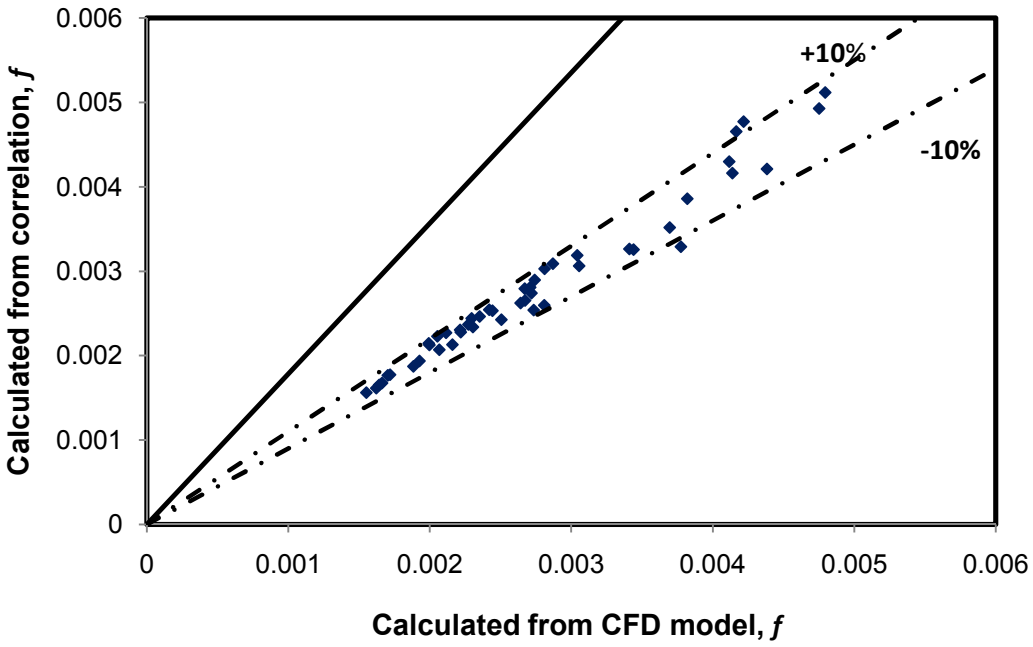

Figure 5.18 Cross plot of experimental and predicted friction factors of Guar data

Figures 5.19 and 5.20 show the plots of Fanning friction factor vs. generalized Reynolds number (N_{Reg}) for the experimental data of Guar polymer solutions and the new correlation for a 3 ½-in. by 1 ¾-in. and 5-in. by 3½--in. eccentric annuli respectively. It can be seen that there is an excellent agreement between the new correlation and the experimental data. This further confirms the accuracy of the proposed correlations. For 60 lb/Mgal Guar polymer solution, it can be observed in Fig. 5.20 that the new correlation matches the experimental data reasonably well, with absolute deviation changing from 0.2% to 6.4% with an average deviation of 3.9%.

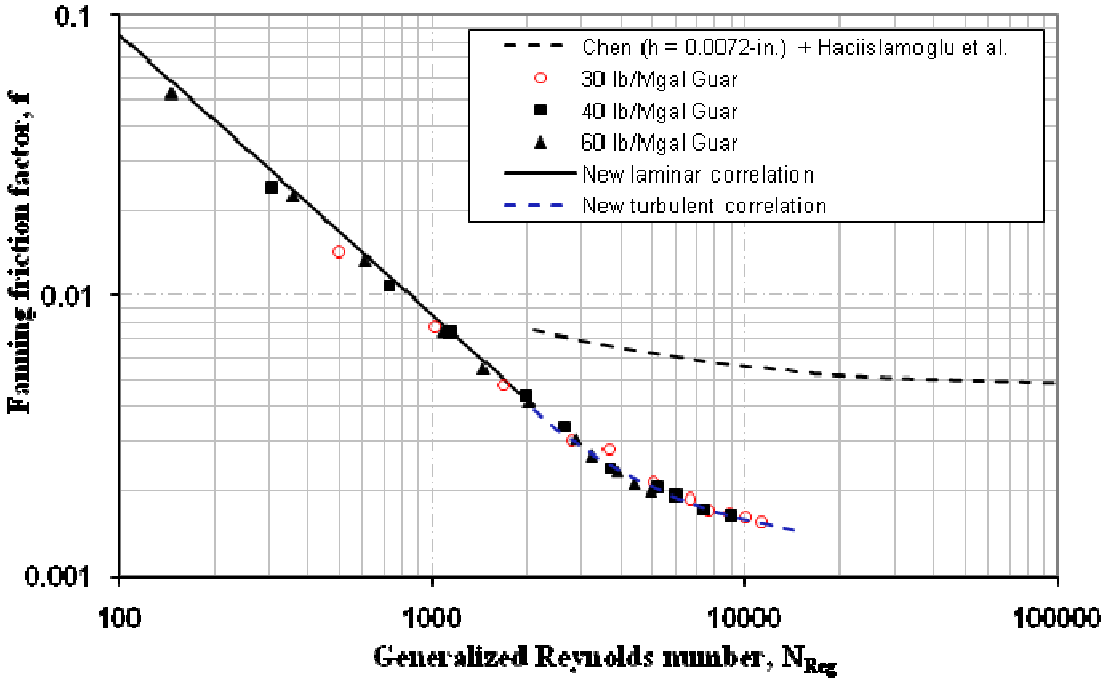

Figure 5.19 Fanning friction factor of Guar fluids in 3 ½-in. by 1 ¾-in. eccentric annulus

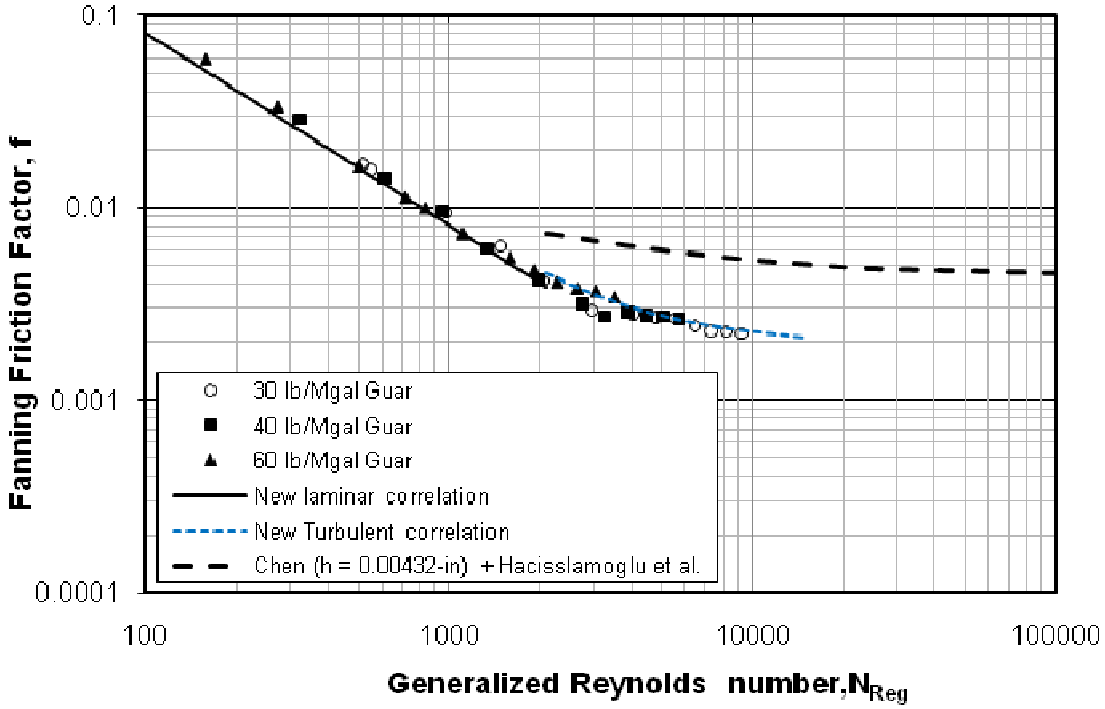

Figure 5.20 Fanning friction factor of Guar fluids in 5-in. by 3 ½-in. eccentric annulus

Example: Turbulent flow of 40 lb/Mgal hydroxyethyl cellulose (HEC) gel in 3½-in. x 1¾-in. eccentric annulus. Clean (proppant-free) HEC gel was pumped through the 210-ft, 3½-in. x 1 ¾-in. eccentric annulus. The rheological properties of the HEC gel were: n = 0.424 and K = 0.04 $lb_f sec^n/ft^2$. Figure 5.21 compares the measured and predicted friction factors from the new empirical correlation. The agreement between the measured data and the predictions are reasonably good. For the range of generalized Reynolds number investigated (2100 - 6,500) the largest deviation between empirical correlation and experimental data is 3.1%. The average deviation is 2.0%. This further confirms the accuracy of the new correlation and also affirms its reliable applicability in

making undemanding hydraulic program calculations for non-Newtonian fluid flow in eccentric annuli.

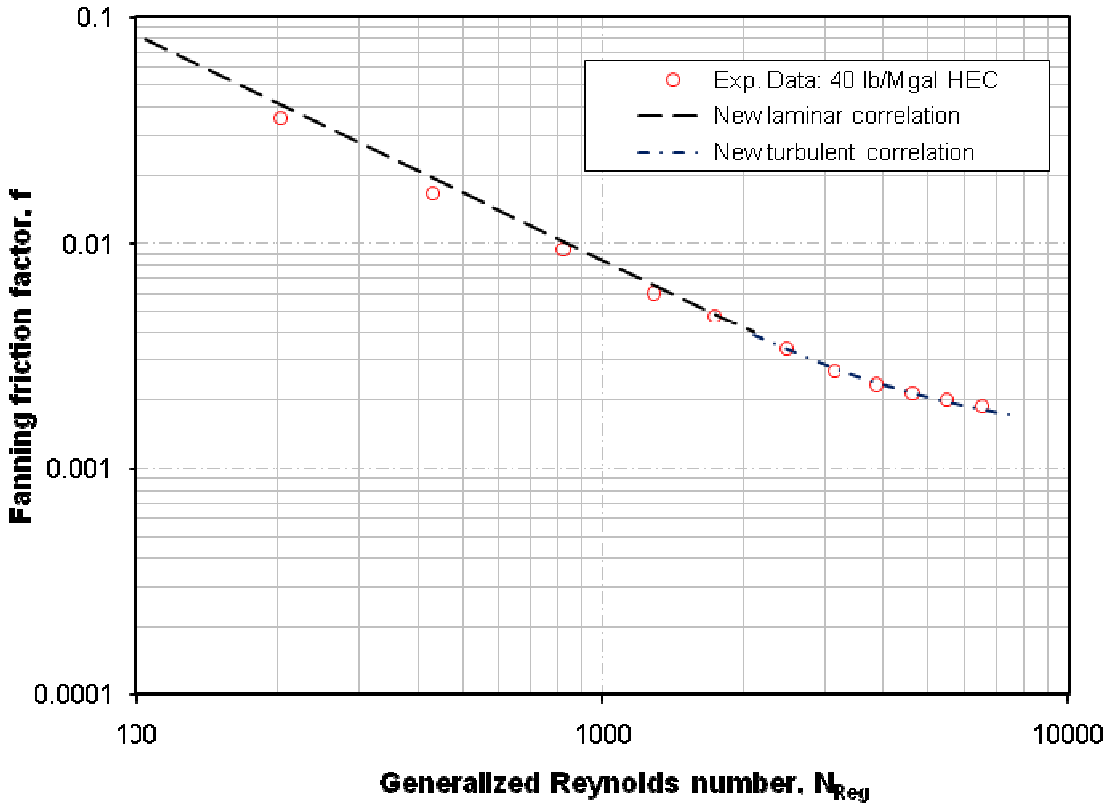

Figure 5.21 Fanning friction factor of 40 lb/Mgal HEC fluid in 3½-in. x 1 ¾-in. eccentric annulus

5.5 Summary

The flow behavior of Guar polymer solutions at several concentrations (20, 30, 35, 40 and 60 lb/Mgal) has been investigated using field scale flow-loop consisting of 5-in. x 3 ½-in., 3½-in. x 2 3/8-in. and 3½-in. x 1¾-in. eccentric annuli. At constant flow rate, the friction pressures increased significantly as guar polymer concentration increases from 20 to 60 lb/Mgal. However, at all polymer concentrations, the fluids showed significant drag reduction in the turbulent flow regime as compared to the friction pressure data

obtained with water for each flow loop. In agreement with results obtained by previous investigators, a significant effect of diameter ratio on the friction pressure behavior in an eccentric annulus was observed. The range of diameter ratio (k = 0.64 to 0.82) used in this study is quite limited, but they do cover a majority, if not all, of tubular configurations used during coiled tubing operations.

Friction factor correlations for turbulent flow in a fully eccentric annulus have been developed based on the field-scale flow test. They can be used in hydraulics design of oilfield operations, involving the flow of drag reducing non-Newtonian fluids through an eccentric annulus. Although, this correlation is developed for non-Newtonian power law fluids, it can be applied along with the unified rheological model introduced by Zamora et al. (2002) to estimate the friction pressure behavior corresponding to other rheological models.

CHAPTER 6

CONCLUSIONS AND RECOMMENDATIONS

6.1 CONCLUSIONS

CFD analyses have been successfully applied to solve the steady, fully-developed laminar flow of a non-Newtonian power law fluid in eccentric annular geometries. From the results of this investigation, the following conclusions can be drawn.

- The CFD code proved to be an appropriate numerical platform to successfully model non-Newtonian fluid flow in eccentric annular geometries as expressed by the consistently good agreement found between the numerical and experimental results.
- The computational investigation of flow in an eccentric annulus, with Newtonian and non-Newtonian fluids, presents a contribution to the understanding of the flow field occurring during fully-developed laminar flow conditions. First, the velocity profile for non-Newtonian fluids are slightly flattened compared with that for a Newtonian fluid in both concentric and eccentric annuli. Second, the axial velocity profile in an eccentric annulus is distorted and the peak velocities vary with location. A high velocity zone in the sector A of the annulus and a low velocity zone (almost stagnant at eccentricities greater than or equal to 0.75) in sector C of the annulus are observed, hence, coexisting laminar and turbulent flow regimes are tenable for fluid flow in an eccentric annulus.

- The narrowing region of an eccentric annulus presents a zone of high shear, and it is distinctly accompanied by a considerable reduction in viscosity. Compared to the maximum fluid viscosities calculated for the wide (A) and narrow (C) gaps in an eccentric annulus, about 42, 60, 78 and 90% reductions in the maximum fluid viscosity were observed in the widening gap (B) for 20, 30, 40 and 60 lb/Mgal guar gels respectively. This phenomenon along with the reduced velocity in the narrow sections reasonably explains the cuttings transport disparity that exists between concentric and eccentric annuli.
- Both eccentricity and annular diameter ratio are important parameters in calculating frictional pressure losses in eccentric annuli. At a constant flow rate, frictional pressure losses are decreased with increasing eccentricity (i.e. about 50% reduction in frictional pressure loss is observed when the annular section is fully eccentric, as compared to concentric annular flow at the same flow rate).
- A good agreement was obtained with the Haciislamoglu et al. correlation, and the results of this study, especially at low values of eccentricity. Hence, a modified version of Haciislamoglu correlation for friction pressure predictions in the annular flow of non-Newtonian Power law fluids with varying eccentricities was developed. The accuracy of the correlations was verified with experimental data.
- It is found that the deviations between the predicted and the experimental friction factors are generally within 10% for the new correlation and within

15% for Haciislamoglu et al. correlation. However, significant deviations with experimental data were observed mainly at very low flow rates, where data could be affected by differential pressure span settings, as generalized Reynolds number increased, the new correlation is accurate within 5%.

- The frictional pressure behavior of 20, 30, 35, 40 and 60 lb/Mgal Guar polymer solutions in fully eccentric annuli have been investigated using field-scale flow loop. It is found that the more concentrated Guar polymer solutions yield higher friction pressures. The Turbulent flow data for low polymer loading (e.g. 20 lb/Mgal Guar) were significantly affected by tubing roughness. However, at all polymer concentrations, the fluids showed significant drag reduction in the turbulent flow regime as compared to the friction pressure data obtained with water for each flow loop.
- Empirical correlations of Fanning friction factor as a function of generalized Reynolds number for non-Newtonian power law fluids in turbulent flow have been developed based on field –scale experimental data. Evaluation of these correlations indicated that the most data points used for the development of the correlations, the deviations between correlations and the experimental data were within 5%.

6.2 RECOMMENDATIONS FOR FUTURE RESEARCH

The presented simulation highlights the practicability of employing such CFD code to expediently and economically conduct an array of parametric studies involving non-Newtonian fluids associated with drilling and completion operations, in opposition to the lengthy and costly alternative of assembling, instrumenting and running field scale or laboratory experiments. Hence, I recommend the following experimental and CFD studies for future research:

- Conduct CFD simulations for the effect of tubing roughness on friction factor. Since, there are no available correlations to calculate roughness effect in both coiled tubing and eccentric annulus, and it is not practically feasible to construct one with a controlled roughness. Numerical experiments can fill this knowledge gap.
- The present study has been undertaken without inner tubing rotation; in the future, similar study should be extended to helical flow for non-Newtonian Power law fluids and other Rheological models.
- Conduct field scale experimental study using drag reducing polymer fluids, with a wide range of diameter ratios and annular eccentricities, so as to understand the turbulent flow behavior of these fluids in eccentric annulus and develop an empirical correlation to characterizing the friction pressure gradients.

REFERENCES

Akgun, F. and Jawad, R. H.: "Determination of Friction Pressure of Fluids Flowing Turbulently Through an Eccentric Annulus," International Journal of Petroleum Science and Technology, Vol. 1, No. 1 (2007), pp. 37-49.

Ahmed Kamel, A. H..: "Flow Behavior of Surfactant Based Fluids" PhD Dissertation, University of Oklahoma, 2008**.**

Annabattula, P. E. I.: "A CFD Model to Predict Pressure Loss Coefficient in Circular Ducts with a Motorized Damper," MS Thesis, University of Nevada, 2008

Azouz, I., Shirazi, S. A., Pilehvari, A. and Azar, J. J.: "Numerical Simulation of Laminar Flow of Power Law Fluids in Conduits of Arbitrary Cross-Section" Recent Developments in non-Newtonian Flows and Industrial Applications, ASME FED-Vol. 124(1991), 73-79.

Azouz, I., Shirazi, S. A., Pilehvari, A. and Azar, J. J.: "Numerical Simulation of Laminar Flow of Yield Power Law Fluids in Conduits of Arbitrary Cross-Section" Journal of Fluids Engineering, December 1993, Vol. 115, 710-716

Bailey, M., Blanco, I., and Rosine, R.: "Reel-to-Injector Fluid-Flow Analysis Using CFD Software", SPE paper 100141, presented at 2006 SPE/ICoTA Coiled Tubing and Well Intervention Conference and Exhibition held in The Woodlands, TX, 4-5 April, 2006.

Batra, R. L. and Eissa, M.: "Helical Flow of Sutterby Model Fluid," Polymer-Plastics Technology and Engineering, 33 (1994) 489-501.

Bilgesu, H. I., Ali, M. W., Aminian, K., and Ameri, S.: "Computational Fluid Dynamics (CFD) as a Tool to Study Cutting Transport in Wellbores," SPE 78716, SPE Eastern Regional Meeting, Lexington, Kentucky, 23-25 October, 2002.

Bittleston, S. H. and Hassager, O.: "Flow of Viscoplastic Fluids in a rotating concentric annulus," Journal of Non-Newtonian Fluid Mech. 42, (1992) 19-36.

Bern, P. A., Morton, E. K., Zamora, M., May, R., Moran, D., Hemphill, T., Robinson, L., Cooper, I., Shah, S. N., and Flores, D. V.: "Modernization of the API Recommended Practice on Rheology and Hydraulics: Creating easy Access to Integrated Wellbore Fluids Engineering," SPE Drilling and Completions, September, 2007, pp. 197-204.

Beverly, C. R. and Tanner, R. I.: "Numerical analysis of three dimensional Bingham Plastic Flow," Journal of Non-Newtonian Fluid Mech. 42, (1992) 85-115.

Bird, D. J., Armstrong, R. C., and Hassager, O.: Dynamics of Polymeric Liquids, John Wiley & Sons, 2nd ed., vol. 1, New York City (1987).

Bird, R. B., Stewart, W. E., and Lightfoot, E. N.: Transport Phenomena, John Wiley & Sons, New York City (1960).

Bode, D. J., Noffke, R. B., and Nickens, H. V.: "Well-Control Methods and Practices in Small-Diameter Well Bores," JPT, November 1991, pp. 1380-1386.

Bourgoyne, A. T., Chenevert, M. E., Millheim, K., and Young, F. S.: Applied Drilling Engineering, SPE Textbooks Series, Richardson, TX (1986).

Bourne, D. E., Figueiredo, O., and Charles, M. E.: "Laminar and Turbulent Flow in Annuli of Unit Eccentricity," The Canadian Journal of Chemical Eng., Vol. 46, (October, 1968), pp. 289-293.

Caetano, E. F., Shoham, O., and Brill, J. P.: "Upward Vertical Two-Phase Flow Through an Annulus- Part 1: Single-Phase Friction Factor, Taylor Bubble Rise Velocity, and Flow Pattern Prediction," Journal of Energy Resources Tech., Vol. 114 (1992), pp. 1-13.

Chaplin, M.: "Water Strcture and Science, Guar gum", Retrieved February 12, 2008, from: http://www.lsbu.ac.uk/water/hygua.html

Chen, N.H.: "An Explicit Equation for Friction Factor in Pipe,", Industrial Engineering Chemical Fundamentals, Vol.18 (1979), No. 3, pp. 296-297.

Chen X., "Application of Computational Fluid Dynamics (CFD) to Flow Simulation and Erosion Prediction in Single-Phase and Multiphase Flow", PhD Dissertation, The University of Tulsa, 2004.

Chin, W. C.: "Borehole Flow Modeling in Horizontal, deviated, and Vertical Wells," Gulf Publishing Co., Houston, TX (1992).

Chin, W. C.: "Computational Rheology for Pipeline and Annular Flow," Gulf Professional Publishing, 2001, pp. 25-68.

Colebrook, C. F.: "Turbulent Flow in Pipes, with Particular Reference to the Transition Region between the Smooth and Rough Pipe Laws," Journal of the Institution of Civil Engineers (1938-1939) 11, p133-156.

Cross, M. M.: "Rheology of non-Newtonian Fluids: A New Flow Equation for Pseudoplastic Systems," Journal of Colloid Sc., Vol. 20, pp. 417-437 (1965)

Delwiche, R.A., Lejeune, M. W. D., Mawet, , P. F. B. N., and Vigghetto, R.: "Slimhole Drilling Hydraulics," SPE 24596, presented at the SPE Annual Technical Conference, Washington, D. C., October 4-7, 1992.

Demirdal, B.: "The Study of Flow of paraffin Based Synthetic Drilling Fluid at Elevated Pressure and Elevated Temperature (EPET) conditions," MS Thesis, University of Tulsa, Tulsa, OK, May 2001.

Demirdal, B., and Cunha, J. C.: "Pressure Losses of Non-Newtonian Fluids in Drilling Operations," SPE paper 108711-MS presented at the International Oil Conference and Exhibition, Veracruz, Mexico, 27-30 June, 2007.

De Sousa, J. T. V., Prohaska, M., Bencic, A., and Milheim, K. K.: "Optimization of Slimhole Dual-Body by Experiments and Computational Fluid Dynamics," SPE 54595, SPE Western Regional Meeting, Anchorage, Alaska, May 26-28, 1999.

Dogde, N. A.: "Friction Losses in Annular Flow," Paper 63-WA-11, presented at the Winter Annual Meeting of the ASME, Philadelphia, Pa, Nov. 17-22, 1963, pp. 1-7.

Drew, T. B., Koo, E. C., and McAdams, W. H.: "The Friction Factors for Clean Round Pipes," Trans., AIChE, 28, p. 56-72, (1932).

Edwards, J.K., "Development, Validation and Application of a Three-Dimensional CFD-Based Erosion Prediction Procedure", PhD Dissertation, The University of Tulsa, 2000.

Elder, R. L., Tourlidakis, A., and Yates, M. K. (Editors): Advances of CFD in Fluid Machinery Design, Professional Engineering Publishing, London, UK (2003).

Ellison, T. K., Hatziavramidis, D. T., Sun, B., and Godaspow, D.: "Computational Fluid Dynamics (CFD) Model for Phase Separation at Branching Tee Junctions," SPE 38274, SPE Western Regional Meeting, Long Beach, California, June 25-27, 1997.

Erdal, F. M., Shirazi, S. A., Shoham, O., and Kouba, G. E.: "CFD Simulation of Single-Phase and Two-Phase Flow in Gas-Liquid Cylindrical Cyclone Separators," SPE 36645, SPE Annual Technical Conference and Exhibition, Denver, Colorado, Oct. 6-9, 1996.

Escudier, M. P., Gouldson, I. W., Oliveira, P. J., and Pinho, F. T.: "Effects of Inner Cylinder Rotation on Laminar Flow of a Newtonian Fluid through an Eccentric Annulus," Int. Journal of Heat and Fluid Flow, 21 (2000) 92 – 103

Escudier, M. P., Oliveira, P. J., Pinho, F. T., and Smith, S.: "Fully Developed Laminar Flow of non-Newtonian Liquids through Annuli: Comparison of Numerical Calculations with Experiments," Experiments in Fluids 33 (2002a) 101 – 111

Escudier, M. P., Oliveira, P. J., Pinho, F. T., and Smith, S.: "Fully Developed Laminar Flow of Purely Viscous non-Newtonian Liquids through Annuli, including the effects of eccentricity and inner cylinder rotation," Int. Journal of Heat and Fluid Flow, 23 (2002b) 52 - 73

Exlog staff, 1985. In: Whittaker, A. (Ed.), Theory and Application of Drilling Fluid Hydraulics. International Human Resources Development, Boston, MA.

Farber, S.: "Pressure Loss Modeling of Non-Symmetric gas Turbine Exhaust Ducts using CFD," MS Thesis, Concordia University, Montreal, Quebec, Canada, 2008

FLUENT Manual published by FLUENT Incorporated Network Services, Centerra Resource Park, Lebanon, NH, 2006.

Frankiewicz, T. and Lee, C. M.: "Using Computational Fluid Dynamics (CFD) Simulations to Model Fluid Motion in Process Vessels on Fixed and Floating Platforms," SPE 77494, SPE Annual Tech. Conference and Exhibition, San Antonio, Texas, Sept. 29 – Oct. 2, 2002.

Fredrickson, A. G., and Bird, R. B., "Non-Newtonian Flow in Annuli," Ind. Engr. Chem. (March 1958) 50, No. 3, 347-52

Goel, N., Shah, S. N., and Grady, B. P.: "Correlating viscoelastic measurements of fracturing fluid to particles suspension and solids transport," Journal of Petroleum Science and Engineering, 35 (2002), pp. 59-81.

Goel, N.: "Viscoelastic Measurements of Fracturing Fluid for Proppant Transport Application," PhD Dissertation, The University of Oklahoma, Norman, Ok, U.S.A., 2001.

Gregory, J., Walls, A. H., Sinai, Y. L. and Owens, M. P.: "CFD Modelling of the Dispersion and Burning of a Limited Oil Inventory from an Offshore Installation," SPE 35806, International Conference on Health, Safety and Environment, New Orleans, Louisiana, June 9-12, 1996.

Guckes, T. L.: "Laminar Flow of Non-Newtonian Fluids in an Eccentric Annulus," Paper 74-Pet-57 presented at the 1974 ASME Petroleum Mechanical Engineering Conference, Dallas, Sept. 15-18.

Gun, D. J., and Darling, C. W. W.: "Fluid Flow and Energy Losses in non-Circular Conduits," Trans. of the Inst. of Chemical Engineers, Vol. 41 (1963), pp. 163-173.

Haaland, S. E.: "Simple and Explicit Formulas for the Friction factor in Turbulent Pipe flow," ASME Journal of Fluids Engineering, Vol.105 (1983), 83.

Haciislamoglu, M.: “Non-Newtonian Fluid Fow in Eccentric Annuli and its Application to Petroleum Engineering Problems,” PhD Dissertation, Louisiana State University, 1989

Haciislamoglu, M. and Cartalos, U.: "Practical Pressure Loss Predictions in Realistic Annular Geometries," SPE paper number 28304 presented at the SPE 69th Annual Tech. Conf. New Orleands, Sept. 25-28, 1994, pp. 113-126.

Haciislamoglu, M. and Langlinais, J.: "Non-Newtonian Flow in Eccentric Annuli," Journal of Energy Resources Technology, Vol. 112 (1990), pp. 163-169.

Haciislamoglu, M. and Langlinais, J.: "Effect of pipe Eccentricity on Surge Pressures," Journal of Energy Resources Technology, Vol. 113 (1991), pp. 157-160.

Haige, W. and Yinao, S.: “Flow of Robertson-Stiff Fluids through an Eccentric Annulus,” Applied Mathematics and Mechanics, 19 (10), Oct. 1998

Hartnett, J. P. and Kostic, M.: “Turbulent Friction Factor Correlation for Power-law Fluids flowing in Ducts of Arbitrary Cross-Section,” Int. Comm. Heat Mass Transfer, 1990, 17, pp. 59-65.

Hanks, R. W. and Larsen, K. M.: “The Flow of Power-Law Non-Newtonian Fluids in Concentric Annuli, “Ind. & Eng. Chem. Fund. Vol. 18, No. 1 (1979), pp. 33-35.

Heyda, J.F.: “A Green’s Function Solution for the Case of Laminar Incompressible flow Between Non-Concentric Circular Cylinders,” J. Franklin Inst. (Jan. 1959) 267, No. 1, 25-34.

Hussain, Q. E. and Sharif, M. A. R.: “Analysis of Yield-Power-law fluid Flow in Irregular Eccentric Annuli,” Journal of Energy Resources Tech., Vol. 120 (1998), pp. 201-207.

Iyoho, A. W. and Azar, J. J.: “An Accurate Slot Model for Non-Newtonian Flow Through Eccentric Annuli,” SPEJ (Oct. 1981) 565-72.

Jain, A. K.: “Accurate Explicit Friction Factor,” Journal of Hydraulic Division, ASCE Vol. 102, HY5, May 1976.

Jensen, T. B. and Sharma, M. P.: “Study of Friction Factor and Equivalent Diameter Correlations for Annular flow of Non-Newtonian Drilling Fluids,” Journal of Energy Resources Technology, Vol. 109 (1987), pp. 200-205.

Jones, O. G. and Leung, J. C. M.: “An Improvement in the Calculation of Turbulent Friction in Smooth Concentric Annuli,” Journal of Fluid Engineering, Vol. 103, Dec. 1981.

Jonsson, V. K., and Sparrow, E. M.: “Experiments on Turbulent Flow Phenomena in Eccentric Annular Ducts,” Journal of Fluid Mechanics, Vol. 25, Part 1, 1966, pp. 65-86.

Kostic, M. and Hartnett, J. P.: “Predicting Turbulent Friction Factor of non-Newtonian Fluids in Non-Circular Ducts,” Int. Comm. Heat Mass Transfer, 1984, 11, pp. 345-352.

Kozicki, W., Chou, C. H., and Tiu, C.: “Non-Newtonian Flow in Ducts of Arbitrary Cross-Sectional Shape,” Chem. Eng. Sci., 1966, 21, pp. 665-679.

Lamb, H.: Hydrodynamics, Sixth Edition, Dover Publications, New York, 1945, pp. 585-587.

Locket, T. J.: “Numerical Simulation of Inelastic non-Newtonian Fluid Flows in Annuli,” PhD Dissertation, U. of London, London, UK (1992)

Luo, Y., and Peden, J. M.: "Flow of Non-Newtonian Fluids Through Eccentric Annuli," SPE Production Engineering, February. 1990, pp. 91-96.

Luo, C.: “Distribution of Velocities and Velocity Gradients in Mixing and Floculation Vessels: Comparison Between LDV Data and CFD predictions,” PhD Dissertation, New Jersey Institute of technology, 1997

Manzar, M. A. and Shah, S. N.: “Particle Distribution and Erosion During the Flow of Newtonian and Non-Newtonian Slurries in Straight and Coiled Pipes,” Engineering Applications of Computational Fluid Mechanics, Vol. 3, No. 3, pp. 296 - 320 (2009)

McCann, R. C., Quigley, M. S., Zamora, M. and Slater, K. S.: “Effects of High Speed Pipe Rotation on Pressures in Narrow Annuli,” SPE Drilling and Completions, June 1995, pp 96-103.

Meter, D. M. and Bird, R. B.: “Turbulent Newtonian Flow in Annuli,” AIChE Journal, Vol. 7 (1961), pp. 41-45.

Meuric, O. F. J, Wakeman, R. J., Chiu, T. W., and Fisher, K. A.: “Numerical Flow Simulation of Viscoplastic Fluids in Annuli,” Can. Journal of chemical Engineering, Vol. 76, Feb. 1998, 27-40

Mishra, N.: “Investigation of Hole Cleaning Parameters using Computational Fluid Dynamics in Horizontal and Deviated Wells,” MS thesis, West Virginia University, 2007.

Mitsuishi, N. and Aoyagi, Y.: "Non-Newtonian Fluid Flow in an Eccentric Annulus," Journal of Chemical Eng., Japan (1973) 6, No. 5, 402-08.

Moises A. S., and Shah, S. N.: "Friction Pressure Correlations of Newtonian and Non-Newtonian Fluids through Concentric and Eccentric Annuli", SPE paper 60720, presented at SPE/ICoTA held in Houston, TX, April, 2000.

Moran, L. and Savery, M.: "Fluid Movement Measurements Through Eccentric Annuli: Unique results Uncovered," SPE paper 109563, presented at the SPE Annual Technical Conference and Exhibition held in Anaheim, CA, November 11-14, 2007.

Nouri, J. M., Umur, H. and Whitelaw, J. H.: "Flow of Newtonian and non-Newtonian Fluids in Concentric and Eccentric Annuli," Journal of Fluid Mechanics, Vol. 253, August 1993, pp 617 – 641

Ogugbue, C. C. and Shah, S. N.: "Friction Pressure Correlations for Oilfield Polymeric Solutions in Eccentric Annulus," paper OMAE2009-80044 presented at the International Conference on Ocean, Offshore and Artic Engineering, Honolulu, Hawaii, U.S.A., May 31 – June 5, 2009.

Ooms, G., Kampman-Reinhartz, B. E.: "Influence of Drillpipe Rotation and Eccentricity on Pressure Drop over Borehole with Newtonian Liquid during Drilling," SPE Drill. & Completion 15(4), December 2000, pp. 249-253.

Ozbayoglu, M. E. and Omurlu, C.: "Analysis of the Effect of Eccentricity on Flow Characteristics of Annular Flow of Non-Newtonian Fluids Using Finite Element Method," SPE 100147, SPE/ICOTA Coiled Tubing and Well Intervention Conference and Exhibition, The Woodlands, Texas, U.S.A., 4-5 April, 2006.

Papanastasiou, T. C.: "Flows of Materials with Yield," Journal of Rheology, Vol. 31 (1987), pp. 385-404.

Patankar, S. V. and Spalding, D. B.: "A Calculation procedure for heat, mass and momentum transfer on three-dimensional parabolic flows", Int. Journal Heat and Mass Transfer, 15, 1787 – 1806, 1972.

Patankar, S. V.: Numerical Heat Transfer and Fluid Flow, Hemisphere Publishing Corporation, 1980.

Park, J.: "Computational Fluid Dynamics Simulation and Experimentation of bubbly two-Phase Flow in Horizontal Configuration," PhD Dissertation, The University of Wisconsin-Milwaukee, 2007

Pereira, F. A. R., Barrozo, M. A. S. and Ataide, C. H.: "CFD Predictions of Drilling Fluid Velocity and Pressure Profiles in Laminar Helical Flow," Brazilian Journal of Chemical Engineering, 24 (4), pp. 587-595, Oct. – Dec., 2007

Redberger, P. J. and Charles, M. E.: "Axial Laminar Flow in a Circular Pipe Containing a Fixed Eccentric Core," Canadian Journal of Chemical Engineering, August 1962, 148-151.

Redberger, P. J. and Charles, M. E.: "Axial Laminar Flow Correction," Canadian Journal of Chemical Engineering (1963), 41, 86.

Reed, T. D. and Pilehvari, A. A.: "A New Model for Laminar, Trasitional, and Turbulent Flow of Drilling Muds," SPE Paper 25456 presented at the Production Operations Symposium, Oklahoma City, OK, U.S.A, March 21-23, 1993.

Rehme, K.: "Turbulent Newtonian Flow in Smooth Concentric Annuli with Small Ratios," J. of Fluid Mech., Vol. 64, 1974, pp. 263-287.

Roache, P. J.: Fundamentals of Computational Fluid Dynamics, Hermosa Publishers, Albuquerque, New Mexico, U.S.A., 1998.

Roberto P. R.: "Finite Element Modeling of Annular Flows with Application to Slim Hole Drilling Hydraulics," PhD Dissertation, The University of Texas at Austin, 1994.

Rosine, R., Bailey, M., and Blanco, I.: "Fluid-Flow Phenomena in CT Using CFD", SPE paper 94057, presented at 2005 SPE/ICoTA Coiled Tubing Conference held in Houston, TX, 12-13 April, 2005.

Rothfus, R. R., Monrad, C. C., and Seneca, V. E.: "Velocity Distribution and Fluid Friction in Smooth Concentric Annuli," Ind. Eng. Chem., Vol. 42 (1950), pp. 2511.

Rothfus, R. R., Sartory, W. K., and Kermode, R. I., "Flow in Concentric Annuli at High Reynolds Numbers," AIChE Journal, Vol. 12 (1966), pp. 1086-1091.

Shah, S. N.: "Effects of Pipe Roughness on Friction Pressure of Fracturing Fluids," SPEPE 5 (2): 151-156, 1990.

Shah, S. N., Singhal, N. and Jain, S.: "Determination of Friction Pressure Losses in Straight and Coiled Tubing by CFD Simulations," AIAA / ASME symposium held in Oklahoma City, OK, Feb. 2004.

Shah, S. N. and Ogugbue, C. C.: "Comparative evaluation of drilling and completion polymer fluids," Paper EXPL-2-CE-116, proceedings of the VI International (INGEPET) seminar, October 13-17, 2008, Lima, Peru.

Shergides, C. K.: "Estimate Friction Factor Accurately," Chemical Engineering, March 5, 1984, pp. 63-64.

Shklyar, A. and Arbel, A.: "Accelerated convergence of the numerical simulation of incompressible flow in general curvilinear co-ordinates by discretizations on the double-staggered grids," Int. J. Numer. Meth. Fluids 2008; 57:205–236

Singhal, N., Shah, S. N. and Jain, S.: "Friction Pressure Correlations for Newtonian and Non-Newtonian Fluids in Concentric Annuli," SPE Production and Operations Symposium, Oklahoma City, OK, April 2005

Snyder, W. T. and Goldstein, G. A.: "An Analysis of Fully Developed Laminar Flow in an Eccentric Annuli," AIChE Journal, Vol. 11 (1965), pp. 462-467.

Subramanian, R.: "A Study of Pressure Loss Correlations of Drilling Fluids in Pipes and Annuli," MS Thesis, U. of Tulsa, Oklahoma, 1995.

Subramanian, R. and Azar, J. J.: "Experimental Study on Friction Pressure Drop for NonNewtonian Drilling Fluids in Pipe and Annular Flow," SPE 64647 presented at the SPE International Oil and Gas Conference and Exhibition held in Beijing, China, 7-10 November 2000.

Tam, K. C. and Tiu, C., "A General Correlation for Purely Viscous Non-Newtonian Fluids flowing in Ducts of Arbitrary Cross-Section," Can. Journal Chem. Eng., 1988, 66, pp. 542-549.

Tao, L. N. and Donovan, W. F.: "Through Flow in Concentric and Eccentric Annuli of Fine Clearance With and Without Relative M b otion of the Boundaries," Trans., ASME (1955) 77, 1291-1301.

Tiu, C. and Bhattacharyya, S.: "Flow Behavior of Power Law Fluids in the Entrance Region of Annuli," The Can. Journal of Chem. Eng., Vol. 51 (1973), pp. 47-54.

Tiu, C. and Bhattacharyya, S.: "Developing and Fully Developed velocity Profiles for Inelastic Power Law Fluids in an Annulus," AIChE Journal, Vol. 20 (1974), pp. 1140-1144.

Ton-That, Q. A. and Camarero, R.: "Solution of incompressible fluid flows based on velocity field corrections, a different approach from the pressure correction methods", Numerical Methods in Laminar and Turbulent Flow, Vol. 5, pt 1, 102-113, 1987

Tosun, I.: "Axial laminar Flow in an Eccentric Annulus: An Approximate Solution," AICHE Journal (Sept. 1984) 30, No. 5, 877-78.

Tu, J., Yeoh, G. H. and Liu, C.: Computational Fluid Dynamics, A Practical Approach, Butterworth-Heinemann, ELSEVIER, First Edition, 2008.

Tzabiras, G., Diraas, A. and Loukakis, T.: "A Numerical method for the calculation of incompressible, steady, separated flows around airfoils", Int. J. Numerical Methods fluids, 6, 789-908, 1986.

Speigel, M. R.: Mathematical Handbook of Formulas and Tables, McGraw-Hill Book Co., 1968, pp. 125-128.

Uner, D., Ozden, C., and Tosun, I.: "An Approximate Solution for Non-Newtonian Flow in Eccentric Annuli," Ind. And eng. Chem. (1988) 27, No. 4, 698-701.

Van Doormaal, J. P. and Raithby, G. D.: "Enhancement of the Simple Method for Predicting Incompressible Fluid Flows," Numerical Heat Transfer: Part A: Applications, Volume 7, Number 2 (1984), pp. 147-163.

Vaughn, R. D.: "Axial Laminar flow of Non-Newtonian Fluids in Narrow Eccentric Annuli," SPEJ (Dec. 1965) 277-80; Trans., AIME, 234.

Watson, G. R., Barton, N. A., Hargrave, G. K.; "Using New Computational Fluid Dynamics Techniques to Improve PDC Bit Performance," SPE 37580, SPE/IADC Drilling Conference, Amsterdam, The Netherlands, March 4-6, 1997.

Whitcomb, P. J., Gutowski, J., and Howland, W. W.: "Rheology of Guar Solutions," Journal of Applied Polymer Science, Vol. 25, pp. 2815-2827 (1980).

Winkler, H. W.: "Single and Two-Phase Vertical Flow Through 0.996 x 0.625 inch Fully Eccentric plain Annular Configuaration," Ph.D dissertation, The University of Texas at Austin, 1968.

Xu, J., Shirazi, S. A., Doty, D. R., Schmidt, Z., and Blais, R. N.: "Predictions of Turbulent Friction in Rod Pumped Wells," SPE 39800, SPE Permian Basin Oil and Gas Recovery Conference, Midland, Texas, 25-27 March, 1998.

Yao, D. and Robello, S. G.: "Annular Pressure Loss Predictions for Various Stand-off Devices," IADC/SPE 112544, IADC/SPE Drilling Conference, Orlando, Florida, U.S.A., 4-6 March, 2008.

Yu, S.: "Non-Newtonian Fluid Flow in Annuli" PhD Dissertation, McMaster University, Canada, July 1994.

Zamora, M. and Power, D.: "Making a case for AADE Hydraulics and the Unified Rheological Model," Paper AADE-02-DFWM-HO-13 presented at the AADE "Drilling

and Completion Fluids and Waste Management" Technology Conference, Houston, Texas, U.S.A, April 2-3, 2002.

Zamora, M., Roy, S. and Slater, K.: "Comparing a Basic set of drilling Fluid Pressure-Loss Relationships to Flow Loop and Field Data," Paper AADE-05-NTCE-27 presented at the AADE National Technical Conference and Exhibition, Houston, Texas, U.S.A, April 5-7, 2005.

APPENDIX A

GAMBIT JOURNAL FILES FOR GRID GENERATION

A.1: Hexahedral Mesh for a Concentric annulus 40(r) x 80(θ) x 200(z), d_1 = 1.375in, d_2 = 0.875in.

```
/ Journal File for GAMBIT 2.3.16, Database 2.3.14, ntx86 SP2006032921
vertex create "origin" coordinates 0 0 0
vertex create "topdp" coordinates 0 0.875 0
vertex create "middletop" coordinates 0 1.125 0
vertex create "topcsg" coordinates 0 1.375 0
vertex create "ctrtbg" coordinates 0 0 0
vertex create "dwntbg" coordinates 0 -0.875 0
vertex create "dowmmiddle" coordinates 0 -1.125 0
vertex create "dwncsg" coordinates 0 -1.375 0
vertex create "xaxisdp" coordinates 0.875 0 0
vertex create "xaxiscsg" coordinates 1.375 0 0
edge create "updown" straight "topdp" "middletop"
edge create "toptop" straight "middletop" "topcsg"
edge create "downup" straight "dwntbg" "dowmmiddle"
edge create "downdown" straight "dowmmiddle" "dwncsg"
edge create "csg1" center2points "origin" "topcsg" "xaxiscsg" minarc arc
edge create "csg2" center2points "origin" "xaxiscsg" "dwncsg" minarc arc
edge create "tbg1" center2points "ctrtbg" "topdp" "xaxisdp" minarc arc
edge create "tbg2" center2points "ctrtbg" "xaxisdp" "dwntbg" minarc arc
undo begingroup
edge picklink "downdown" "downup"
edge mesh "downup" "downdown" successive ratio1 1 intervals 20
undo endgroup
undo begingroup
edge picklink "updown"
```

```
edge mesh "updown" successive ratio1 1 intervals 20
undo endgroup
undo begingroup
edge picklink "toptop"
edge mesh "toptop" successive ratio1 1 intervals 20
undo endgroup
edge merge "csg1" "csg2" forced
edge merge "tbg1" "tbg2" forced
undo begingroup
edge picklink "tbg1"
edge mesh "tbg1" successive ratio1 1 intervals 80
undo endgroup
undo begingroup
edge picklink "csg1"
edge mesh "csg1" successive ratio1 1 intervals 80
undo endgroup
face create "inlet" wireframe "updown" "toptop" "downup" "downdown" "csg1" \
  "tbg1" real
face mesh "inlet" map size 1
vertex create "end" coordinates 0 0.875 200
edge create "z axis" straight "topdp" "end"
undo begingroup
edge picklink "z axis"
edge mesh "z axis" successive ratio1 1 intervals 100
undo endgroup
volume create translate "inlet" onedge "z axis" withmesh
physics create "inlet" btype "VELOCITY_INLET" face "inlet"
physics create "outlet" btype "OUTFLOW" face "face.8"
physics create "wallcsg" btype "WALL" face "face.5"
physics create "wall tbg" btype "WALL" face "face.4"
physics create "symmetry" btype "SYMMETRY" face "face.7" "face.6" "face.3" \
```

```
  "face.2"
 physics create "fluid" ctype "FLUID" volume "volume.1"
 export fluent5 \
  "CA-2.75-1.75_40_80_100(200in).msh"
```

A.2: Hybrid Mesh for case c, eccentricity = 0 96, d_1 = 1.0-in, d_2 = 2.0-in., Grid Size = 0.0327-in.

```
/ Journal File for GAMBIT 2.3.16, Database 2.3.14, ntx86 SP2006032921
/ Identifier "default_id2812"
vertex create "origin" coordinates 0 0 0
vertex create "ctrdp" coordinates 0 -0.48 0
vertex create "downtbg" coordinates 0 -0.98 0
vertex create "downcsg" coordinates 0 -1 0
vertex create "upcsg" coordinates 0 1 0
vertex create "uptbg" coordinates 0 0.02 0
edge create "symdown" straight "downtbg" "downcsg"
edge create "symup" straight "upcsg" "uptbg"
vertex create "x axis dp" coordinates 0.5 -0.48 0
vertex create "x axis csg" coordinates 1 0 0
edge create "csg" center2points "origin" "upcsg" "x axis csg" minarc arc
edge create "csg2" center2points "origin" "downcsg" "x axis csg" minarc arc
edge create "tbg2" center2points "ctrdp" "downtbg" "x axis dp" minarc arc
edge create "tbg3" center2points "ctrdp" "uptbg" "x axis dp" minarc arc
edge merge "tbg2" "tbg3" forced
edge merge "csg" "csg2" forced
face create "inlet" wireframe "symdown" "symup" "csg" "tbg2" real
undo begingroup
edge picklink "symdown"
edge mesh "symdown" successive ratio1 1 intervals 1
undo endgroup
undo begingroup
```

```
edge picklink "symup"
edge mesh "symup" successive ratio1 1 intervals 30
undo endgroup
undo begingroup
edge picklink "tbg2"
edge mesh "tbg2" successive ratio1 1 intervals 48
undo endgroup
undo begingroup
edge picklink "csg"
edge mesh "csg" successive ratio1 1 intervals 97
undo endgroup
face mesh "inlet" tripave size 1
vertex create "x axis" coordinates 1 0 0
vertex create "end" coordinates 1 0 120
edge create "z axis" straight "x axis" "end"
undo begingroup
edge picklink "z axis"
edge mesh "z axis" successive ratio1 1 intervals 360
undo endgroup
volume create translate "inlet" onedge "z axis" withmesh
physics create "inlet" btype "VELOCITY_INLET" face "inlet"
physics create "outlet" btype "OUTFLOW" face "face.6"
physics create "wall tbg" btype "WALL" face "face.3"
physics create "wall csg" btype "WALL" face "face.4"
physics create "symmettry" btype "SYMMETRY" face "face.2" "face.5"
physics create "FLUID" ctype "FLUID" volume "volume.1"
edge delete "z axis" lowertopology
export fluent5 "0.96EA_2.0_1.0_0.02_30_48_97_360(120).msh"
```

A.3: Hexahedral Mesh for case a, eccentricity = 0 43, 32(r) x 128(θ) x 100(z)

```
/ Journal File for GAMBIT 2.3.16, Database 2.3.14, ntx86 SP2006032921
vertex create "origin" coordinates 0 0 0
vertex create "topdp" coordinates 0 0.17281 0
vertex create "middletop" coordinates 0 0.267905 0
vertex create "topcsg" coordinates 0 0.363 0
vertex create "ctrtbg" coordinates 0 -0.05719 0
vertex create "dwntbg" coordinates 0 -0.28719 0
vertex create "dowmmiddle" coordinates 0 -0.3251 0
vertex create "dwncsg" coordinates 0 -0.363 0
vertex create "xaxisdp" coordinates 0.23 -0.05719 0
vertex create "xaxiscsg" coordinates 0.363 0 0
edge create "updown" straight "topdp" "middletop"
edge create "toptop" straight "middletop" "topcsg"
edge create "downup" straight "dwntbg" "dowmmiddle"
edge create "downdown" straight "dowmmiddle" "dwncsg"
edge create "csg1" center2points "origin" "topcsg" "xaxiscsg" minarc arc
edge create "csg2" center2points "origin" "xaxiscsg" "dwncsg" minarc arc
edge create "tbg1" center2points "ctrtbg" "topdp" "xaxisdp" minarc arc
edge create "tbg2" center2points "ctrtbg" "xaxisdp" "dwntbg" minarc arc
undo begingroup
edge picklink "downdown" "downup"
edge mesh "downup" "downdown" successive ratio1 1 intervals 16
undo endgroup
undo begingroup
edge picklink "updown"
edge mesh "updown" successive ratio1 1 intervals 16
undo endgroup
undo begingroup
edge picklink "toptop"
```

```
edge mesh "toptop" successive ratio1 1 intervals 16
undo endgroup
edge merge "csg1" "csg2" forced
edge merge "tbg1" "tbg2" forced
undo begingroup
edge picklink "tbg1"
edge mesh "tbg1" successive ratio1 1 intervals 128
undo endgroup
undo begingroup
edge picklink "csg1"
edge mesh "csg1" successive ratio1 1 intervals 128
undo endgroup
face create "inlet" wireframe "updown" "toptop" "downup" "downdown" "csg1" \
  "tbg1" real
face mesh "inlet" map size 1
vertex create "end" coordinates 0 0.17281 60
edge create "z axis" straight "topdp" "end"
undo begingroup
edge picklink "z axis"
edge mesh "z axis" successive ratio1 1 intervals 100
undo endgroup
volume create translate "inlet" onedge "z axis" withmesh
physics create "inlet" btype "VELOCITY_INLET" face "inlet"
physics create "outlet" btype "OUTFLOW" face "face.8"
physics create "wallcsg" btype "WALL" face "face.5"
physics create "wall tbg" btype "WALL" face "face.4"
physics create "symmetry" btype "SYMMETRY" face "face.7" "face.6" "face.3" \
  "face.2"
physics create "fluid" ctype "FLUID" volume "volume.1"
export fluent5 \
  "HEC Model_32_128_100(60in).msh"
```

APPENDIX B

VELOCITY AND VISCOSITY PROFILES

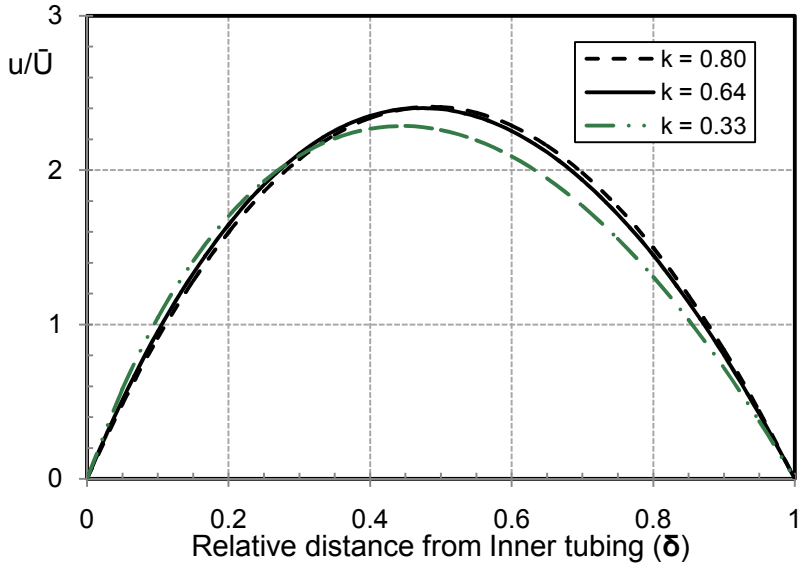

Figure A.1 Axial velocity profile of a Newtonian fluid (sector A), N_{Reg} = 800, ε = 0.5

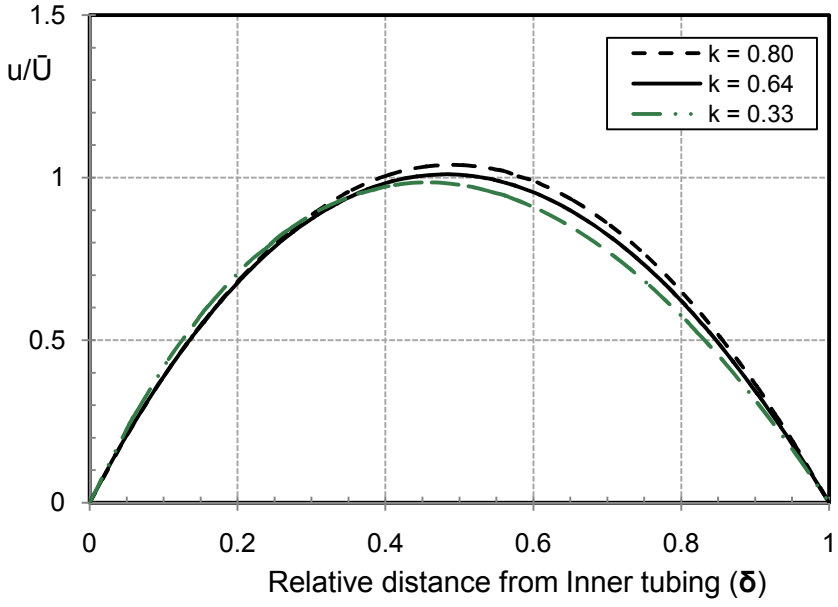

Figure A.2 Axial velocity profile of a Newtonian fluid (Sector B), NReg = 800, ε = 0.5

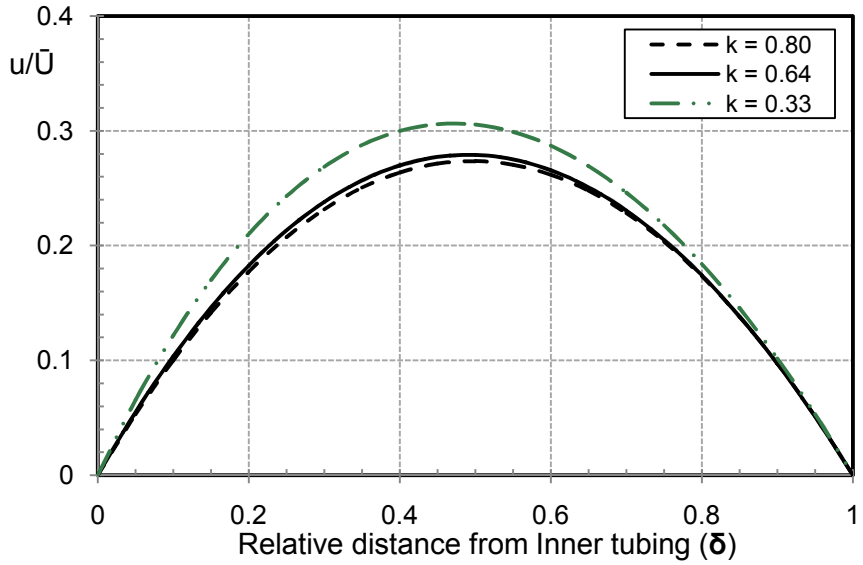

Figure A.3 Axial velocity profile of a Newtonian fluid (Sector C), N_{Reg} = 800, ε = 0.5

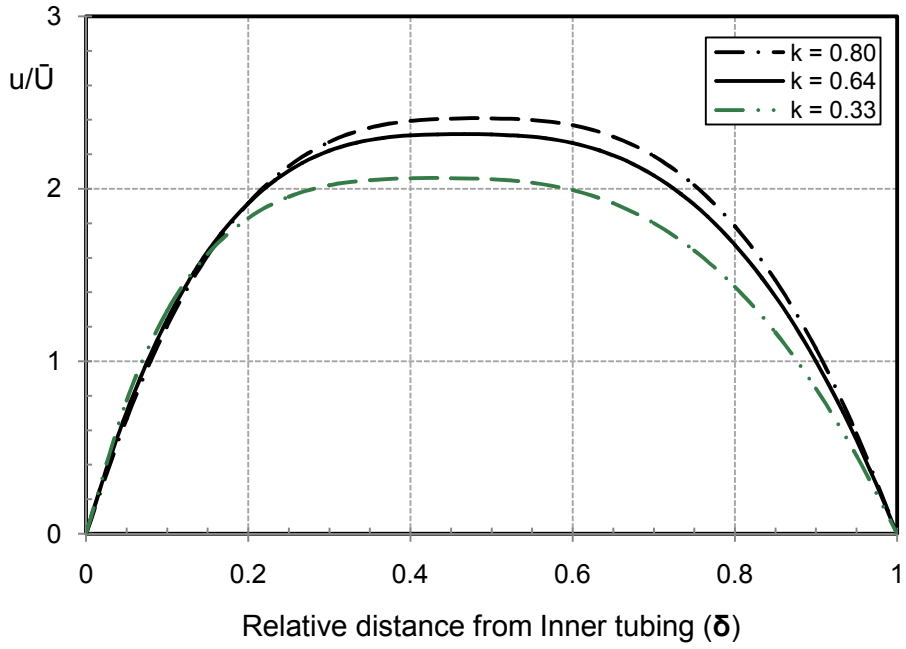

Figure A.4 Axial velocity profile of a non-Newtonian fluid (30 lb/Mgal guar, n=0.55) for sector A, N_{Reg} = 400, ε = 0.5

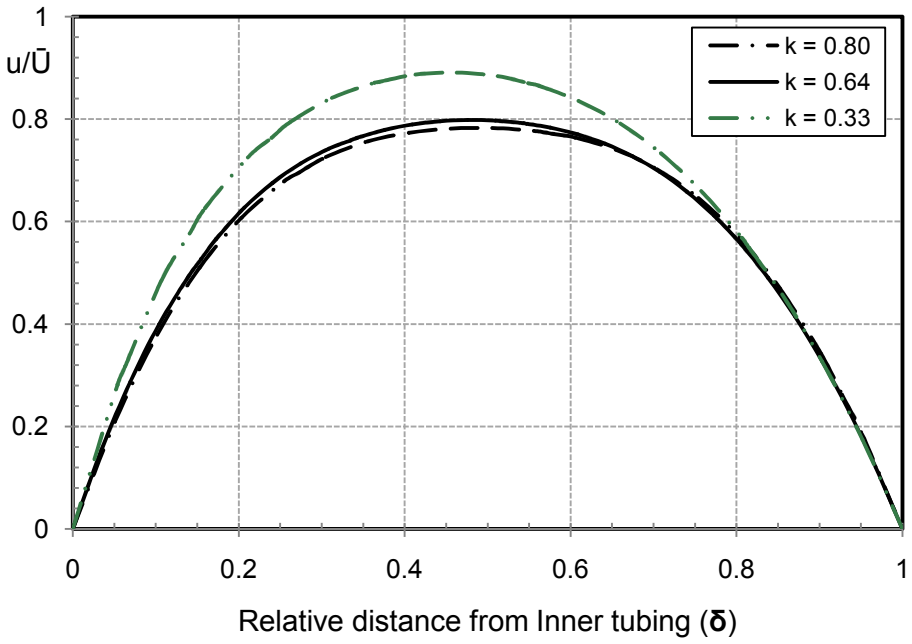

Figure A. 5 Axial velocity profile of a non-Newtonian fluid (30 lb/Mgal guar, n=0.55) for sector B, N_{Reg} = 400, ε = 0.5

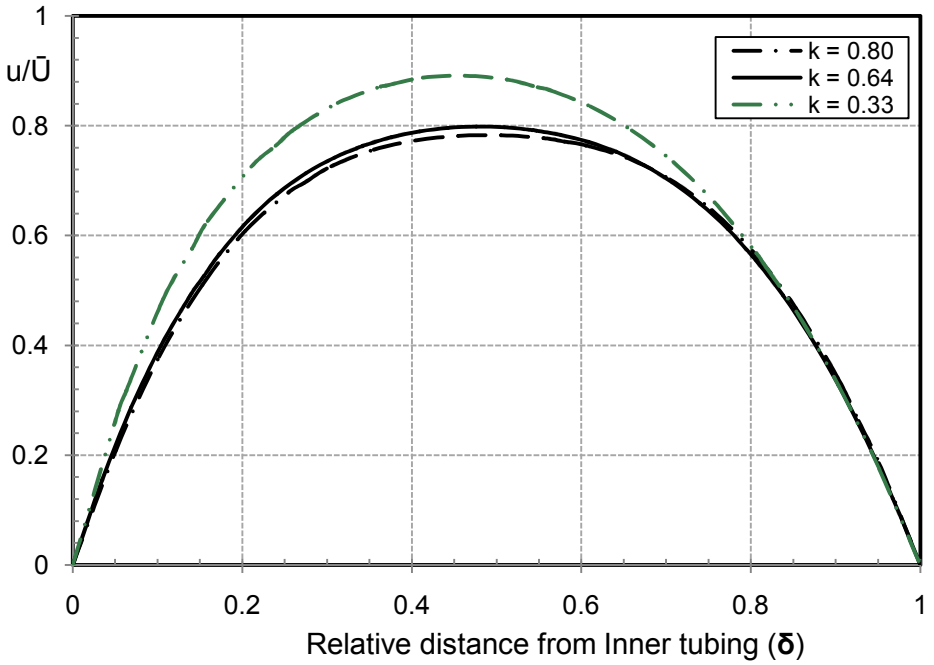

Figure A.6 Axial velocity profile of a non-Newtonian fluid (30 lb/Mgal guar, n=0.55) for sector C, N_{Reg} = 400, ε = 0.5.

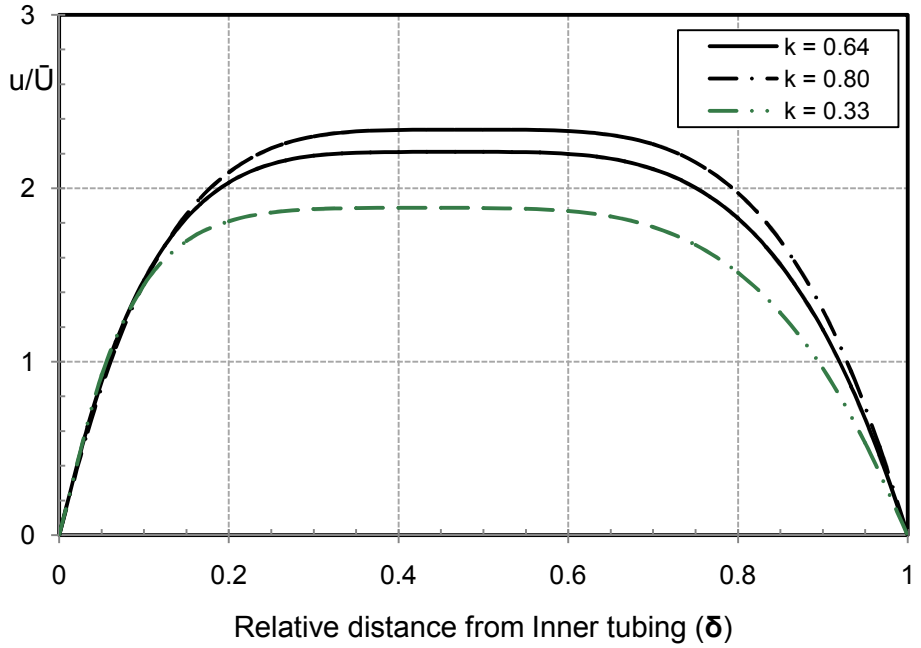

Figure A.7 Axial velocity profile of a non-Newtonian fluid (60 lb/Mgal guar, n=0.36) for sector A, N_{Reg} = 124, ε = 0.5

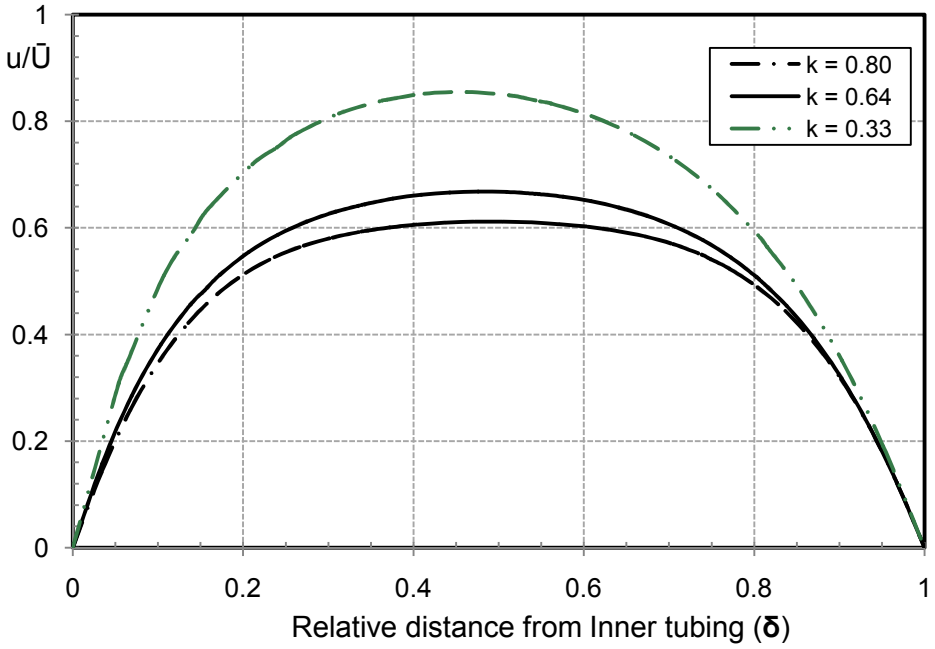

Figure A.8 Axial velocity profile of a non-Newtonian fluid (60 lb/Mgal guar, n=0.36) for sector B, N_{Reg} = 124, ε = 0.5.

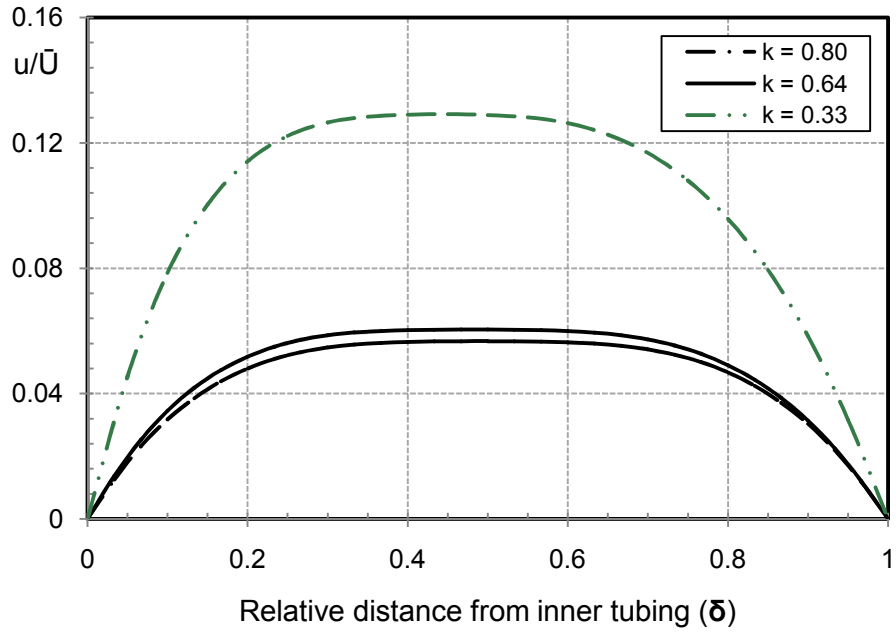

Figure A.9 Axial velocity profile of a non-Newtonian fluid (60 lb/Mgal guar, n=0.36) for sector C, N_{Reg} = 124, ε = 0.5.

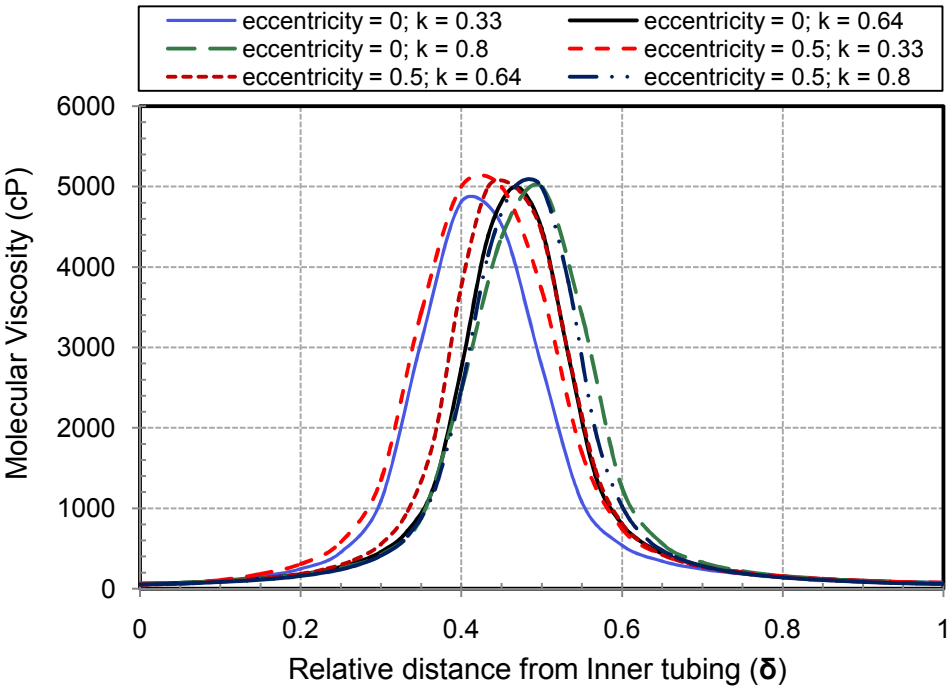

Figure A.10 Molecular velocity profile (sector A) for the laminar flow of 60 lb/Mgal guar (n = 0.36), N_{Reg} = 124.

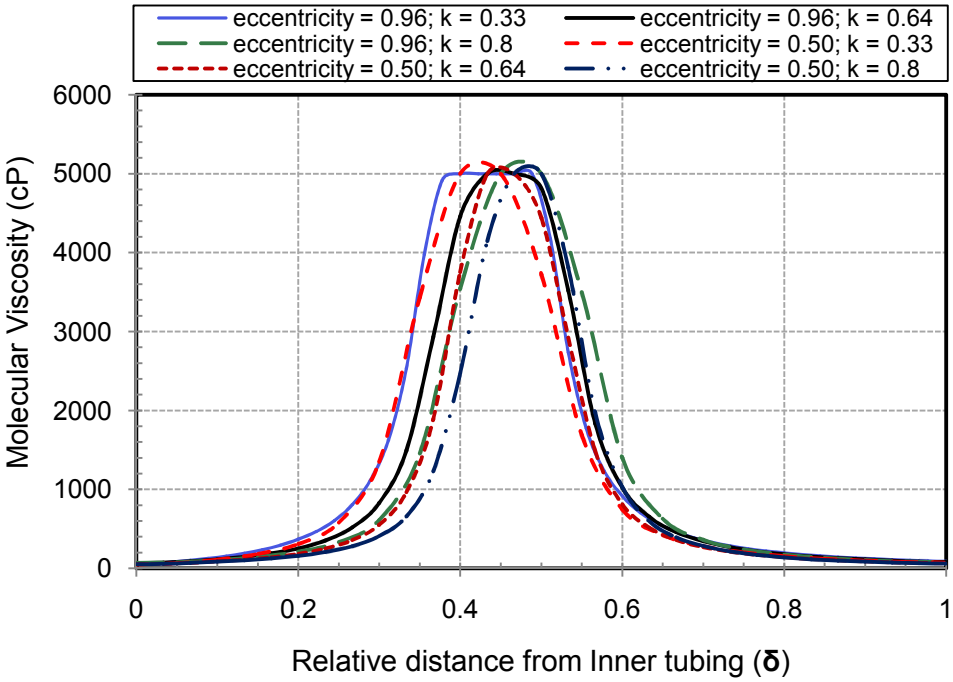

Figure A. 11 Molecular velocity profile (sector A) for the laminar flow of 60 lb/Mgal guar (n = 0.36), N_{Reg} = 124, ε = 0.5 and 0.96.

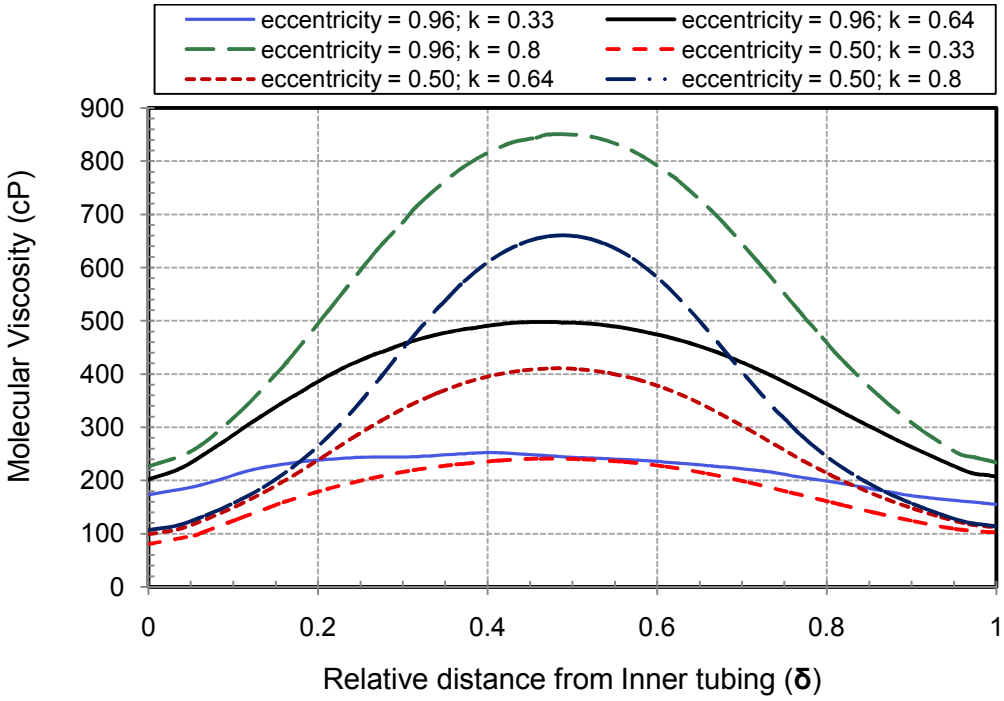

Figure A.12 Molecular velocity profile (sector B) for the laminar flow of 60 lb/Mgal guar (n = 0.36), N_{Reg} = 124, ε = 0.5 and 0.96.

APPENDIX C

NOMENCLATURE

a	Constant variable in Eq. (2.2)
A	Correlation constant, *dimensionless,* Eq. (2.19)
B	Flow behavior index of a RS fluid, *dimensionless*, Eq. (2.19)
b_1	Constant variable in Eq. (2.30)
b_2	Constant variable in Eq. (2.30)
C	Shear rate correction index in RS model, s^{-1}, Eq. (2.19)
c	radial clearance, R_o - R_i, in., Eq. (2.16)
d_1	outer diameter of inner pipe, in.
d_2	inner diameter of outer pipe, in.
d_{eff}	effective diameter of outer pipe, in., Eq. (2.39)
d_h	hydraulic diameter of outer pipe, in., Eq. (2.35)
e	offset distance between the centers of the inner and outer pipes, L
f	Fanning friction factor, *dimensionless*
G	Correlation constant, *dimensionless,* Eq. (2.40)
gpm	gallons per minute
h	tubular roughness projection in Eq. (5.17)
h_s	slot height, in., Eq. (2.16)
k	diameter ratio of annulus, d_1/d_2
K	Consistency index of power law fluid ($lb_f s^n/ft^2$)
K_a	Consistency index of power law fluid for annular flow, ($b_f s^n/ft^2$)
K_p	Consistency index of power law fluid for pipe flow, ($b_f s^n/ft^2$)
K_v	Consistency index of power law fluid from Fann Model 35 viscometer, ($b_f s^n/ft^2$)
L	length between pressure ports (*ft*)
n	Power law flow behavior index, *dimensionless*
N	Rotor speed of viscometer in revolutions per minute *(rpm)*, Eq. (5.1)
N_{Re}	Reynolds number

N_{Reg} generalized Reynolds number, *dimensionless*

Q flow rate, gal/min

Q_D dimensionless flow rate

R_i inner radius (outer radius of inner pipe), (*in.)*

R_o outer radius (inner radius of outer pipe), (*in.)*

r_h Hydraulic radius*, in., Eq. (2.30)*

S *s*pring factor of Fann Model 35 viscometer, Eq. (5.2)

T Correlation constant, *dimensionless,* Eq. (2.36)

u local fluid velocity in velocity profile plots, (*ft/sec*)

$\bar{U}$ average fluid velocity, (*ft/sec*)

Y Correlation constant, Eq. (2.42)

Z Correlation constant, *dimensionless,* Eq. (2.41)

GREEK SYMBOLS

α Correlation constant, *dimensionless,* Eq. (3.12)

ρ fluid density, (lb_m/gal)

σ Constant in Eq. 5.5, *dimensionless*

β ratio of bob to cup radius for Model 35 Fann Viscometer

ΔP pressure drop (*psi*)

$\Delta P_{conc.}$ pressure drop in concentric annulus (*psi*), Eq. 2.20

$\Delta P_{ecc.}$ pressure drop in eccentric annulus (*psi*), Eq. 2.20

ε constant variable used to describe bipolar coordinate system, Eq. 2.2

ε_i constant variable used to describe bipolar coordinate system, Eq. 2.5

ε_o constant variable used to describe bipolar coordinate system, Eq. 2.6

f_∞ Correlation constant, *dimensionless,* Eq. (2.24)

Π_1 Correlation constant, Eq. (2.35)

Π_2 Correlation constant, Eq. (2.35)

θ angular coordinate, (rad.)

ϕ General variable (representing transport properties; u, v,w, T, ¥ & g) in *Eq*. (3.3)

Ø	Correlation constant, *dimensionless,* Eq. (2.24)
Ω	Correlation constant, *dimensionless,* Eq. (2.44)
λ	dimensionless radial position at which velocity is maximum, Eq. (2.29)
ρ	fluid density, (lb_m/gal)
$\dot{\gamma}$	Shear rate, (s^{-1})
$\dot{\gamma}_w$	wall shear rate, (s^{-1})
τ	Shear stress, (lb_f/ft^2)
τ_w	wall shear stress, (lb_f/ft^2)
μ	fluid (water) viscosity (cP)
μ_a	apparent viscosity, *cP*
μ_D	Dimensionless viscosity
ξ	eccentricity, *dimensionless*
ψ	constant variable in Eq. 2.7